



**Die Bedeutung von Ceramiden und Sphingomyelinasen
für Dynamische Membranveränderungen in T-Zellen**

**The Role of Ceramides and Sphingomyelinasen
for Dynamic Membrane Processes
in T Cells**

Thesis for a doctoral degree
at the Graduate School of Life Sciences,
Julius-Maximilians-Universität Würzburg

Section: Infection and Immunity

submitted by

Lena Collenburg

from Kiel

Würzburg 2017

Submitted on:

Members of the *Promotionskomitee*:

Chairperson: Prof. Dr. Thomas Hünig

Primary Supervisor: Prof. Dr. Sibylle Schneider-Schaulies

Supervisor (Second): PD Dr. Niklas Beyersdorf

Supervisor (Third): Prof. Dr. Markus Sauer

Supervisor (Fourth):

Date of Public Defence:

Date of Receipt of Certificates:

Affidavit

I hereby declare that my thesis entitled "The Role of Ceramides and Sphingomyelinases for Dynamic Membrane Processes in T Cells" is the result of my own work. I did not receive any help or support from commercial consultants. All sources and/or materials applied are listed and specified in the thesis. Furthermore, I verify that this thesis has not yet been submitted as part of another examination process neither in identical or similar form.

Würzburg,

Date

Signature

Eidesstattliche Erklärung

Hiermit erkläre ich an Eides statt, die Dissertation „Die Bedeutung von Ceramiden und Sphingomyelinasen für Dynamische Membranveränderungen in T-Zellen“ eigenständig, d.h. insbesondere selbständig und ohne Hilfe eines kommerziellen Promotionsberaters, angefertigt und keine anderen als die von mir angegebenen Quellen und Hilfsmittel verwendet zu haben.

Ich erkläre außerdem, dass die Dissertation weder in gleicher noch in ähnlicher Form bereits in einem anderen Prüfungsverfahren vorgelegen hat.

Würzburg,

Datum

Unterschrift

Table of Contents

1	Introduction	1
1.1	T Cells in the Immune System.....	1
1.2	Chemokines in the Immune System	1
1.3	Chemokine Receptors.....	2
1.4	Actin Dynamics in T Cell Polarisation and Migration.....	3
1.5	T Cell Circulation and Migration into Tissues.....	8
1.6	Sphingolipids and Ceramides	8
1.7	Neutral Sphingomyelinase 2.....	10
1.8	Visualisation of Lipids.....	11
1.9	Function of Membrane Platforms.....	12
1.10	Sphingolipid Enriched Domains in T Cell Activation	13
1.11	Aim of the Thesis	15
2	Materials	16
2.1	Cell Lines	16
2.2	Primary Cells	16
2.3	Mice	16
2.4	Media, Buffers and Solutions	17
2.5	Plastic Materials.....	21
2.6	Antibodies and Dyes	22
2.7	Chemokines, Cytokines, Inhibitors.....	23
2.8	Equipment	24
3	Methods	25
3.1	Cell Culture.....	25
3.1.1	Cell Lines	25
3.1.2	Cryoconservation	25
3.1.3	Isolation of Primary Human T Cells and DCs.....	26
3.2	T Cell Transfection and Inhibitor Treatment	28
3.3	NSM/ASM Assay	28
3.4	RNA Isolation, cDNA Transcription and PCR.....	29
3.5	General Analysis.....	31
3.5.1	Confocal Microscopy.....	31
3.5.2	Flow Cytometry	31
3.6	Click Chemistry.....	32

3.6.1	Dye Testing for Click Labelling.....	32
3.6.2	Click Labelling	32
3.6.3	Bacterial Sphingomyelinase Treatment	32
3.6.4	T Cell Stimulation for N ₃ -cer Uptake	33
3.6.5	Dynabead/T Cell Contacts	33
3.6.6	DC/T Cell Contacts	33
3.6.7	Co-Stimulation on Planar Surfaces	33
3.6.8	Cell Preparation for Lipidomics	34
3.6.9	Live/Dead Staining	34
3.6.10	Ca ²⁺ Flux Measurement.....	34
3.6.11	CD69 Surface Staining.....	35
3.7	Bead/T Cell Contacts	36
3.8	T Cell Migration	37
3.8.1	2D Migration on Collagen.....	37
3.8.2	3D Migration in a Collagen Matrix	37
3.8.3	Polarisation on Planar Surfaces.....	38
3.8.4	Adhesion Assay on HBMECs.....	39
3.8.5	T Cell Polarisation on HBMECs	39
3.8.6	Transendothelial Migration	40
3.9	Isolation of Murine CD4⁺ T Cells and Homing Assays	41
3.9.1	Mouse Section	41
3.9.2	Lysis of Erythrocytes by Hypoosmotic Shock	41
3.9.3	CD4 ⁺ T Cell Isolation	41
3.9.4	In Vivo Homing.....	42
3.10	Statistical Analysis	42
4	Results.....	43
4.1	Functionalised Ceramide Analogues to Study Dynamic Redistribution of Sphingolipids in Living T Cells.....	43
4.1.1	Toxicity Testing of Azide-Functionalised Ceramides	43
4.1.2	Selection of Suitable Dyes	46
4.1.3	Incorporation of Functionalised Compounds into T Cells.....	49
4.1.4	Visualisation of Functionalised Ceramides in T Cells	51
4.1.5	Optimising N ₃ -C ₆ -cer Uptake in Primary T Cells	53
4.1.6	T Cell Activation After N ₃ -C ₆ -cer/ N ₃ -C ₆ -cer Incorporation	55
4.1.7	N ₃ -C ₆ -cer Redistribution After Cell Stimulation.....	56
4.1.8	Ceramide Localisation in T Cell/DC Conjugates	59
4.2	Membrane and Vesicle Dynamics	60

4.2.1	T Cell/Bead Contact Formation	61
4.2.2	Migration of N ₃ -C ₆ -cer Labelled T Cells.....	62
4.3	NSM in Directed T Cell Migration	63
4.3.1	Influence of the NSM on 2D Migration	63
4.3.2	Transendothelial Migration	65
4.3.3	Influence of the NSM on 3D Migration	67
4.3.4	In Vitro Migration of Murine T Cells.....	70
4.3.5	In Vivo Migration of Murine T Cells	72
4.3.6	CXCR4 Expression on T Cells	73
4.3.7	Sphingomyelinase Activity upon SDF-1 α Contact	74
4.3.8	LFA-1 Affinity Maturation.....	75
4.3.9	Phosphorylation of Src, ZAP70 and Erk 1/2.....	78
4.3.10	T Cell Polarisation	79
5	Discussion.....	83
5.1	N ₃ -ceramides Allow for Analysis of Ceramide Redistribution in Living T cells.....	83
5.2	NSM Ablation.....	86
5.3	NSM in T Cell Polarisation	87
5.4	Adhesion and Transendothelial Migration	88
6	Summary	92
7	Zusammenfassung.....	93
8	Bibliography.....	95
9	Abbreviations.....	101
10	Acknowledgements	105
11	Publication List.....	106
12	Curriculum Vitae	107

1 Introduction

1.1 T Cells in the Immune System

The activity of the immune system has to balance between induction of responses to danger signals and infectious agents, and, at the same time, avoidance of overshooting responses causing immunopathology [1]. Immune cells develop from hematopoietic stem cells which differentiate into a plethora of different cells with different functions. T cells are generated from stem cells that migrate into the thymus. In the thymus two lineages arise, the $\alpha\beta$ - and the $\gamma\delta$ -T cells according to the T cell receptor (TCR) they express [2]. T cells with a correctly rearranged TCR undergo a thymic selection process during which those bearing TCRs specific for self-antigens are depleted by apoptosis, while those specific for non-self-antigens survive and continue to differentiate into naïve T cells [3]. $CD8^+$ and $CD4^+$ T cells are the major $\alpha\beta$ -T cell subsets leaving the thymus. They circulate between secondary lymphoid tissues like the lymph nodes and the spleen, and the blood [4]. $CD8^+$ T cells play a major role in the defence against viruses and intracellular pathogens due to their cytolytic activity and $IFN\gamma$ production [5]. $CD4^+$ T cells are also called T helper cells, as their major role is to activate further immune cells like B cells or macrophages. By that they drive the humoral and cell-mediated immunity.

1.2 Chemokines in the Immune System

Directional immune cell circulation is regulated through chemotactic signals that rely on the interaction of chemokines and their specific receptors. This complex system allows the recruitment of antigen presenting cells or effector cells to inflamed or pathogen exposed areas or secondary lymphatic tissues, but also tissue homing and maintenance of the immune compartment under homeostatic conditions [6].

The chemokine superfamily consists of 50 members (8 to 10 kDa in size), which specifically bind to at least one of the 22 G-protein coupled seven-transmembrane signalling receptors. These receptors are divided into families according to their binding motifs [7]. Based on the cystein motifs in their N-termini, chemokines are grouped into

CXC and CC chemokines (the two major groups encoded by gene clusters on chromosomes 4q13.3 and 17q12) or C and CX₃C chemokines (minor groups). Chemokines are mainly leukocyte attractants but also fulfil other tasks in the immune system. They are produced by blood and tissue cells and can play “inflammatory” or “homeostatic” roles. Upon the sensing of infections with their pattern recognition receptors, dendritic cells (DCs), macrophages or $\gamma\delta$ -T cells together with local tissue cells start producing effector cell attracting chemokines. These cells are recruited and activated and then also produce chemokines to enhance the inflammatory milieu and optimise the immune reaction. Main inflammatory cytokines are CXCL6, CXCL8, CXCL1 or CXCL2. In the absence of an acute immune reaction, chemokines regulate immune cell homeostasis. Important chemokines for these functions are CXCL12, CXCL13, CCL19 and CCL21. They regulate haematopoiesis, homeostasis of leukocytes, follicular activities or immune cell homing into spleen and LN [8].

1.3 Chemokine Receptors

Chemokine receptors belong to the γ subfamily of rhodopsin-like seven-membrane receptors. All leukocytes express specific sets of chemokine receptors which are divided into two groups: most of them are G protein–coupled and signal by activating pertussis toxin-sensitive G_i-type G proteins. The second, smaller group is referred to as atypical chemokine receptors which sense and translate chemokine gradients in a G protein–independent manner [9]. Chemokine receptors are activated mainly by the different chemokine families: XCR by C chemokines, CCR by the eleven different CC chemokines, CXCR by the six different CXC chemokines and CX₃CR by CX₃C chemokines. Additionally, there are the four atypical receptors ACKR1 to 4. Expression patterns are specific for each immune cell subset, and they change upon activation to allow differential tissue homing. For instance, dendritic cells (DCs) undergo a chemokine receptor switch (from CCR5 to CCR7) that allows them to sense and follow LN-produced chemokines such as CCL21, which is key to LN homing and priming of T cell responses there [10, 11].

The receptor ligand interaction is a two-step process. First, the C-terminus of the chemokine interacts with the N-terminus and the extracellular loops of the receptor. This is followed by the chemokine’s N-terminus’ interaction with the seven transmembrane bundle of the receptor to stabilise it in its active conformation to initiate signal trans-

duction by G-proteins or arrestins [12]. Chemokine receptor ligation activates PI3-kinase (PI3K) which interacts with the adaptor DOCK2, thereby allowing the assembly of a complex including Crk and ELMO and downstream activation of several Rac-dependent pathways [13, 14]. Rac-dependent pathways are crucial for actin cytoskeletal rearrangements which are particularly important in both physical reshaping of immune cells (cell polarisation), their motility and their migration.

Because our current work focusses on the interaction of CXCR4 and CXCL12/SDF-1 α , this is explained in more detail.

CXCR4 selectively binds SDF-1, which is present in two splice isoforms. Both bind the receptor with similar affinity [15], thereby regulating processes like haematopoiesis, organogenesis, and vascularisation [16]. CXCR4 signalling also mediates metastasis in various cancers and is a co-receptor for HIV. CXCR4 is expressed on many cells of the haematopoietic lineage. Its expression is upregulated on T cells by calcium, cyclic AMP, IL2, IL4 and other mediators, but also upon CD3/CD28 co-stimulation, while inflammatory signals like IFN γ , TNF α and IL1 β lead to CXCR4 downregulation. The receptor can form dimers; this process is enhanced by SDF-1 binding. CXCR4 activation is pertussis toxin-sensitive and depends on the activation of G $_i$ -proteins, which initiate activation of Src-kinase, PLC γ and PI3K, and finally cell migration and adhesion [17]. Being not specific for CXCR4, chemokine receptor ligation mediated cytoskeletal changes are initiated via ZAP70, different Src-kinases and further downstream Cdc42. Along with Cdc42 the actin polymerisation machinery is activated which is a prerequisite for allowing cell locomotion [18].

1.4 Actin Dynamics in T Cell Polarisation and Migration

T cells are found throughout the body and they act in very distinct localisations. Naïve T cells move through secondary lymphoid organs in search for their cognate antigen. Upon an antigen encounter, they expand and differentiate into activated effector cells which migrate into peripheral tissues where they clear antigens [19]. Subsequently, the pool of antigen-specific activated effector cells undergoes a phase of massive contraction, and the residual population differentiates into memory cells which stay in the tissue for immunosurveillance [20]. Hence, each of these cell populations must be recruited to and maintained within different sites. This is regulated by the chemokine system explained above [21].

To be able to move through the organism, T cells need to adapt their cytoskeletal and membrane activity. At a cellular level, T cells need to polarise and reorganise their receptors and signalling machinery. Leukocytes, and so also T cells, are recruited into tissues by a multi-step process of leukocyte-endothelial interactions [22].

The resting endothelium does not interact with circulating leukocytes as it lacks surface molecules for interaction [23]. Two initial steps allow for the attachment of leukocytes to the endothelial cells lining post-capillary venules. First, the endothelium is activated by TNF and IL-1 secreted by stimulated macrophages, and secondly, the dilatation of blood vessels at the site of the inflammation leads to the slowing of the blood flow and a movement of the large leukocytes (compared to red blood cells) to the vessel walls [24]. Here, E- and P-selectin ligands on leukocytes bind the respective selectins on the inflamed endothelial cells with low affinity. The binding is too weak to induce a firm adhesion, hence the short binding leads to leukocyte rolling on the endothelium [25, 26]. The inflamed endothelial cells locally express chemokines which are recognised by the rolling T cells bearing the respective receptor repertoire. This leads to increasing integrin affinity. Upon chemokine receptor engagement small GTPases like Ras1 or Rap1 activate integrins responsible for a firm adhesion to the endothelium [27]. For this, it is important that chemokine receptors localise to the leading edge and the microtubule organising centre as well as the actin regulatory proteins ezrin and moesin organise to the uropod [28]. These signals induce the formation of a defined “front” and a defined “rear” in migrating T cells. In the front the lamellipodium with the chemokine receptors is formed. Now, T cells can acquire motility, which can result in migration. For T cell crawling, integrins need to switch between high and low affinity states to allow an attachment to and release from the endothelial ligands, which are ICAM-1, ICAM-2 or VCAM-1 [29]. This regulation is enabled via signalling through GPCRs recognising the chemokines displayed on the endothelium [30]. Transmigration or diapedesis can then occur in two ways, between endothelial cells (paracellular) or through individual endothelial cells (transcellular). Transcellular migration occurs in about 30 % of the cases [31]. For paracellular transmigration T cells move through tight junctions between single endothelial cells. These tight junctions loosen up in the inflamed endothelium, and the receptors PECAM-1, JAM-1 or CD99 translocate there allowing for the squeezing of the T cell through the gap [32]. In paracellular transmigration F-actin and caveolin-1 rich channels are built by bending epithelial actin stress fibres [33]. The T cells move through the resulting gap without rupturing the fibres, and a ring of actin

quickly seals the opening after passage [34]. Both ways of this diapedesis involve several steps, starting with the formation of T cell protrusions into the endothelial gap (tight junction or transcellular “channel”), followed by the formation of a leading edge underneath the epithelium. Next, the nucleus is lobulated and squeezed through, followed by complete cell passage and pore sealing [35, 36].

The lamellipodium is a thin region which dynamically forms and retracts actin-based protrusions. Aligned actin bundles, as visualised in Figure 1, form fingerlike structures, referred to as filopodia, which mediate sensing of directional information and translate these into actin polymerisation. The lamellipodium contains actin filaments which rapidly extend to push the leading edge forward and retract when the membrane tension is too high. This creates a retrograde actin flow which, when coupled with extracellular matrix adhesion, generates the cell movement [37].

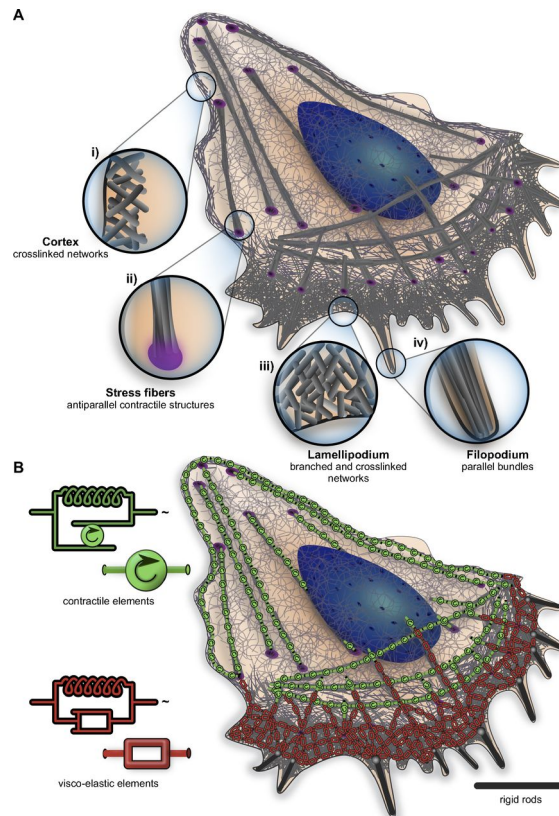


Figure 1: Actin structures in migrating T cells. The upper image shows four different actin structures in distinct regions of migrating T cells. The lower image illustrates the flexibility of the actin stress fibres that can contract, and the lamellipodium containing elastic elements which are recycled. Laurent Blanchoin et al., *Physiological Reviews*, 2014 [38]

Mechanically, actin cytoskeletal rearrangements are connected to signalling pathways via the nucleation factors of the WASP/Scar family (Figure 2). These interact with small GTPases like Cdc42 or Rac through their N-terminal CRIB motifs. WASP proteins are anchored to the plasma membrane via their PH domains which bind acidic phospholipids. WASP can interact with Src family kinases through its SH3 domain, and all

WASP/Scar family proteins interact directly with actin via a respective binding domain [39]. WASP is one of several nucleation promoting factors which enable formation of actin filaments (F-actin) from actin monomers. Other important actin nucleation factors are the actin-related proteins 2 and 3 (Arp 2/3) which are the core of a 7-protein complex. It is located in actin-rich spots in the lamellipodium of crawling cells, and is associated there with the pointed end of newly generated actin fibres to assemble the filaments of an existing actin branch at an angle of 70° [37].

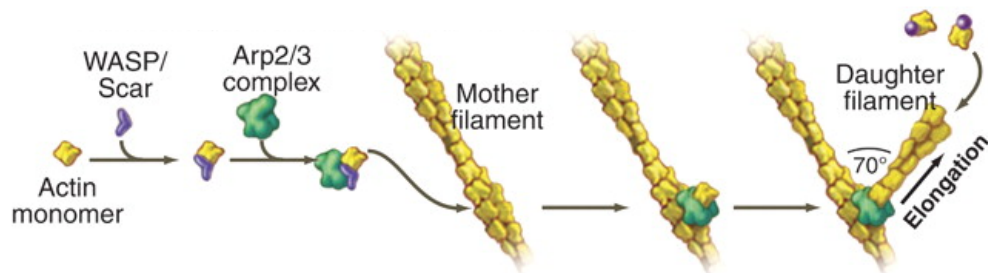


Figure 2: Branching nucleation by the Arp 2/3 complex. The nucleation-promoting factor WASP binds an actin monomer and the Arp 2/3 complex. The whole complex binds to the side of a mother filament and starts a daughter filament which grows from the Arp 2/3 complex. Thomas D. Pollard and John A. Cooper, Science, 2009 [40]

The actin nucleation machinery and the chemokine receptors are of major importance in the leading edge of the cells. For cell movement, this extension has to be coordinated with a retraction of the cell rear. Therefore, coordinated asymmetrical adhesion and detachment happening at the two opposing poles of the cell is crucial in this process (Figure 3). The T cell uropod is highly organised and very active during migration. Various intracellular adhesion molecules (ICAM-1 to -3), CD43, CD44 and the actin binding proteins ezrin and moesin are located here [41]. Actin stress fibres are formed which allow the contraction of the rear end. These are unbranched actin filaments that contain myosin II, but also depend on Arp 2/3 activity to be formed.

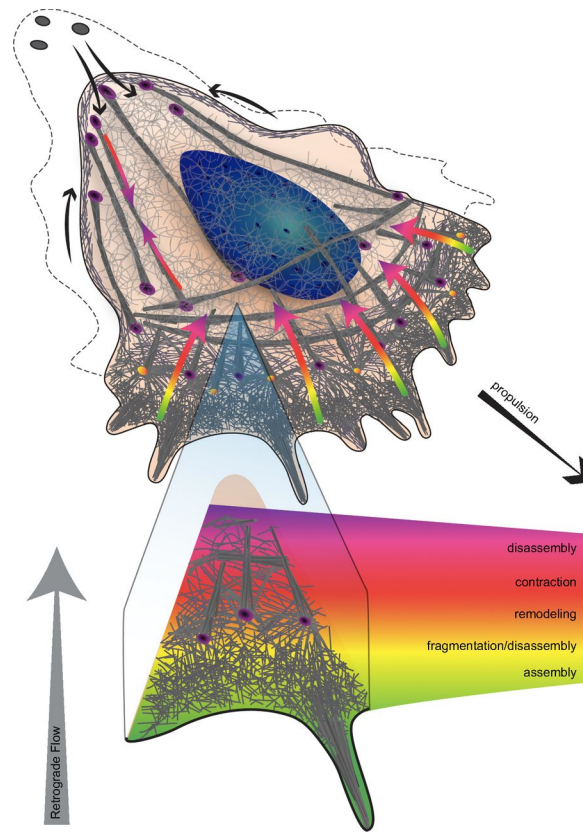


Figure 3: Dynamic actin remodelling in migrating T cells. Laurent Blanchoin et al., *Physiological Reviews*, 2014 [38]

During migration the actin network is assembled in the front of the lamellipodium and disassembled in the back of the lamellipodium, generating monomers for further extension of actin fibres and the forward force production. The rear of the cell retracts by stress fibre contraction and actin disassembly [38].

The cytoskeleton is linked to the intracellular environment in a bi-directional manner via integrins. These are organised in focal adhesions where talin and vinculin link them to actin filaments. Integrins can be present in three different conformations - the bent form, the extended form with closed headpiece and the extended-open form - which define their binding affinity. The integrin lymphocyte function-associated antigen-1 (LFA-1) is expressed by all leukocytes and interacts with different ICAMs on neighbouring cells. Binding of activated LFA-1 to ICAM-1 generates a force that stabilises the open form, especially underneath the mid-body and in the front of the T cell, allowing the forward movement [42].

1.5 T Cell Circulation and Migration into Tissues

T cells move between peripheral tissues, secondary lymphoid organs and the blood. The lymphatic system is a network of blind-ended capillaries that start in the tissue, merge and finally drain into lymph nodes [43]. T cells from the tissue enter LNs via the afferent lymphatic vessels where they pass through junctions in between lymphatic endothelial cells. They are guided there by chemokines from lymphatic endothelial cells and interact with adhesion molecules that allow adhesion and migration (see above) [44]. Most recirculating naïve T cells enter LNs from the blood via high endothelial venules (HEV) or from upstream LN. For extravasation from the blood through HEV T cells perform a multistep process of rolling on the endothelium, integrin activation by chemokines, stable adhesion and finally migration through the endothelium [45, 46]. Within the LN T cells have to cross the subcapsular sinus to enter the cortex and interact with B cells or DC, or they leave the LN directly through the sinus. Movement within the LN is regulated by the chemokines CCL19 and CCL21 [47]. LN egress is regulated by sphingosine-1-phosphate (S1P) which is produced by erythrocytes (red blood cells) and the blood endothelium. T cells upregulate S1P receptors which are essential for migration of the T cells out of the LN and into the blood [48].

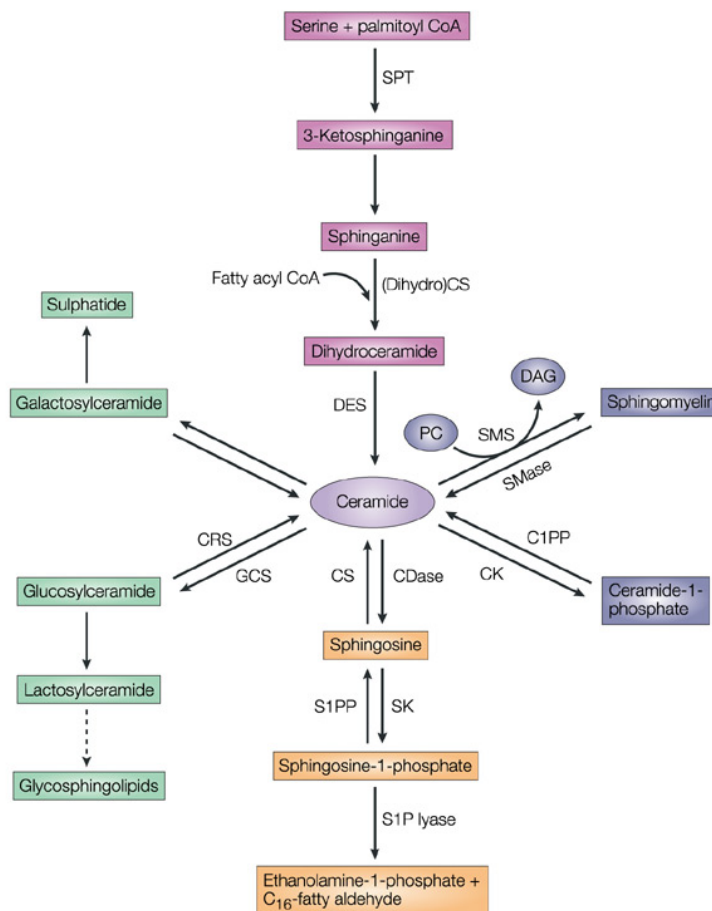
The spleen is the second important lymphoid organ. Lymphocytes enter through branches from the splenic artery, referred to as central arteries, into the white pulp which is highly organised into areas with B cells and T cells [49]. Because the spleen has no HEV or afferent lymphatics, cell entry here is less restricted than in LNs. Antigens are delivered through the blood and are sampled by APCs which present these to T cells [50].

1.6 Sphingolipids and Ceramides

Sphingolipids are molecules containing a sphingoid backbone, and the addition of various other chemical structures give rise to a broad range of molecules with a variety of functions and properties.

Sphingolipids are present in eukaryotic cells and here mainly within membrane bilayers where they define their physical properties. They can be formed in the cell in different ways. The amino acid serine and the fatty acid palmitate are basic building modules for sphingolipid *de novo* biosynthesis.

Ceramide is a simple sphingolipid, consisting of an acyl chain and sphingosine. It can be further modified by a phosphate group (to yield ceramide-1-phosphate), phosphor-ylcholine or sugar moieties give rise to sphingomyelin or glycosphingolipids, respectively. Ceramide can be broken down by ceramidases. These variations in the chemical structure allow a compartmentalisation within the cell where different ceramide species in different organelles can perform a plethora of functions [51]. To regulate different cellular functions, the sphingolipid metabolism is highly regulated and allows rapid and versatile conversion and formation of the bioactive molecules ceramide, sphingosine and sphingosine-1-phosphate [52].



Nature Reviews | Cancer

Figure 4: Sphingolipid metabolism. Besim Ogretmen & Yusuf A. Hannun, Nature Reviews Cancer, 2004 [53]

The synthesis of most lipids is initiated in the endoplasmatic reticulum (ER) from where they have to redistribute to various cellular sub-compartments. As lipids cannot leave membranes easily due to their hydrophobicity, their trafficking has to be vesicular or, if non-vesicular, aided by lipid transfer proteins such as CERT [54]. To a major extent, cellular ceramide originates in the ER compartment and is translocated by CERT which

can extract ceramide from membranes to the Golgi compartment. There, it is further converted, for instance to sphingomyelin [55, 56].

A second way to generate ceramide is the breakdown of complex sphingolipids and the recycling of sphingosine in the salvage pathway which involves several enzymes, including sphingomyelinases, cerebrosidases, ceramidases, and ceramide synthases [57]. Finally, ceramide is the result of sphingomyelin breakdown by sphingomyelinases. These can be activated upon exogenous stress signals [58], their steady state activity is, however, important for maintaining the sphingolipid rheostat conditions [59]. Sphingolipids impact on membrane fluidity and stiffness and thereby modulate crucial lateral and vertical sorting processes of membrane proteins and membrane proximal signalling complexes [60]. Thereby, their rheostat and regulated activity efficiently modulates various cellular functions such as cell apoptosis, differentiation or proliferation [61, 62]. As they can condense into large membrane domains which promote transmembrane signalling, their generation upon cell activation is an important process [63]. This process is catalysed by the hydrolysis of sphingomyelin by sphingomyelinases and the self-association of ceramide molecules [64].

1.7 Neutral Sphingomyelinase 2

Sphingomyelinases (SMases) are central molecules in the sphingolipid metabolism because they hydrolyse sphingomyelin to ceramide and phospho-choline. Seven SMases are known in mammalian cells: a lysosomal acid SMase, a secreted acid SMase (ASM in the human, Asm in the murine system), an alkaline SMase and four neutral SMases (NSM in the human, Nsm in the murine system). They are differentially compartmentalised within the plasma membrane, lysosomes, the Golgi and the ER which allows a regulated synthesis of ceramide in these distinct localisations. Of the three NSMases the NSM1 locates to the ER and the nucleus, the NSM3 to the Golgi and the ER and the NSM2 to the inner leaflet of the plasma membrane and the Golgi. Recently, a mitochondria-associated NSM has been characterised which regulates mitochondrial sphingolipids and thereby impacts cellular viability [65].

The NSM2 is of major interest in this project (NSM will be used as an equivalent for NSM2 in the further thesis). It is a 71 kDa membrane-associated enzyme that is activated and shuttles between the Golgi and the PM in response to stimulation by, e.g., $\text{TNF}\alpha$, PMA or oxidative stress by H_2O_2 [66]. In T cells, NSM activity is also stimulated

upon CD95, CD40L or Fc γ receptor ligation, as well as CD3 or CD3/CD28 engagement, showing a role in T cell activation and turnover [59, 67]. Recent findings indicate that the generation of ceramides on the inner leaflet of the plasma membrane not only influences T cell activation but also the regulation of the cytoskeletal responses to extracellular stimuli [68, 69].

1.8 Visualisation of Lipids

Lipids are major components of the plasma membrane which is organised in two leaflets, forming a lipid bilayer into which proteins are inserted. These can specifically interact with certain lipids, but they are mainly organised due to the ionic and highly polar lipid head groups which turn towards the aqueous phase out of the membrane bilayer and the nonpolar tails which are embedded in the hydrophobic bilayer [70]. Furthermore, the lipids can be packed in higher or lower order domains. Domain definition and fluidity is often based on the composition of cholesterol and sphingolipids of a different fatty acid chain length and degree of saturation [71, 72].

Understanding the spatial distribution of lipids in the plasma membrane is important as it is crucial for the cell function. It is therefore of major interest to analyse the domain organisation and the distribution of single lipids in this complex environment which is highly sensitive to interference of specific lipid labelling with their native distribution.

Singer and Nicolson proposed the fluid mosaic model in 1971 where they postulated that lipids and proteins can move freely in a membrane bilayer by diffusion, and are organised randomly [70]. About ten years later this model was partially negated, and it was hypothesised that proteins interact with the cytoskeleton and are so constrained in their movement (“fencing”) [73]. Also lipids were thought to be laterally distributed non-homogenically and form organised domains that may have functional and structural roles [74]. These so called “lipid rafts” are enriched in cholesterol and sphingomyelin, and so differ from the surrounding membrane [75]. The localisation of GPI-anchored proteins in these detergent-insoluble membrane sheets supports this idea and addresses the membrane lipid organisation and its impact on protein movement [76]. Still, the analysis of lipids remains challenging; mostly rafts are analysed due to their resistance to solubilisation by the non-ionic detergent Triton X-100, their sensitivity to cholesterol depletion [77], or they are detected using cholera toxin B, which binds to ganglioside GM1 which is localised in lipid rafts [78].

Ceramide-enriched membrane platforms are different structures which form rapidly after stimulation-dependent sphingomyelinase activation and ceramide self-aggregation. They play roles in e.g. trimerisation of Fas for optimal function after activation [79] or CD95 clustering as one of many transmembrane receptors [80].

What both lipid membrane structures have in common is that the visualisation of lipids bears a major problem: Antibody staining may interfere with the lipids as they can cluster small lipids in the membrane. As fixation of membranes only crosslinks proteins, the lipids are still free to move in-between them, and so the bivalent antibodies can move lipids together creating clusters that are not naturally present in the cell. Therefore, the analysis of e.g. stimulation-induced lipid domains is not trivial with standard methods such as staining.

Recent advances in the development of the bio-orthogonal chemical reporter strategy, based on metabolic labelling and click chemistry, opens new opportunities in the field of membrane lipid research [81]. Erdmann et al. developed a trans-cyclooctene-containing ceramide lipid and a tetrazine-tagged near-IR dye allowing for live cell Golgi imaging [82]. Several similar lipid probes have been developed allowing the analysis of enzyme activity in the lipid metabolism, localisation of specific lipid moieties or lipid-protein interactions [83-85].

1.9 Function of Membrane Platforms

Ceramide-enriched membrane platforms are created upon sphingomyelinase activation following different aforementioned stimuli, such as co-stimulation and self-aggregation of ceramides by lateral sorting. These ceramide-enriched platforms are formed, and proteins are recruited there or excluded from there to allow for effective complex formation and signal induction [86, 87].

Another field where sphingomyelinases show to be of great importance is in vesicle fusion processes. The acid sphingomyelinase is an important regulator of wound repair in mammalian cells [88]. Upon membrane wounding and subsequent influx of extracellular calcium, lysosomes containing the ASM are translocated to the plasma membrane. Here they fuse and bring the ASM to the outer leaflet of the plasma membrane. The very abundant sphingomyelin is hydrolysed to ceramide, generating ceramide-rich platforms. Due to the tighter packing of ceramide these areas favour invagination and hence the endocytosis of the damaged membrane part [89]. The local increase in ceramide concentration by ASM activity is also necessary for microvesicle formation

at the plasma membrane. In glia cells treated with ATP, the ASM is translocated to the outer leaflet of the membrane and induces microvesicle budding [90].

The ASM is important for endocytosis, but not for exocytosis as shown for cytotoxic granule secretion in T cells. Upon ASM ablation, fusion of cytotoxic granules with the plasma membrane is still functional, only the content discharge seems to depend on ASM activity [91]. Also ROS-induced lysosome exocytosis is independent of ASM function [92].

Budding of exosomes from multivesicular endosomes also requires ceramide, but in this case generated by NSM activity at the inner leaflet of the membrane. The addition of ceramides or NSM activation enhances exosome shedding, the inhibition of the NSM with the specific inhibitor GW4869 results in less exosome release [93]. Crucial for exosome formation is the sorting of cargo by raft microdomains via lateral segregation within endosomal membranes, and here the NSM activity on the inner leaflet of the membrane is of importance [94].

Sphingolipid turnover has also been shown to be important for killing of ingested pathogens in macrophages [95, 96]. Sphingomyelin is abundant not only in the plasma membrane but also in the membranes of endo-lysosomal vesicles. Utermöhlen et al. demonstrated the importance of ASM function for phago-lysosomal fusion and hence the killing of ingested microbes. Upon ASM ablation both organelles only formed an insufficient pore and separated again without fusion and discharge of lysosome contents needed for pathogen killing [97].

1.10 Sphingolipid Enriched Domains in T Cell Activation

The interaction of defined lipid membrane domains and the cytoskeleton contribute to both, further lipid ordering and cytoskeletal dynamics (Figure 5). Several cytoskeletal components like actin, tubulin, vinculin or filamin can localise to lipid rafts and take part in the communication with the extracellular matrix by interacting with integrins, cadherins, occludins and other cellular adhesion molecules [98]. Additionally, it has been shown that within these domains cholesterol and sphingolipids are important for the clustering of the aforementioned cytoskeletal proteins and thereby contribute to cellular migration, cell growth, endothelial and epithelial barrier formation, and immune cell activation [99]. The enrichment of cholesterol and phospholipids into tightly packed membrane lipid rafts is essential for T cells to acquire a migratory phenotype and chemokine receptor clustering [100]. Reducing sphingomyelin and increasing

ceramide levels has shown to inhibit integrin adhesion and thereby cell motility, underscoring the role of sphingolipid metabolism and especially sphingomyelin activity for T cell motility and function [101].

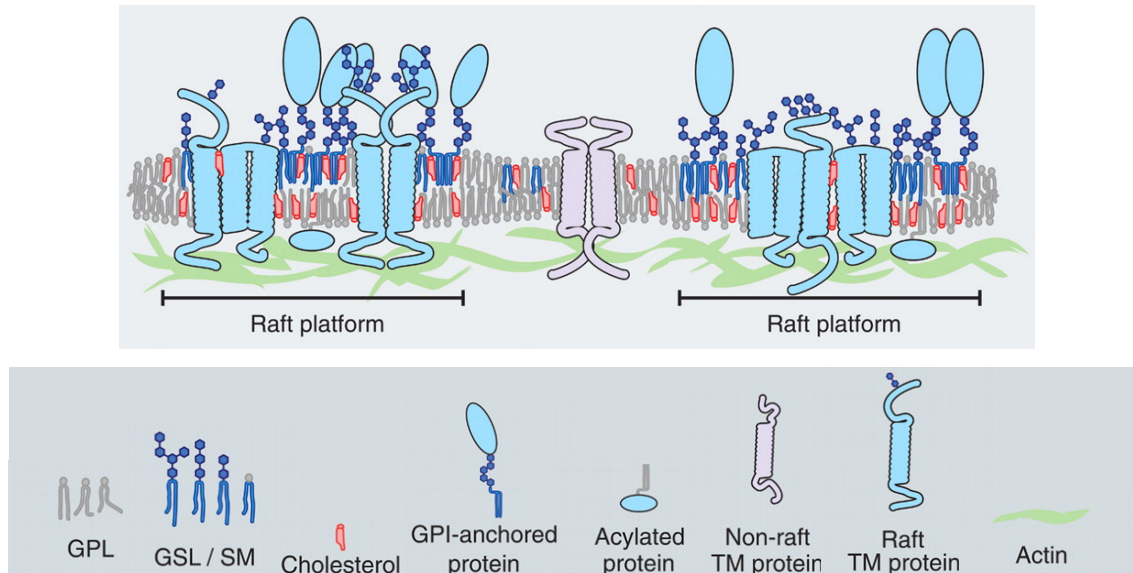


Figure 5: Organisation of lipid membrane domains. Adapted from Daniel Lingwood & Kai Simons, *Science*, 2010 [102]

A main factor for T cell motility are cytoskeletal dynamics, and it has been shown that ceramide accumulation, sphingomyelinase activity and actin remodelling are directly dependent. Measles virus contact with T cells induces local activation of sphingomyelinases and T cell paralysis, accompanied by a cytoskeletal collapse [103, 104]. Hence it is a suitable model to study the impact of ceramides overproduction on the cytoskeleton. NSM activation in physiological co-stimulation of primary T cells results in the generation of ceramide only in the lamellum, but is excluded from areas of high actin turnover, like the centre of the immune synapse [105]. When ceramide levels are increased following prolonged NSM activation (occurring in co-stimulated T cells after a measles virus exposure), a loss of cell spreading, hence cytoskeletal collapse, and tyrosine phosphorylation of proteins is observed. Upon NSM inhibition contrasting effects are observed: T cell hyper-responsiveness to a co-stimulus revealed by enhanced actin dynamics and an overshooting phosphorylation of signalling proteins [69].

1.11 Aim of the Thesis

Previous work of our group has established a role of sphingomyelinases in the regulation of T cell responses to TCR or pathogen stimulation, and this became particularly evident at the level of actin cytoskeletal dynamics. The formation of lipid membrane microdomains is crucial for receptor clustering and signal induction, and therefore, ceramide accumulation by membrane sphingomyelin breakdown is needed for signaling-complex-assembly. Pathogen-induced overshooting of SMase activation substantially impacted the formation of membrane protrusions, with T cell spreading as well as a front/rear polarisation upon CD3/CD28 co-stimulation [103]. On the other hand, NSM activation is part of the physiological TCR signal [67], indicating that a spatiotemporally balanced NSM activation is crucial for its physiological function. It involves actin cytoskeletal reorganisation and T cell polarisation. These two functions are also of central importance in directional T cell migration and motility in tissues.

This thesis aims on defining the role of NSM in compartmentalisation of the T cell membrane in polarisation and migration. Therefore, functional studies on the impact of NSM activity in these processes had to be complemented by the development of tools to study ceramide compartmentalisation in living T cells.

2 Materials

2.1 Cell Lines

Table 1: Cell lines

Cell line	Cell type	Species	Origin
CRISPR/Cas9 NSM KD Jurkat T cells	lymphoblast T cells	human	University Bern, Prof. Dr. Annette Draeger
HBMEC	brain microvascu- lar endothelial cells	human	Virology Würzburg
Jurkat	lymphoblast T cells	human	Virology Würzburg

2.2 Primary Cells

Primary cells were isolated from leukocyte reduction chambers supplied by the University Hospital of Würzburg, Institute for Transfusion Medicine and Haemotherapy (ethically approved, vote S. Schneider-Schaulies).

2.3 Mice

Table 2: Mice used in the project

Type	Origin
C57Bl/6.WT	Virology Würzburg
Thy1.1 congenic C57Bl/6	Virology Würzburg TVA Number: 55.2-2531.01-56/14

2.4 Media, Buffers and Solutions

Table 3: Chemicals and solutions

Chemical	Company or Recipe
3, 6 µm beads	Polysciences
Agarose, ultrapure	BioFroxx
ATP (10mM)	Thermo Fischer
ATV	136,89 M NaCl 5,36 M KCl 3,22 M D(+)-glucose 6,90 M NaHCO ₃ 0,05 % trypsin 0,54 M EDTA ad aqua dest., pH 7,4
BSA	Serva
C ₁₆ -ceramide	Avanti Polar Lipids
C ₆ -ceramide	Avanti Polar Lipids
CFSE labelling washing buffer	5% FCS in PBS
Chloroform	AppliChem
Collagen I High Concentration Rat Tail	Corning
Collagen type IV	Sigma-Aldrich
Complete, EDTA-free, Protease Inhibitor Cocktail	Roche
DMSO	AppliChem
dNTP Mix, 10 mM each	Thermo Scientific
Dynabeads Human T-Activator CD3/CD28	Invitrogen
Dynabeads M-450 Tosylactivated	Invitrogen
EDTA	Sigma-Aldrich
EGTA	Sigma-Aldrich
Endothelial Cell Growth Medium MV (Ready-to-use)	PromoCell
Ethanol	AppliChem

FACS buffer	PBS (w/o Ca ²⁺ /Mg ²⁺) 0,5 % (w/v) BSA 0,02 % (w/v) NaN ₃
FCS	Biochrome AG
First Strand cDNA Synthesis Kit	Fermentas
Fluo-4	Invitrogen
Formaldehyde 16 %	Electron Microscopy Science
Gel Red	Sigma-Aldrich
HBSS	Biowest
Heparin	Sigma-Aldrich
Histopaque-1077	Sigma-Aldrich
HMU-PC	Moscerdam Substrates
HMU-PC solution	1,35 mM HMU-PC 0,25 M Na-acetate 30 µM Na-taurochlorate ad aqua dest., pH 7,4 or 5,2
HPLC-grade water	AppliChem
Human Fibronectin	Prospec
Ingenio Solution	Mirus
Isopropanol	AppliChem
Lysis buffer	50 mM Tris-HCl 100 mM NaCl 1 mM DTT ad aqua dest., pH 7,4
MagniSort CD4 T cell isolation kit mouse	Affymetrix
MEM	Gibco
Methanol	AppliChem
Mounting media	Southern Biotech
Mouse T cell media	RPMI-1640 5 % FCS 10 % SSC 1 % Pen/Strep

Na ₂ SO ₄	AppliChem
NBD-C ₆ -ceramide	Avanti Polar Lipids
NSM Assay resuspension buffer	20 mM HEPES pH 7,4 15 mM MgCl ₂ 10 mM β-glycerolphosphate protease inhibitor cocktail ad aqua dest.
NSM/ASM Assay lysis buffer	20 mM HEPES pH 7,4 2 mM EDTA 5 mM EGTA 5 mM DTT 1 mM Na-orto-vanadate 10 mM β-glycerolphosphate protease inhibitor cocktail ad aqua dest.
NSM/ASM Assay stop buffer	0,2 M glycine 0,2 M NaOH 0,25 % Triton-X ad aqua dest., pH 11
NTE	0,1 M Tris 1 M NaCl 0,01 M EDTA ad aqua dest.
PBS	137 mM NaCl 2,7 mM KCl 10 mM Na ₂ HPO ₄ x H ₂ O 1,8 mM KH ₂ PO ₄ 1 mM CaCl ₂ x 2 H ₂ O 0,5 mM MgCl ₂ x 6 H ₂ O ad aqua dest.
PBS (w/o Ca ²⁺ , Mg ²⁺)	137 mM NaCl 2,7 mM KCl 10 mM Na ₂ HPO ₄ x H ₂ O 1,8 mM KH ₂ PO ₄

	ad aqua dest.
Penicillin/Streptomycin (100 i.e./mL)	Sigma-Aldrich
Phusion® High-Fidelity DNA Polymerase	New England Biolabs
Pluronic F-127, 20 % in DMSO	VWR International
Poly-L-Lysine	Sigma-Aldrich
Propidium Iodide	immunotools
Puromycin	Sigma-Aldrich
RPMI-1640	Gibco
Sphingomyelinase (Bacillus cereus)	Sigma-Aldrich
Staphylococcal Enterotoxin A/B	Sigma-Aldrich
TAE-buffer	25 mM Tris 0,57 % (v/v) acetic acid 0,6 M EDTA ad aqua dest., pH 8,0
Triton-X	Sigma-Aldrich
TRizol reagent	Invitrogen
Trypanblue	0,25 % (w/v) in PBS (w/o Ca ²⁺ /Mg ²⁺)
Ultrapure glycogen	Invitrogen
α -/ω-N ₃ -C ₁₆ -ceramide	Organic Chemistry, Würzburg
α -/ω-N ₃ -C ₆ -ceramide	Organic Chemistry, Würzburg

2.5 Plastic Materials

Table 4: Plastic materials

Material	Company
0,40 x 20 mm BL/LB cannula	Braun
1 mL syringe	Dispomed
12-well microscopy slide	ibidi
125, 75 25 cm ² cell culture flasks	Greiner Bio One
18-well angiogenesis slide	ibidi
6-, 12-, 24-well cell culture plates	Greiner Bio One
70 µM cell strainer	SPL Life Sciences
8-well live microscopy slide	ibidi
96-well flat bottom plate	Falcon
96-well flat bottom plate, black	Nunc
Cover glass for IF	Marienfeld-Superior
Cryo-tubes	Greiner Bio One
Electroporation cuvettes	VWR
FACS-tubes	Falcon
Leucocyte reduction chambers	University Hospital Würzburg
Nylon wool	Hartenstein
Petri dishes	Greiner Bio One
Pipette tips	Brand
Plastic pipettes (5, 10, 25 mL)	Sarstedt
Plastic tubes (50, 10 mL)	Greiner Bio One
PVC-tube	Rauclaire-e
Reaction tubes (0,5, 1,5, 2,0 mL)	Eppendorf
Syringe (60 mL)	Infuject
Syringe stamp	Infuject
Transwell 6,5 mm insert 3,0 µm membrane	Corning Incorporated
µ-Slide VI ^{0,4}	ibidi

2.6 Antibodies and Dyes

Table 5: Antibodies and dyes

Antigen/Target	Clone	Company	Dilution
Actistain 488		Cytoskeleton	1:100 (IF, FACS)
Alexa Fluor 488 α CD11a/CD18	m24	Biolegend	1:50 (FACS)
Alexa Fluor 647 α CD11a	HI111	Biolegend	1:100 (FACS)
Cell proliferation dye eFluor 670		Affymetrix	5 μ M
CFSE		eBioscience	5 μ M
Click-IT Alexa Fluor 488 DIBO Alkyne		Life technologies	1:200 (IF)
DBCO-Sulfo-Cy5		Jena Bioscience	1:200 (IF)
IF 2 nd antibodies Alexa 568 goat- α -rabbit Alexa 488 goat- α -mouse Alexa 568 goat- α -mouse		Life technologies	1:100 1:100 1:100
NBD-C ₆ -ceramide		Life Technologies	1:1000 (IF)
Viability Dye (APC Cy7)		Thermo Fischer	1:150 (FACS)
α CD11a (LFA-1)	MEM-83	Thermo Scientific	
α CD28	CD28.2	Beckton-Dickinson Biosciences Pharmingen	1:1000
α CD3	UCHT-1	Beckton-Dickinson Biosciences Pharmingen	1:1000
α CD3-PE		immunotools	1:100 (FACS)
α CD4-APC		immunotools	1:100 (FACS)
α CD4V421 (Brilliant Violet)		BD Bioscience	1:300 (FACS)
α CD69-PE		Immunotools	1:100 (FACS)

α Cdc42		Santa Cruz Bio- tech	1:100 (IF)
α CXCR4		Abcam	1:100 (IF, FACS)
α CXCR4-APC		BioLegend	1:100 (FACS)
α LFA-1 α -chain, active conformation	NKI-L16	Gift from IMJ Reinieren-Beeren, Nijmegen	
α pERM		Cell Signalling	1:100 (IF)
α Thy1.1-PE		eBioscience	1:2000 (FACS)

2.7 Chemokines, Cytokines, Inhibitors

Table 6: Small active molecules

Chemical	Company
Amitriptyline	Sigma-Aldrich
CCL19	immunotools
CCL21	immunotools
CCL4	immunotools
CXCL10	immunotools
ES048	Gift from Christoph Arenz
GM-CSF	Berlex
GW4869	Sigma Aldrich
IL4	Milteny Biotec
INF γ	Milteny Biotec
Ionomycin	Sigma-Aldrich
LPS	Sigma-Aldrich
PMA	Sigma-Aldrich
SDF-1 α (CXCL12)	ReproTech
TNF α	Milteny Biotec

2.8 Equipment

Table 7: Equipment

Equipment	Company
Accu-jet pro	Brand
Agarose-Gel Chamber	Virology, University Würzburg
Centrifuge Mikro 200	Hettich
Centrifuge Rotanta 460 R	Hettich
Confocal microscope LSM 780	Zeiss
FACS LSR II	Becton Dickinson
FACScan Calibur	Becton Dickinson
Fluorescent microscope DMI8	Leica
Heating block	Liebisch
Incubator 37 °C, 5 % CO ₂	Heraeus
Laminar work flow	Gelman
Microliter pipettes	Brand, Eppendorf
Millicell-ERS	Millipore
Millifuge	Millipore
PCR cycler	ML Research
Safire2 – Fluorescence plate reader	Tecan
Shaker platform WS5	Edmund Bühler
Ultra-Centrifuge	Thermo Scientific
Vortex Mixer	Neo Lab
Water bath	Kotterman

3 Methods

3.1 Cell Culture

3.1.1 Cell Lines

All cells are cultured in plastic flasks suitable for cell culture with filter lids in a humidified incubator at a temperature of 37 °C and a 5 % CO₂ atmosphere. Jurkat T cells are cultured in RPMI 1640 media supplemented with 10 % heat inactivated fetal calf serum (FCS). For heat inactivation the serum is heated to 56 °C for 1 h. Cells are sub-cultured every 2 to 3 days at a ratio of 1:3 to maintain a density between 1*10⁵ and 1*10⁶ viable cells per mL. In case of CRISPR/Cas9 NSM KD Jurkat T cells 1 µg/mL puromycin is added to the cell culture media for selection of CRISPR/Cas9 expressing cells.

HBMEC cells are cultured in endothelial cell growth medium MV containing the following ingredients:

Fetal calf serum	0.05 mL/mL
Endothelial cell growth supplement	0.004 mL/mL
recombinant human epidermal growth factor	10 ng/mL
Heparin	90 µg/mL
Hydrocortisone	1 µg/mL

Cells are cultured until confluence, detached with ATV for about 5 min, and 1/5 is seeded then into a fresh flask.

3.1.2 Cryoconservation

For long-term storage, 1*10⁷ cells are centrifuged (5 min, 280 x g, RT) and the pellet is resuspended in 1 mL FCS/10 % DMSO, before cooling it to -80 °C over night. After freezing, cells are stored at -140 °C. For thawing, normal cell culture media is heated to 37 °C, frozen cells are quickly thawed and diluted in 10 mL of the medium. The medium is changed after 24 h to minimise cellular stress.

3.1.3 Isolation of Primary Human T Cells and DCs

Peripheral blood monocyte cells (PBMC) from healthy donors from leucocyte reduction chambers are used for T cell and DCs isolation. First the blood is diluted with PBS 1:2 (final volume about 50 mL) and layered on to Histopaque (25 mL blood to 7 mL Histopaque). During density gradient centrifugation (30 min, 160 x g, RT) cells separate according to their density, and the layer of PBMCs can be extracted from the gradient.

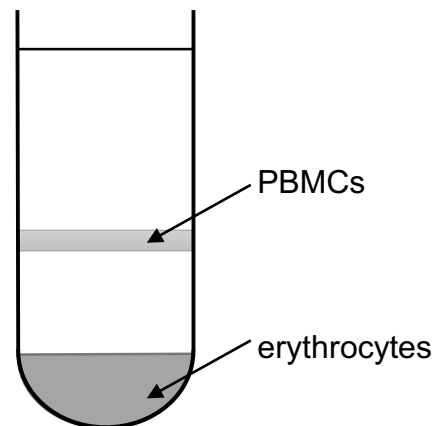


Figure 6: Layer distribution after density gradient centrifugation.

The cells are washed three times with PBS and resuspended in RPMI/10 % FCS to a density of 5×10^6 cells/mL.

Monocytic cells are isolated by plastic adherence. The cell suspension is transferred into 75 cm² cell culture flasks and incubated for 2 h at 37 °C in the incubator. During this time monocytic cells attach to the plastic, while T or B cells do not. Fresh cell culture medium is added to the adherent monocytes and they are left in the incubator o.n. for generation of moDCs.

Monocytes are differentiated into immature dendritic cells by culture in RPMI supplemented with 10 % FCS and human GM-CSF (500 U/mL) and IL-4 (250 U/mL) for four days, while adding fresh cytokines every 48 h. These immature DCs are matured by addition of LPS to the cell culture medium over night.

The non-adherent fraction of the PBMCs (PBLs) are used as a source for primary human T cells. T cells can be enriched by nylon wool column purification. B cells show a higher affinity for nylon wool than T cells at the right temperature and FCS concentrations. For preparation of the columns, 1,5 g of nylon wool are put into 50 mL syringes and autoclaved. A plastic hose is attached to the opening of the syringe and a metal clamp is used to control the flow.

Prior to the loading of the cells, the column is equilibrated with 30 mL warm RPMI supplemented with 5 % FCS. The medium is allowed to flow through the column, afterwards fresh RPMI/5 % FCS is added until the nylon wool is fully submerged. Then $1,5 \cdot 10^8$ PBLs are added in 7 mL RPMI/5 % FCS. RPMI/5 % FCS is added to fully cover the wool with media. The column with the cells is incubated at 37 °C for 45 min. The cells are allowed to slowly drop out of the column and the wool is washed with 25 mL RPMI/5 % FCS. The flow through is the population enriched in T cells, which are centrifuged and resuspended in RPMI/10 % FCS at a concentration of $4 \cdot 10^6$ T cells per mL for culturing.

To estimate the purity of the T cells after isolation, these are stained with α CD3 and α CD4 antibodies for 15 min on ice, washed twice and analysed by FACS. CD3 and CD4 positive cells are T cells and the frequencies are added and compared to frequencies before T cell isolation. About 80 to 90 % purity is achieved by the nylon wool purification.

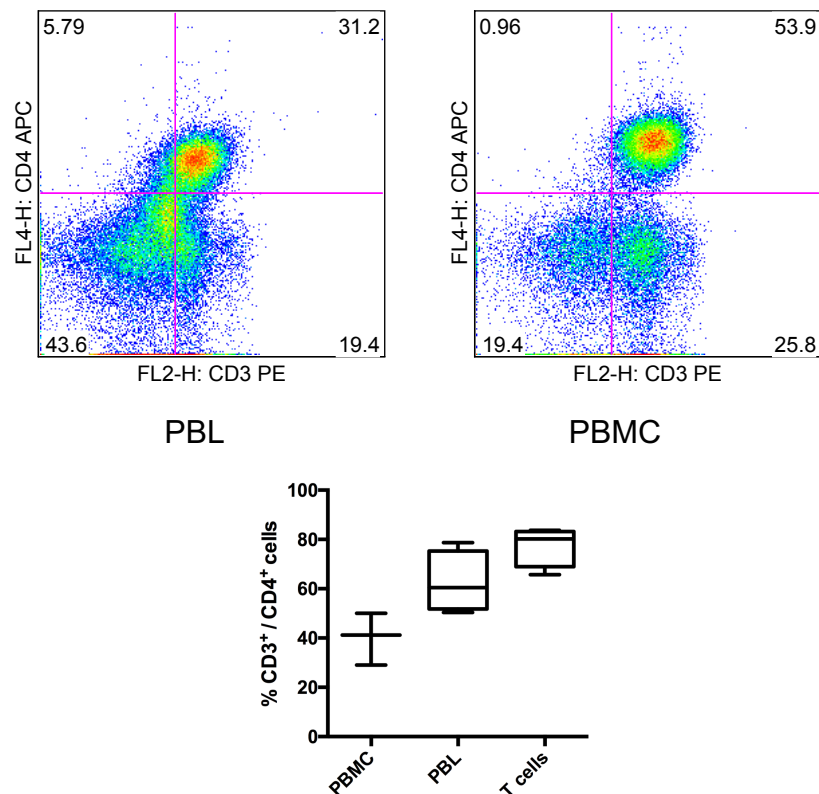


Figure 7: CD3⁺ and CD4⁺ cells among blood cells before and after the two purification steps (plastic and nylon wool adhesion).

3.2 T Cell Transfection and Inhibitor Treatment

For genetic ablation of the NSM, primary T cells are transfected with siRNA targeting the NSM gene. The following siRNAs are used:

nSMase2 sense: 5'-UGCUACUGGCUGGUGGACC-3'

nSMase2 anti-sense: 5'-GGCUCCACCAGCCAGUAGCA-3'

For transfection 8×10^6 to 1×10^7 cells are taken up in 100 μ L transfection medium and 100 pM siRNA are added. The cells are transferred into a fresh electroporation cuvette and electroporated with Amaxa pre-installed program U-014. After electroporation, cells are transferred into 3 mL pre-warmed RPMI/10 % FCS in a 12-well plate. Electroporation is repeated twice on day 1 and 3, maximum gene knock-down is achieved on day 5. Knock down is validated via PCR or NSM assay.

Various inhibitors are used for cell manipulation; concentrations for cell viability and sufficient inhibition have been optimised in the laboratory:

Table 8: Inhibitors for T cell treatment

Target enzyme	NSM	NSM	ASM
Inhibitor	GW4869	ES048	Amitriptyline
Concentration	1,5 μ M	1,5 - 3 μ M	10 μ M

3.3 NSM/ASM Assay

To measure the NSM or ASM enzyme activity, a substrate is used that is converted by both enzymes to a reaction product which emits detectable fluorescent light.

3×10^5 to 5×10^5 Jurkat or primary T cells are pelleted and resuspended in 40 μ L lysis buffer, the suspension is placed at -80 °C for 2 min and then thawed in the 37 °C water bath again for 2 min. This freeze/thaw procedure is repeated five times to ensure complete cell lysis. Afterwards, the cell debris is removed by centrifugation for 1 min at $3400 \times g$. The following mix is prepared for triplicates per sample plus one background measurement:

For NSM Assay:

Resuspension buffer	10 μ L
HMU-PC (pH 7,4)	10 μ L
ATP (10 mM)	2,2 μ L

For ASM Assay:

Lysis buffer	10 μ L
HMU-PC (pH 5,2)	10 μ L
EDTA (30 mM)	1,3 μ L

10 μ L sample are added to the mix in 0,5 mL tubes; for background measurement only lysis buffer is added. The samples are placed at 37 °C o.n., and the reaction is then stopped by addition of 100 μ L stop buffer. Samples are transferred to a black flat bottom 96-well plate, and fluorescence is measured in the fluorescence reader. For data analysis the background value is subtracted from the sample values.

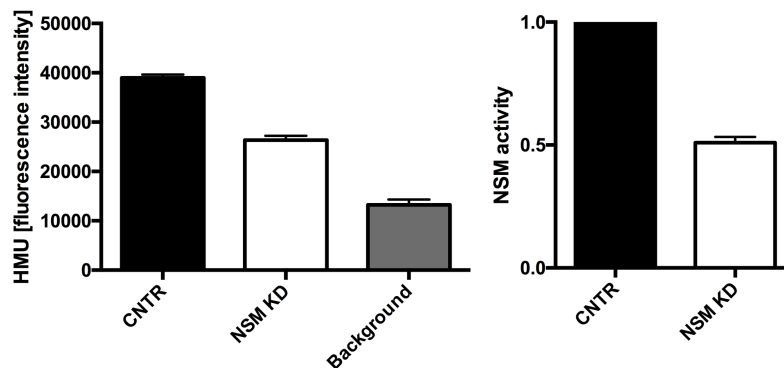


Figure 8: NSM Assay. The left graph shows the HMU fluorescence signal. The right graph shows the relative NSM activity calculated from the HMU signal after background subtraction.

3.4 RNA Isolation, cDNA Transcription and PCR

Genetic knockdown efficiency can be measured at mRNA level by isolating RNA from T cells, transcribing it into cDNA, followed by a PCR with NSM-specific primers. $5 \cdot 10^5$ primary T cells are pelleted and resuspended in 1 mL TRIzol. Samples are incubated at RT for 5 min for cell lysis. After the incubation 200 μ L chloroform are added and the samples are gently mixed for 15 secs before incubation at RT for 3 min. To induce the separation of molecules, the samples are centrifuged for 15 min at 15000 x g at 4 °C. Proteins will move to the lower organic (chloroform) phase, RNA to the upper aqueous phase, and DNA accumulates at the interphase. The upper phase is transferred to a

fresh tube. 10 µg RNase-free glycogen as well as 500 µL isopropanol are added, mixed and centrifuged for 10 min at 15000 x g at 4 °C. The supernatant is removed, and the RNA is washed with 1 mL 75 % ethanol. After centrifugation for 5 min at 9500 x g at 4 °C, the ethanol is removed, the RNA pellet is dissolved in 25 µL HPLC water for 10 min at 55 °C. The RNA content is determined, and 1 to 5 µg are used for cDNA synthesis.

cDNA synthesis is started using oligo(dT)₁₈ primers provided in the First Strand cDNA Synthesis Kit according to the manufacturer's instructions.

For the PCR reaction the cDNA is used undiluted and at a dilution of 1:100 to estimate the knockdown efficiency. The following mix is prepared in a 0,5 µL tube for the PCR reaction:

5x Phusion HF buffer	4 µL	
dNTPs	10 mM	(0,4 µL)
forward primer	10 µM	(1 µL)
reverse primer	10 µM	(1 µL)
DMSO	0,6 µL	
Phusion polymerase	0,2 µL	
cDNA	2 µL	
nuclease-free water	ad 20 µL	

Primers used are:

NSM forward primer: GCAGCTTCAAGTGTCTCAACAG

NSM reverse primer: GTAGTGGGTGAACAGGGAGTGT

PCR is performed with the following program:

Initial denaturation:	60''	98 °C
Primer annealing:	30''	60 °C
<u>Elongation:</u>	<u>30''</u>	<u>72 °C</u>
35 cycles of:	30''	98 °C
	30''	60 °C
	<u>30''</u>	<u>72 °C</u>
Final elongation:	10'	72 °C
Storing:	∞	4 °C

To analyse the PCR product 4 µL of the sample is mixed with 2 µL Gel Red and the samples are applied to a 2 % agarose/TAE gel. The DNA bands are detected under UV light.

3.5 General Analysis

3.5.1 Confocal Microscopy

Imaging is performed with the confocal laser scanning microscope LSM 780 from Zeiss, which is equipped with an incubation system and a 403 Plan-Apochromat oil objective (NA 1.4). Fluorescence dyes are excited with laser lines of 488 nm and 633 nm. For live cell imaging, cells are kept in normal cell culture medium and transferred into ibidi slides appropriate for live cell imaging.

3.5.2 Flow Cytometry

For flow cytometry, cells are introduced into a laminar flow in which they are singularised and pass a laser which allows detection of the size (FSC, forward scatter), granularity (SSC, sideward scatter) and fluorescent labelling. Different fluorescent labels and their intensities are measured and allow the characterisation of different subpopulations in a mixture of cells. For this purpose, cells are either labelled by antibodies linked to fluorescent dyes, dyes are incorporated into cells, or cells are labelled by click-chemistry. All measurements are performed with a FACScan Calibur or LSR II, and for data analysis either CellQuestPro or FlowJo 8.5.3. software are used.

3.6 Click Chemistry

3.6.1 Dye Testing for Click Labelling

To select suitable dyes which are unable to diffuse into intact living cells, 1×10^5 Jurkat or primary T cells are incubated with different clickable dyes (25 μM in RPMI) for 30 min at 37 °C and then washed three times with PBS. Dye uptake is analysed by confocal microscopy.

3.6.2 Click Labelling

For labelling 2×10^5 Jurkat T cells or primary T cells are washed and resuspended in HBSS. Clickable ceramides ($\text{N}_3\text{-C}_6\text{-ceramide}$, $\text{N}_3\text{-C}_{16}\text{-ceramide}$ (alpha and omega)) and NBD- $\text{C}_6\text{-ceramide}$ are used at concentrations from 5 to 25 μM and incubated with the cells for 30 min at RT. After feeding, the cells are washed with HBSS or PBS twice and resuspended in the staining solution. The staining solution containing 20 μM Click-IT Alexa Fluor 488 DIBO Alkyne (DIBO 488) or DBCO-Sulfo-Cy5 in HBSS is added for 5 to 10 min at RT. After the click reaction, the cells are washed three to four times with 700 μL HBSS before resuspending the cells in HBSS and keeping them at RT until microscopic analysis.

For primary T cells the feeding buffer may be supplemented with 0,25 % pluronic F-127 to enhance the solubility of the lipids in the buffer and enhance uptake rates. $\text{N}_3\text{-C}_{16}\text{-ceramide}$ is fed over night at 37 °C, as the incorporation rate is very low after 30 min.

3.6.3 Bacterial Sphingomyelinase Treatment

To increase the amount of ceramide at the cell surface, T cells are treated with bacterial sphingomyelinase (2000 U/mL) in standard cell culture medium for 30 min at 37 °C.

3.6.4 T Cell Stimulation for N₃-cer Uptake

T cell stimulation prior to feeding of clickable lipids increases their uptake rate. For high density stimulation, primary T cells are kept at 8×10^6 cells per well of a 12-well plate for 3 to 4 days [106]. Alternatively, cells are activated using 1 $\mu\text{g/ml}$ mouse- αCD3 and/or αCD28 antibodies cross-ligated with goat- α -mouse in solution or addition of T cell stimulatory dynabeads (coated with $\alpha\text{CD3}/\alpha\text{CD28}$ antibodies) at a dilution of 1:1000 for 30 min.

3.6.5 Dynabead/T Cell Contacts

T cells are fed and clicked as described before and then contacted with dynabeads. For this purpose, ibidi-slides are prepared by coating with Poly-L-lysine (1:10 in PBS) for 10 min at 37 °C, followed by three times washing with PBS and air-drying of the slides. 2×10^5 clicked T cells are mixed with 5 μL dynabeads and co-incubated in a 1,5 mL tube for 10 min. Then the cells with beads are transferred to the PLL-coated slides and allowed to settle for 5 min at 37 °C before microscopic analysis.

3.6.6 DC/T Cell Contacts

T cells are prepared as described before and thoroughly washed to remove any free dye which could be taken up by the DCs. To optimise DC/T cell contact formation, DCs are loaded with 1 $\mu\text{g/mL}$ SEA and SEB for 15 min at 37 °C. Then they are added to a well of a PLL-coated 8-well ibidi slide suitable for live cell microscopy and allowed to adhere for 15 min at 37 °C. 2×10^5 clicked T cells are added to the DCs, and conjugates are allowed to form for 15 min at 37 °C before live cell microscopy.

3.6.7 Co-Stimulation on Planar Surfaces

T cells are fed with the clickable ceramide as described before, but 50 μL RPMI with 10 % FCS is used instead of HBSS, cells are then transferred to ice for 15 min. Next, stimulatory antibodies are added (αCD3 , αCD28 or both), and the mixture is left on ice for further 15 min to allow antibody binding without stimulation of the cells. The cells are then transferred onto slides pre-coated with 10 $\mu\text{g/ml}$ goat- α -mouse IgG and incubated at 37 °C for 10 min before addition of the clickable dye for additional 5 min to the medium (2 times concentrated, 50 μL per well). Afterwards, the medium is removed,

and the cells are washed four times with 200 μ L HBSS. Finally, 100 μ L RPMI/10 % FCS are added, and the cells are microscopically analysed for ceramide clusters.

3.6.8 Cell Preparation for Lipidomics

Jurkat or primary T cells are fed with the clickable lipids as described and subsequently washed three times. After complete removal of the washing buffer, the cell pellet is dissolved in 500 μ L methanol and stored at -80 °C until analysis (performed by Dr. Lukasz Japtok (Potsdam University)). As standards for measurements, the feeding solution (25 μ M in HBSS) and 25 μ M lipid in methanol are prepared.

3.6.9 Live/Dead Staining

To estimate compound toxicity, cells are analysed by propidium iodide (PI) staining with a PI staining solution (1:20 in PBS) for 5 min on ice followed by two washing steps and immediate FACS analysis. PI is only incorporated into dead cells with porous cell membrane, while it is excluded from living cells.

3.6.10 Ca²⁺ Flux Measurement

For detection of Ca²⁺ mobilisation, primary T cells are washed in 70 μ L PBS. 500 μ L Hanks Hepes buffer free of calcium and magnesium ions are added, re-centrifuged, and cell are resuspended in the same buffer with 1 μ M Fluo-4. After incubation for 30 min at 37 °C, cells are washed and resuspended in the same buffer without Fluo-4 and kept at 37 °C for another 30 min for complete de-esterification of the intracellular amino acid esters. After pelleting, cells are resuspended in 300 μ L HBSS containing calcium and magnesium ions. The solution is split into two FACS tubes and measured to estimate the background signal. As a positive control 2,5 mM ionomycin is added, and samples are immediately measured to see the maximal cellular response. For co-stimulation 20 μ g/mL α CD3 and α CD28 antibodies are mixed with a goat- α -mouse antibody for 10 min at RT. This antibody mix is added to the T cells, and the Ca²⁺ response is measured for about 5 to 8 min.

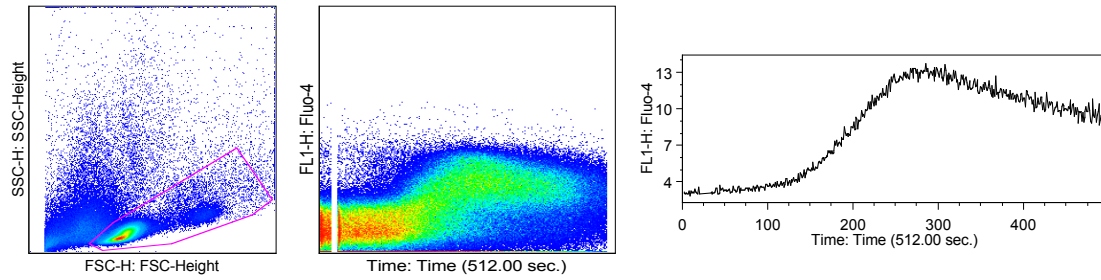


Figure 9: Ca^{2+} flux measurement via flow cytometry. FSC/SSC distribution of cells and the live-gate of T cells (left). Fluo-4 signal of single T cells after antibody addition (middle) and average Fluo-4 signal for the T cell population (right).

3.6.11 CD69 Surface Staining

T cells are treated with ceramides as before and then stimulated with PMA/ionomycin or αCD3 and αCD28 for 20 min to over night. Further sample treatment includes fixation with 4 % FA in PBS for 10 min, permeabilisation with 0,1 % Triton-X in PBS for 5 min and staining with 1:100 αCD69 for 1 h on ice. Measurement is performed by flow cytometry.

3.7 Bead/T Cell Contacts

Beads of 1, 3 or 6 μm diameter are coated with αCD3 and αCD28 antibodies according to the manufacturer's instructions and coating efficiency is estimated by microscopic analysis after staining with an $\alpha\text{-mouse-Alexa 488}$ antibody.

For analysis $5 \cdot 10^5$ cells are used per sample. Beads of different sizes are added to the cells at the following ratios:

3 μm 1:10

6 μm 1:2

Beads and cells are incubated in 1,5 μL tubes in 50 μL 0,5 % BSA/RPMI per $5 \cdot 10^5$ cells for 15 to 60 min at 37 $^\circ\text{C}$. The reaction is stopped by placing the tubes onto ice and analysed either directly by flow cytometry or fixed with 4 % FA for 15 min on ice. For analysis a forward/sideward scatter measurement is used, as beads, cells and cells contacted with beads separate according to size and granularity.

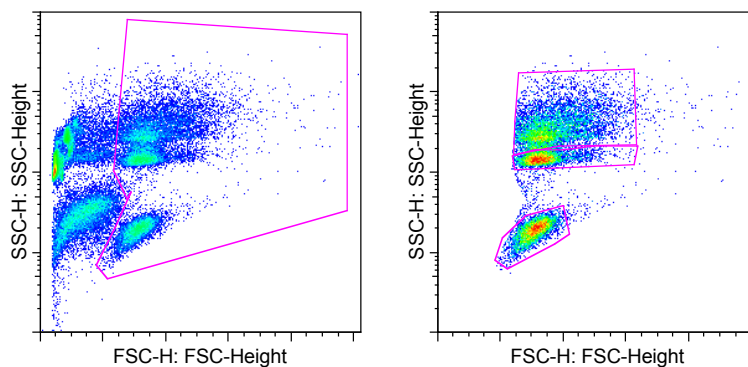


Figure 10: T cell/bead contacts. Left image shows FSC/SSC of ungated cells, right image is gated on living cells and cell/bead contacts. The lower gate includes single cells, the upper gates cells in contact with one or several beads.

3.8 T Cell Migration

3.8.1 2D Migration on Collagen

To analyse their directional movement and speed, living T cells moving on a coated surface are imaged for 90 min. For the 2D migration, the channel of a μ -Slide VI^{0.4} is coated with collagen in PBS for 10 min at 37 °C and washed three times with PBS. $5 \cdot 10^5$ T cells in 50 μ L RPMI/0,5 % BSA and 50 μ L RPMI/0,5 % BSA with 100 ng/mL SDF-1 α are pipetted into the two channels at the same time to create a gradient in the channel. The slide is kept at 37 °C for 15 min for cell attachment before imaging. For imaging the microscope's incubator is pre-heated to 37 °C, images are taken every 45 secs for 90 min.

3.8.2 3D Migration in a Collagen Matrix

To analyse the behaviour of T cells in 3D environments, T cells are embedded in a collagen matrix, a chemokine gradient is established and cells are imaged live for 90 min as before. Rat tail collagen type I polymerises at a neutral pH and 37°C. It is mixed with 10x minimal essential medium, 7 % bicarbonate and the cells in RPMI/10 % FCS in the following amounts to generate a 3,3 mg/mL meshwork:

Bicarbonate	8,5 μ L
MEM	7,5 μ L
Collagen	60 μ L
$1 \cdot 10^6$ T cells in media	75 μ L

To generate matrices with other densities the amount of collagen and the other components have to be adapted accordingly. The first three components are mixed on ice to prevent a premature polymerisation. After addition of the cells, the suspension is incubated at 37 °C for 1 min in the tube and then transferred into the μ -Slide VI^{0.4} where collagen is allowed to polymerise for 20 min at 37 °C, before addition of the chemokine solution (50 μ L with 100 ng/mL SDF-1 α) to one side of the channel and RPMI to the other side. The chemokine quickly diffuses into the gel, so imaging is started after further 20 min of incubation. Manual cell tracking for 2D and 3D migration experiments is

performed with the Fiji plug-in “Manual Tracking” and the following analysis of migration speed, directionality, forward migration index in y-direction (yFMI) and centre of mass displacement in y-direction (yCoM) with the Fiji plug-in “Chemotaxis tool”.

3.8.3 Polarisation on Planar Surfaces

Polarisation of T cells on solid supports can be monitored by an increase of F-actin content or by re-localisation of receptors or other molecules towards the front or the rear of the cell. For the latter, 8-well ibidi slides are coated with fibronectin or collagen (both as described before), and $5 \cdot 10^5$ T cells in 100 μ L RPMI/0,5 % BSA with 100 ng/mL SDF-1 α are added to the wells. For polarisation, the slides are incubated for 30 min at 37 °C. The reaction is stopped, and the cells are fixed by removal of 50 μ L of the medium and addition of 200 μ L 4 % FA. After 15 min, the liquid is removed, the cells are carefully washed three times with PBS before addition of ice cold 0,5 % Triton-X for permeabilisation for 5 min. The cells are washed as before, and unspecific binding sites are blocked with 5 % BSA/PBS for 30 min at RT. For staining, antibodies or phalloidin are added in 1 % BSA/PBS. Staining is performed o.n. at 4 °C, washing is repeated as before, and suitable secondary antibodies are added for 1 h at RT. After final washing, the slides are dried and mounted under coverslips.

The increasing amount of F-actin in polarising cells can be analysed by flow cytometry. $5 \cdot 10^5$ T cells in 50 μ L RPMI/0,5 % BSA are incubated with 100 ng/mL SDF-1 α for different time frames. The reaction is stopped by cell pelleting at 3400 x g for 1 min, removal of the supernatant and addition of 4 % cold FA. After incubation for 15 min on ice, the cells are permeabilised and stained with phalloidin on ice. Finally, the cells are resuspended in 50 μ L FACS buffer for measurement.

3.8.4 Adhesion Assay on HBMECs

To analyse how T cells interact with the endothelium, HBMECs are at “resting” or “inflamed” conditions. For the latter, $3,3 \times 10^4$ HBMECs are seeded into each well of a flat bottom 96-well plate, left o.n. or until confluency, and are then treated with 100 U/mL $\text{TNF}\alpha$ and 500 U/mL $\text{IFN}\gamma$ o.n. to create an inflamed phenotype. Figure 11 shows the upregulation of ICAM-1 upon HBMEC stimulation.

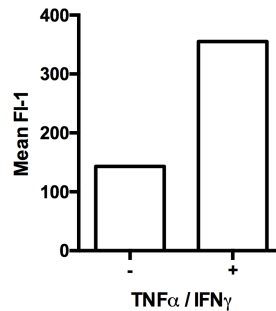


Figure 11: ICAM-1 expression on HBMECs stimulated with $\text{TNF}\alpha$ and $\text{IFN}\gamma$. Graph shows mean fluorescence intensity after o.n. stimulation.

T cells are labelled by addition of 2,5 μM CFSE for 5 min, followed by washing three times and addition to the HBMEC cell layer. After a 30 min attachment period, the wells are washed two times with 100 μL PBS to remove non-adherent T cells. 100 μL lysis buffer are added to each well and incubated for 30 min at 37 $^{\circ}\text{C}$. Before measurement, the lysis buffer with the cells is mixed by pipetting several times, and the fluorescence is measured with the plate reader.

3.8.5 T Cell Polarisation on HBMECs

To analyse T cell polarisation on an endothelial cell layer, 1×10^5 HBMECs are seeded into 8-well ibidi slides and grown to confluency. 5×10^5 CFSE labelled T cells are added to each well and allowed to adhere for 30 min. The cells are fixed with 4 % FA and mounted under a cover slip as described before. Images are taken and the shape of the T cells is analysed with the Fiji plug in “particle analysis”. The circularity of the cells is taken as a marker. Values close to “1” resemble a perfect circle, whereas values closer to “0” are less circular. Polarised cells have lower roundness values than unpolished ones.

3.8.6 Transendothelial Migration

For this assay HBMECs are seeded onto membranes of filter inserts. $3,3 \cdot 10^4$ HBMECs are seeded in each insert and allowed to grow for one week to allow formation of a dense monolayer whose density can be determined by measuring the electrical resistance, the TEER value. For transmigration $1 \cdot 10^6$ T cells are added per insert and allowed to migrate towards SDF-1 α as before. Transmigrated cells are counted manually or with counting beads. For quantification of adhering T cells, the insert is washed twice to remove non-adherent T cells, before addition of 30 μ L APS to detach the HBMECs and incubation for 5 min at 37 °C. The reaction is stopped with 70 μ L RPMI/10 % FCS, and the cells are counted by flow cytometry with counting beads. T cells can be distinguished from HBMECs by their smaller size.

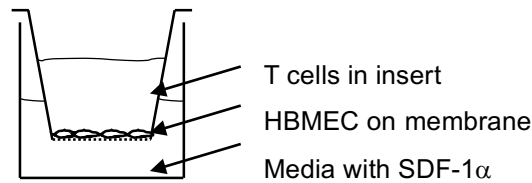


Figure 12: Setup of transendothelial migration assay with HBMECs seeded into filter insert and T cells.

3.9 Isolation of Murine CD4⁺ T Cells and Homing Assays

3.9.1 Mouse Section

For isolation of the lymph nodes and spleen, mice are fixed in a supine position, and the skin is opened without opening the abdominal cavity to allow access to the inguinal, axillary, brachial and cervical lymph nodes. Then the abdominal cavity is opened along the linea alba, and the mesenteric lymph nodes and the spleen are isolated. The organs are kept on ice in HBSS/BSA until preparation of a single cell suspension by grinding them through a 70 µm cell strainer. When blood needs to be taken, the heart is punctured with a cannula, and blood is drained with a syringe.

3.9.2 Lysis of Erythrocytes by Hypoosmotic Shock

Spleenocytes contain large amounts of erythrocytes; to lyse those cells and thereby enrich lymphocytes, the cell suspension is transferred into a 50 mL tube, and the cells are pelleted by centrifugation (280 x g, 5 min, 4 °C). The cells are resuspended in 3 mL ddH₂O by brief vortexing, and immediately supplemented with 3 mL 1,8 % NaCl to prevent lymphocyte lysis. Cell debris is allowed to sediment for 5 min on ice, the supernatant is transferred into a fresh tube and centrifuged as before to recover the lymphocytes.

3.9.3 CD4⁺ T Cell Isolation

CD4⁺ T cells are isolated by negative selection with the MagniSort Negative Selection Protocol III from Affymetrix according to the manufacturer's instructions. Briefly, lymphocytes are counted and taken up in HBSS/BSA at a concentration of 1×10^7 cells/100 µL. 10 µL enrichment antibody cocktail are added per 100 µL of cells and incubated at RT for 10 min. The cells are washed once, before addition of 5 µL negative selection beads per 100 µL. Cells and beads are mixed, incubated for 5 min at RT and placed in a magnet. After further 5 min, the supernatant is poured into a tube, these are the enriched CD4⁺ T cells, and the cells sticking to the tube's wall are discarded. The T cells are counted, treated for following experiments and left o.n. at a concentration of 2×10^6 T cells/mL in a 24-well plate, before using them for migration experiments. Migration experiments are performed as described above for human T cells.

3.9.4 In Vivo Homing

Lymphocytes from Thy1.1 congenic donor mice are isolated and pooled prior to CD4⁺ T cell isolation. CD4⁺ T cells are separated into two parts which are either marked with eFluor 670 or CFSE. For labelling, the cells are washed with PBS to remove any protein from the medium, and incubated with 5 μ M eFluor 670 or CFSE for 10 min at RT. Then medium with 10 % FCS is added and the cells are incubated for 5 min on ice before washing away access dye three times with PBS/10 % FCS. The eFluor 670 labelled cells are incubated with the NSM inhibitor ES048 (1,5 μ M for 2 h or o.n.) at a concentration of 2×10^6 cells/mL in a 12-well plate. Before transfer, the CD4⁺ T cells are washed to remove any inhibitor, and the two individually labelled and treated cell suspensions are mixed at a 1:1 ratio. For transfer 1×10^7 cells are taken up in 200 μ L PBS and injected into the tail vein of WT mice. The acceptor mice are sacrificed after different time frames (1h or 16 h), and lymph nodes, spleen and blood (for 1 h time point) are isolated. For splenocytes the erythrocytes are lysed, and $1,2 \times 10^7$ lymphocytes from spleen or 6×10^6 lymphocytes from lymph nodes and blood are stained for FACS analysis. Antibodies are diluted in FACS buffer, and the cells are stained in 190 μ L staining solution for spleen and 95 μ L for lymph node and blood for 15 min on ice. The cells are washed once and kept on ice until analysis. To lyse the erythrocytes in the blood before analysis, the stained and washed cells are pelleted, resuspended in 100 μ L Fix/Perm Solution and incubated at RT for 30 min. The cells are then washed with PBS and taken up in FACS buffer for analysis.

3.10 Statistical Analysis

All data is analysed and statistically evaluated with Prism 6. Data sets are analysed for Gaussian distribution with the D'Agostino-Pearson omnibus normality test. For normally distributed data a TTest is performed. If no normal distribution is present, the data is evaluated with the Mann-Whitney test. Statistically significant differences are assumed for P-values smaller 0,05.

4 Results

4.1 Functionalised Ceramide Analogues to Study Dynamic Redistribution of Sphingolipids in Living T Cells

The tracing of sphingolipid redistribution has so far been hampered by the lack of suitable reagents. With the advent of bio-orthogonal chemistry to selectively label functionalised molecules, the transfer of this technique into sphingolipids appeared to yield promising tools to close this gap. These chemical compounds were made available in a cooperative project with the group of Professor J. Seibel, Organic Chemistry, University of Würzburg, and the first section of this chapter describes the establishment of suitable experimental conditions for their implementation on living T cells (published in *Journal of Immunology*, 2016 [105] and *Chemistry Communications*, 2016 [107]).

4.1.1 Toxicity Testing of Azide-Functionalised Ceramides

The azide-functionalised ceramides (Figure 13) were synthesised and analysed for purity prior to application in the experiments. The used compounds are N₃-C₆-cer with the N₃-group attached terminally in the ω -position (B), and N₃-C₁₆-cer with the N₃-group in the ω - (C) or the α -position (D), as well as commercially purchased NBD-C₆-ceramide (A), an established marker for the cell membrane and the Golgi apparatus as a control.

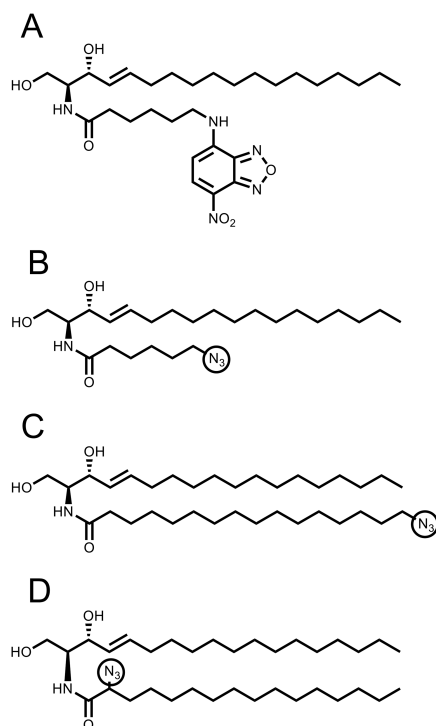


Figure 13: Chemical Structure of NBD-C₆-cer (A), N₃-C₆-cer (B), ω-N₃-C₁₆-cer (C) and α-N₃-C₁₆-cer (D).

First, the toxicity of the compounds for Jurkat and primary human T cells had to be evaluated. For this, a constant concentration (25 μM) of N₃-C₆-cer and NBD-C₆-ceramide was applied to the cells for 10 or 120 min.

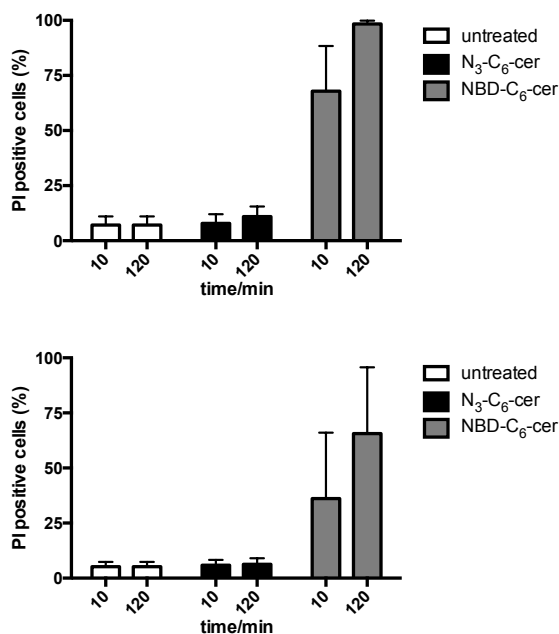


Figure 14: Toxicity of NBD-C₆-cer and N₃-C₆-cer for Jurkat T cells (top) and primary human T cells (bottom). Cells were treated for 10 and 120 min with the compounds, dead cells are PI positive. Bars show averages with standard deviation of n=3.

NBD-C₆-ceramide was already toxic for Jurkat and primary T cells after 10 min, with about 60 % or 30 % dead cells, respectively (Figure 14), while N₃-C₆-cer was non-toxic

for either of the cell types. The NBD- C_6 -ceramide molecule includes the dye and the lipid; therefore, the impact of the dye on the toxicity was analysed also for the clickable compound. The compound was clicked to the dye prior to addition to the cells by mixing both at a 1:1 ratio and incubating them for 10 min at RT. Now the dye was covalently linked to the lipid, generating a molecule comparable to the NBD- C_6 -ceramide.

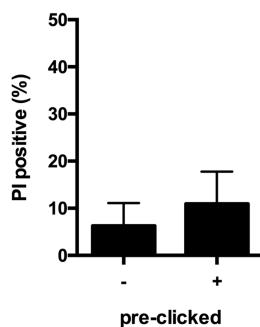


Figure 15: Toxicity of compounds with/without clicked dye. Jurkat T cells treated with N_3 - C_6 -cer (-) or N_3 - C_6 -cer which had been linked to DIBO 488 prior to feeding (+). Bars show averages with standard deviation of $n=3$.

As shown in Figure 15, dye coupling did not increase toxicity of N_3 - C_6 -cer. To determine the concentration-dependent toxicity of the compounds, NBD- C_6 -cer, N_3 - C_6 -cer, ω - N_3 - C_{16} -cer and natural C_6 and C_{16} lipids were applied to Jurkat T cells and primary T cells at three different concentrations for 30 min.

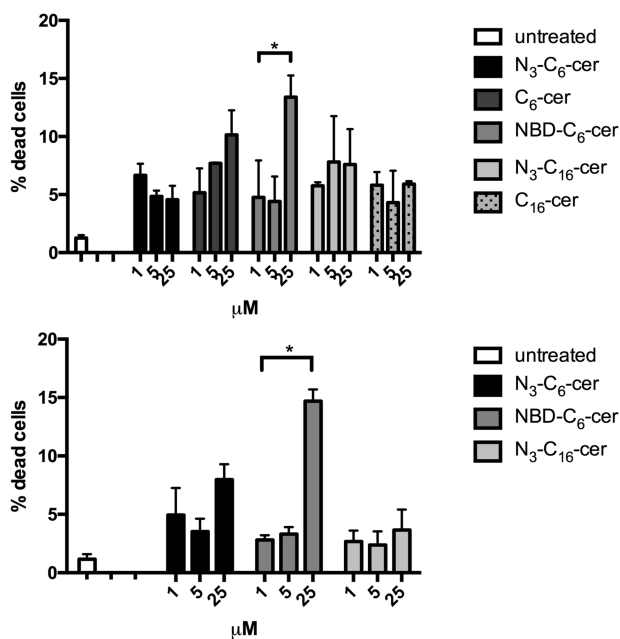


Figure 16: Toxicity of N_3 - C_6 -cer, C_6 -ceramide, NBD- C_6 -cer, ω - N_3 - C_{16} -cer and C_{16} -ceramide for Jurkat (top) and primary T cells (bottom). Compounds were applied to the cells for 30 min at 1, 5 or 25 μ M. Dead cells were stained with Viability Dye. Bars show averages with standard deviation of $n=3$.

While increasing concentrations of NBD- C_6 -cer correlated with enhanced cell death in both cell types, the percentage of dead cells following application of all other compounds did not exceed 10% at any of the concentrations tested (Figure 16). Notably,

the functionalised lipids did not show higher toxicity than their natural counterparts (top diagram for Jurkat T cells in Figure 16).

4.1.2 Selection of Suitable Dyes

In order to receive specific stainings of only the modified lipids with minimal background, functionalised dyes had to be selected which do not penetrate target cells when unattached to a compound.

Table 9: Functionalised dyes tested on Jurkat T cells

Functionalised dye	Diffusion into living Jurkat T cells	Staining pattern
Cyanin-3-alkyne	strong	Golgi, nuclear membrane, structures in the cytoplasm
Cyanin-3-azid	strong	
Cyanin-5-alkyne	strong	
Cyanin-5-azid	strong	
DIBO 647	minor	Spotted, in the cytoplasm
DBCO Sulfo-Cy-3	minor	
Sulfo-cyanin-5-alkyne	minor	
Sulfo-cyanin-3-azid	No	Only dead cells
Sulfo-cyanin-5-azid	No	
DBCO Sulfo-Cy5	No	
DIBO 488	No	

For this purpose, 13 dyes (listed in Table 9) were added to Jurkat T cells which were microscopically analysed 30 min later. Some dyes spontaneously entered into the cells in high amounts and gave an intensive staining of various cellular structures. These dyes were excluded from further experiments. The dyes DIBO 488 and DBCO-Sulfo-Cy5 were selected as suitable as they only clinged to cell debris, but did not enter and stain intact cells (Figure 17).

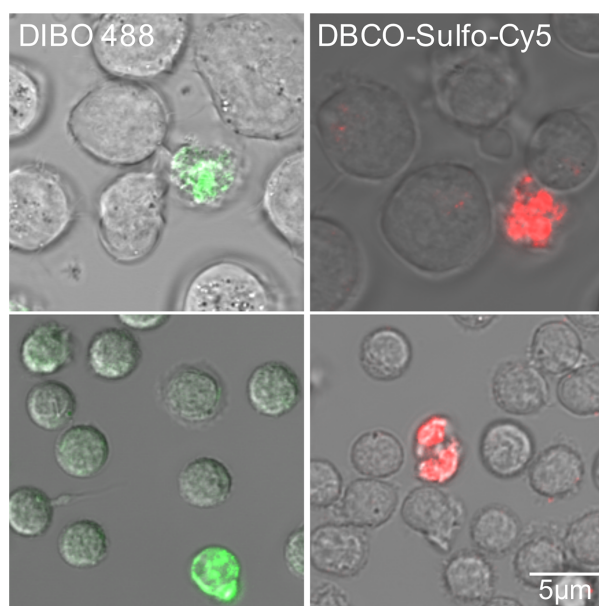


Figure 17: Dye selection. Jurkat (top) and primary T cells (bottom) exposed to 25 μM DIBO 488 (left panel) or DBCO-Sulfo-Cy5 (right panel) showing slight background and cell debris staining.

The chemical structure of both dyes bears an intrinsically high reaction potential as the alkyne bond is located in a strained ring structure. Therefore, copper as a catalyst is not needed for the click reaction. This would be required for click reactions with terminal alkynes but is highly toxic for living cells, which is efficiently avoided by the selected dyes. Performing the click reaction with either of the two dyes, DIBO 488 and DBCO-Sulfo-Cy5, did not reveal any differences in the staining patterns; hence both dyes could be used alternatively in further applications.

To find the optimal dye concentration giving the best background-to-signal-ratio, three different concentrations were added to Jurkat T cells which had been fed with 25 μM $\text{N}_3\text{-C}_6\text{-cer}$.

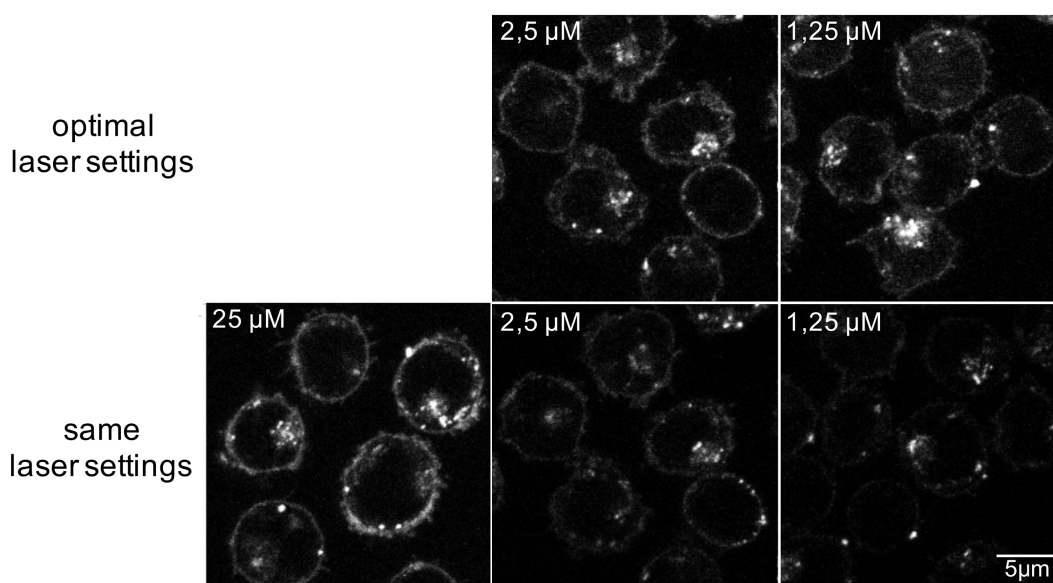


Figure 18: Visualisation of labelling efficiency. Jurkat T cells were exposed to 1,25, 2,5, and 25 μM $\text{N}_3\text{-C}_6\text{-cer}$ and clicked with DIBO 488. Images were taken with the same and optimal laser settings.

The intensity of the labelling increased with increasing dye concentration. With constant laser settings, optimised for the highest dye concentration of 25 μM , the signal intensity decreased with the amount of added dye (Figure 18, bottom row, from left to right decreasing concentration). With optimised laser settings for each dye concentration, the staining patterns were comparable, however, the background-to-signal-ratio was less optimal (Figure 18, upper row). To validate the specificity of the labelling, Jurkat T cells were first incubated with $\text{N}_3\text{-C}_6\text{-cer}$ to introduce the label, and then the click reaction was performed with DBCO-Sulfo-Cy5. Additionally, Cyanin-3-alkyne was added during the click reaction.

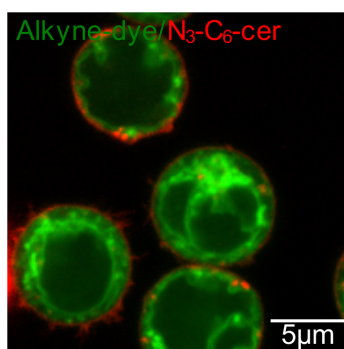


Figure 19: Co-imaging of $\text{N}_3\text{-C}_6\text{-cer}$ and an alkyne dye (Cyanin-3-alkyne). Jurkat T cells were in parallel exposed to $\text{N}_3\text{-C}_6\text{-cer}$ clicked to DBCO-Sulfo-Cy-5 (red) and a non-clickable alkyne dye (green) as a marker for undirected diffusion.

Cyanin-3-alkyne diffuses into the cell already without binding the compound (Table 9) and causes intense signals in the cytosol, but not on the plasma membrane. The labelling with DBCO-Sulfo-Cy5 was confined to the cell membrane, indicating a specific

signal in contrast to the alkyne dye (Figure 19, green signal for Cyanin-3-alkyne and red signal for N_3 - C_6 -cer).

4.1.3 Incorporation of Functionalised Compounds into T Cells

After having established optimal concentrations for both lipid compounds and dyes, the incorporation of the functionalised ceramides was analysed. Jurkat T cells were incubated with 25 μ M N_3 - C_6 -cer and NBD- C_6 -ceramide for up to 75 min, followed by dye coupling for 5 min and analysis by flow cytometry.

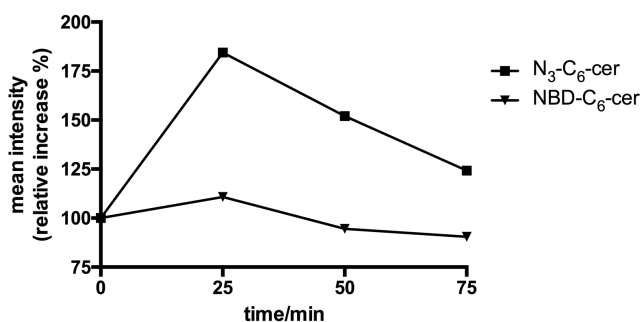


Figure 20: Incorporation of N_3 - C_6 -cer and NBD- C_6 -cer into Jurkat T cells. Cells were fed with 25 μ M of both ceramides, and the uptake was measured by flow cytometry after 25, 50 and 75 min. The graph shows representative results from 3 independent experiments.

Incorporation of NBD- C_6 -ceramide was constant throughout the entire duration of the feeding period, whereas the accumulation of N_3 - C_6 -cer peaked after 25 min and then decreased. Therefore, a feeding period of 25 to 30 min was routinely used.

To estimate the uptake efficiency of N_3 - C_6 -cer, its incorporation levels were analysed by mass spectrometry (Dr. Lukasz Japtok, University Potsdam). Jurkat T cells as well as primary T cells were incubated with the compound for 30 min and its incorporation was determined in cell lysates.

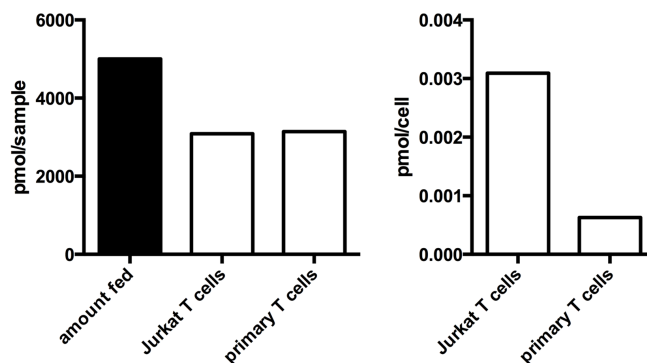


Figure 21: Incorporation of N_3 - C_6 -cer into Jurkat and primary T cells. Cells were incubated with the compound for 30 min, and samples were processed for lipidomic analysis. Bars show representative results for two replicates.

When normalised to the concentration in the feeding medium, uptake levels proved to be as high as 70 %. When stratifying for the cell number in each sample, on a single-cell basis Jurkat T cells incorporated about six times more N₃-C₆-cer than primary T cells (Figure 21).

In order to compare the uptake of the modified ceramides to that of their natural counterparts, N₃-C₆-cer, N₃-C₁₆-cer, C₆-cer, C₁₆-cer and NBD-C₆-cer were added to primary T cells for 30 min. Flow cytometric detection was performed after antibody staining for unmodified ceramides, a 5 min DIBO 488-click reaction for functionalised ceramides or directly in case of NBD-C₆-cer.

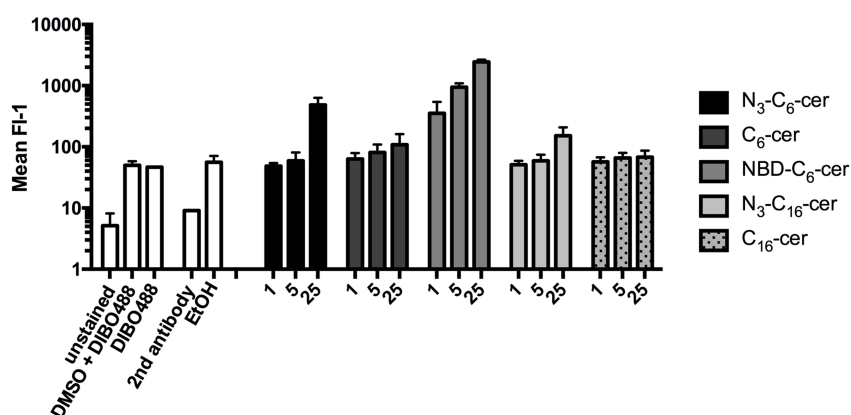


Figure 22: Incorporation of N₃-C₆-cer, C₆-ceramide, NBD-C₆-cer, ω-N₃-C₁₆-cer and C₁₆-ceramide into primary T cells. Cells were fed with either of the 5 compounds, which were visualised by click or antibody staining. Bars show mean fluorescence intensities and averages with standard deviation of n=3.

For control, T cells were incubated with only the secondary antibody or the dye without prior feeding. Except for NBD-C₆-cer, ceramide incorporation was only detectable at the highest concentrations. N₃-C₆-cer showed a 10-fold increase for 25 μM compared to 1 μM, 5 μM or dye controls (black bars, Figure 22). This uptake was substantially higher than for the natural C₆-cer. Both forms of the C₁₆-cer were incorporated highly inefficiently within this time period, the modified molecule showing slightly higher values. Directly comparing N₃-C₆-cer and N₃-C₁₆-cer uptake shows a five times higher incorporation rate for the short chain ceramide. NBD-C₆-cer shows the highest uptake rates already after the addition of 1 μM compound (Figure 22).

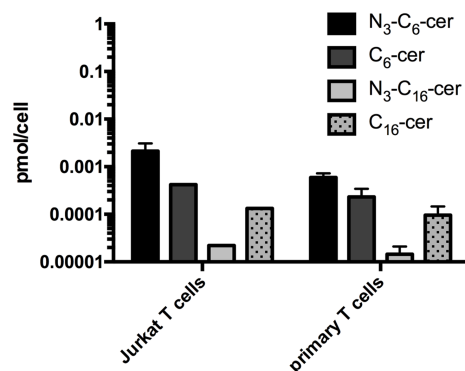


Figure 23: Incorporation of N₃-C₆-cer, C₆-ceramide, ω-N₃-C₁₆-cer and C₁₆-ceramide into Jurkat and primary T cells. Cells were exposed to one of the three compounds for 30 min, and samples were processed for lipidomic analysis. Bars show representative results for two replicates.

The increased incorporation of the short chained ceramides and the higher uptake rates of N₃-C₆-cer compared to C₆-cer also became apparent by mass spectrometry (Figure 23). Remarkably, this enhanced accumulation of C₆-cer after functionalisation was not observed for N₃-C₁₆-cer, which was rather found reduced compared to its unmodified control (light grey bars, Figure 23).

4.1.4 Visualisation of Functionalised Ceramides in T Cells

To compare the localisation and distribution to that of endogenous ceramides, Jurkat T cells fed with N₃-C₆-cer or NBD-C₆-cer were analysed by confocal microscopy.

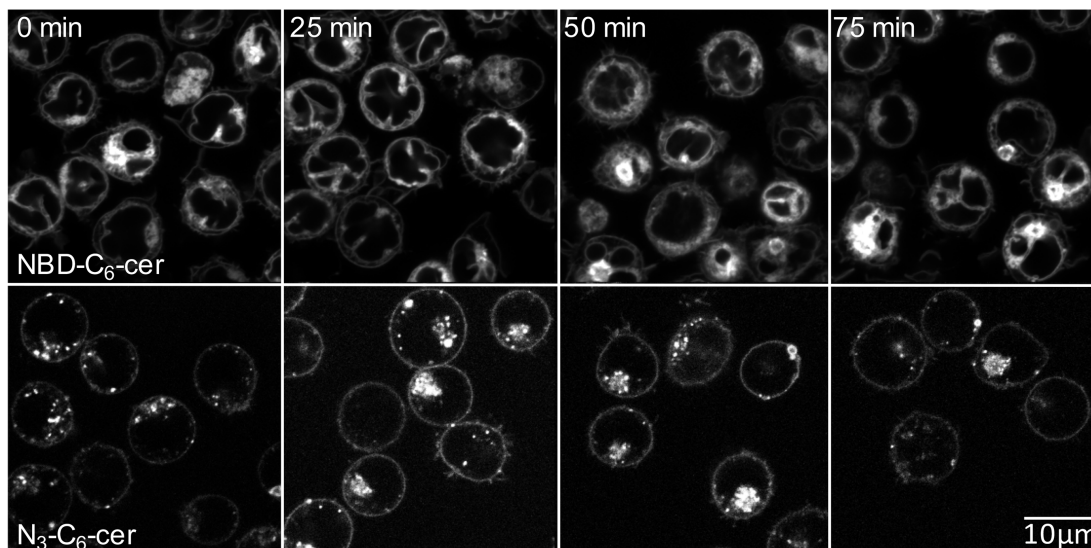


Figure 24: NBD-C₆-cer and N₃-C₆-cer visualisation. Jurkat T cells were exposed to NBD-C₆-cer or N₃-C₆-cer, clicked to DBCO-Sulfo-Cy5 and imaged after 25, 50 and 75 min to estimate uptake and cell morphology.

N₃-C₆-cer fed to Jurkat T cells and clicked to DBCO-Sulfo-Cy5 labelled the plasma membrane and an intracellular structure of which the staining increased with incubation time, indicating an accumulation of clicked N₃-C₆-cer there. Similarly, NBD-C₆-cer (applied at 5 µM to reduce its toxicity) marked the plasma membrane and accumulated in

this intracellular compartment. Though staining patterns of both compounds were similar, staining of intracellular structures with N_3 - C_6 -cer was less pronounced, and fine intracellular vesicles were also seen (lower row, Figure 24). After 75 min, cells exposed to NBD- C_6 -cer (but not those exposed to N_3 - C_6 -cer) revealed substantial morphological changes consistent with a loss of cell integrity, caused by the compound's toxicity (right images, Figure 24).

To identify the large intracellular compartment accumulating the N_3 - C_6 -cer, the compound was co-applied with NBD- C_6 -cer, an established Golgi marker. As evident from the co-localisation of both signals, N_3 - C_6 -cer also appeared to accumulate in this compartment (Figure 25).

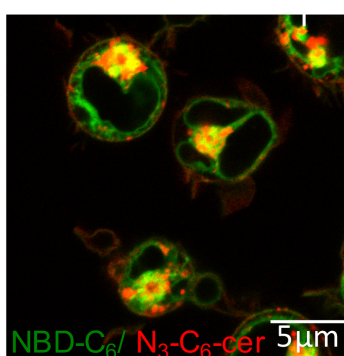


Figure 25: NBD- C_6 -cer and N_3 - C_6 -cer co-localisation. Jurkat T cells were fed with NBD- C_6 -cer (green) and N_3 - C_6 -cer clicked to DBCO-Sulfo-Cy5 (red) and imaged.

As already established in previous experiments, N_3 - C_{16} -cer incorporated less efficiently than N_3 - C_6 -cer within 25 mins (Figure 23), however, did so when feeding periods were prolonged to 16 hours. When clicked then, N_3 - C_{16} -cer efficiently labelled the plasma membrane in Jurkat T cells, indicating that incorporation kinetics are slower. Notably, the compound did not accumulate in the Golgi even after this prolonged feeding period (Figure 26).

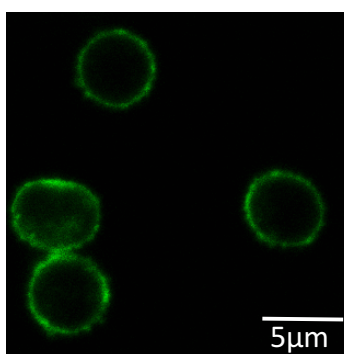


Figure 26: ω - N_3 - C_{16} -cer after o.n. feeding of Jurkat T cells. Jurkat T cells were fed with ω - N_3 - C_6 -cer o.n., clicked to DIBO 488 and imaged.

4.1.5 Optimising N₃-C₆-cer Uptake in Primary T Cells

As shown earlier, unstimulated primary T cells incorporate less N₃-C₆-cer than Jurkat T cells (Figure 21). Because the solubility of lipids in aqueous liquids such as the feeding medium is limited, enhancement of solubility might be favourable for availability of the compounds to T cells. Therefore, the feeding solution was supplemented with 0,2 % pluronic F-127, which increases the solubility of fatty compounds in water.

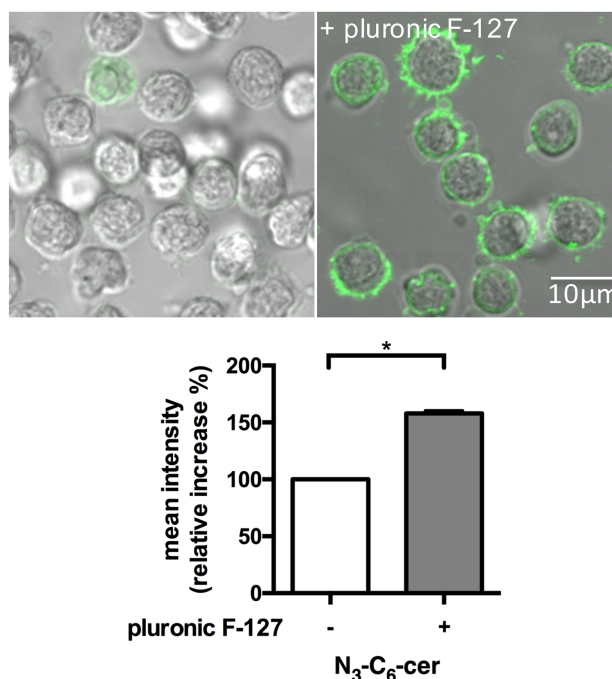


Figure 27: N₃-C₆-cer uptake with pluronic F-127 supplementation. Primary T cells were incubated with N₃-C₆-cer with and without the addition of pluronic F-127. Click reaction was performed with DIBO 488, and uptake was measured by visualisation and FACS. Bars are mean fluorescence intensities with standard deviation for n=3.

Indeed, using an otherwise unchanged feeding protocol, the addition of pluronic F-127 increased the uptake of N₃-C₆-cer into primary T cells by 50 %, while there was no significant enhancement of the uptake into Jurkat T cells (not shown). The difference between the Jurkat and primary T cells' readiness to incorporate different ceramides into their membrane is an interesting finding. It might be explained by slight differences in the cell size, but is more likely due to other changes to the cell membrane relating to the different activation status of the two populations.

To test whether the ability of T cells to incorporate extracellular ceramides into their membrane relates to their activation state, primary T cells were stimulated by high density culture for 5 days. These pre-activated T cells incorporated twice the amount of N₃-C₆-cer (but not N₃-C₁₆-cer) as compared to resting primary T cells (Figure 28, HD).

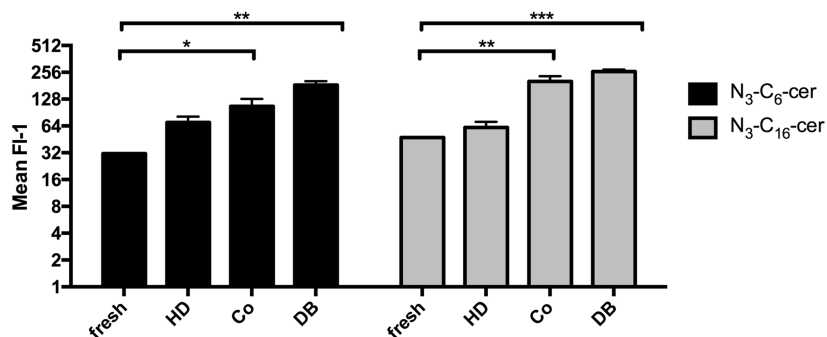
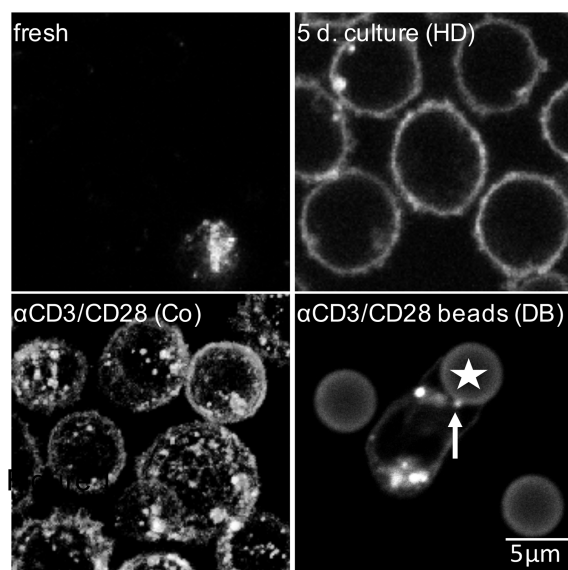


Figure 28: Stimulation-dependent uptake of N_3-C_6 -cer and N_3-C_{16} -cer into primary T cells. Primary T cells were stimulated by high density culture (HD), co-stimulation (Co) or dyna bead contact (DB) prior to incubation with N_3-C_6 -cer or N_3-C_{16} -cer, click reaction was performed with DIBO 488, and uptake was measured by visualisation (images show N_3-C_6 -cer) and FACS. Bars are mean fluorescence intensities with standard deviation for $n=3$.

The labelling efficiency could be enhanced for both the shorter and the longer chained ceramides, after stimulation with $\alpha CD3/CD28$ antibodies either provided on planar surfaces (Figure 28, co-stimulation, Co) or dyna beads (Figure 28, DB). This indicates that activation-dependent alterations of the cell membrane indeed impact the capability of cells to incorporate the functionalised ceramides. Maximum uptake rates were observed after incubation of the T cells with $\alpha CD3/CD28$ -coated beads for 30 min with both ceramides. After this stimulation a pronounced membrane as well as an intracellular vesicular staining below the bead-contact plane could be observed for N_3-C_6 -cer (Figure 28, arrow).

4.1.6 T Cell Activation After N₃-C₆-cer/ N₃-C₆-cer Incorporation

The modified ceramides are taken up by Jurkat T cells and by primary T cells and localised within the cell membrane, intracellular vesicles and the Golgi apparatus. To follow the stimulation-dependent redistribution of ceramides in cellular membranes, it was important to establish that incorporation of the compounds per se did not abrogate stimulatory signals.

Resting primary T cells were incubated with N₃-C₆-cer, N₃-C₁₆-cer and their respective natural counterparts according to the standard protocol. T cells were either kept unstimulated, co-stimulated with α CD/CD28 or stimulated with PMA/Iono for 16 h. Then, surface expression of the early activation marker CD69 was analysed by flow cytometry. Co-stimulation led to an increase of CD69 on the cell surface by 69,7 % in all cultures (middle bars, Figure 29) without compound-relating differences. These also were not apparent, when this parameter was analysed in response to PMA/Iono stimulation (left bars, Figure 29).

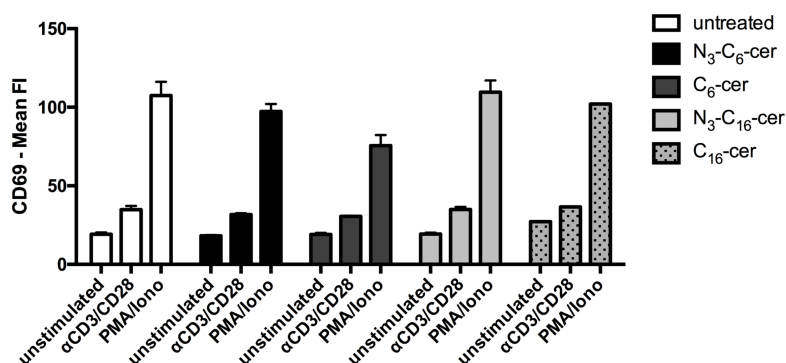


Figure 29: Primary T cell stimulation after ceramide exposure. Cells were fed with N₃-C₆-cer, C₆-ceramide, ω -N₃-C₁₆-cer and C₁₆-ceramide and co-stimulated or stimulated by PMA/Iono over night. Surface CD69 was measured by FACS. Bars represent mean fluorescence intensities with standard deviation for n=3.

To evaluate potential effects shortly after activation, Ca²⁺ mobilisation after CD3/CD28 stimulation was determined in primary T cells pre-exposed to functionalised ceramides by flow cytometry. The light grey lines in each graph represent the untreated cells and the dark grey lines the cells fed with the modified ceramides indicated in each diagram (Figure 30). Thus, as for CD69 upregulation, supplementation of neither the natural nor the modified compounds affected this parameter of T cell activation (Figure 30).

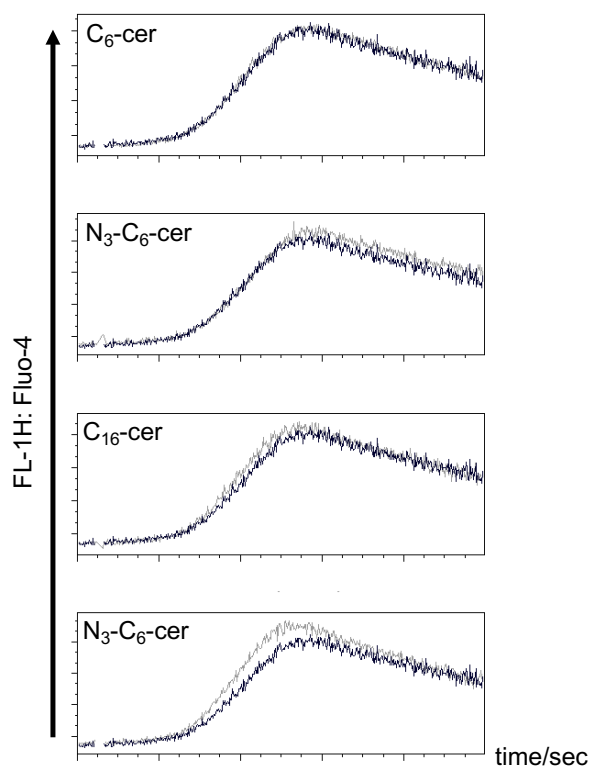


Figure 30: Calcium flux after ceramide exposure. Primary T cells were fed with N_3 - C_6 -cer, C_6 -ceramide, ω - N_3 - C_{16} -cer and C_{16} -ceramide and calcium mobilisation after co-stimulation was measured by FACS. Light grey lines indicate untreated control cells, dark grey lines cells fed with the compounds.

4.1.7 N_3 - C_6 -cer Redistribution After Cell Stimulation

As the modified ceramides did not interfere with T cell activation, their redistribution during activation was analysed. Co-stimulation of T cells leads to an activation of the cytoskeleton, which is visible when T cells spread in response to co-ligation of CD28 and CD3 on a planar surface coated with an antibody cross-linking the two [69]. Figure 31 shows T cells after the addition of α CD3 and/or α CD28 antibodies and an unstimulated control. The dotted line marks the cell boundary and shows the increased cellular size by formation of lamellar extensions in the co-stimulated cells.

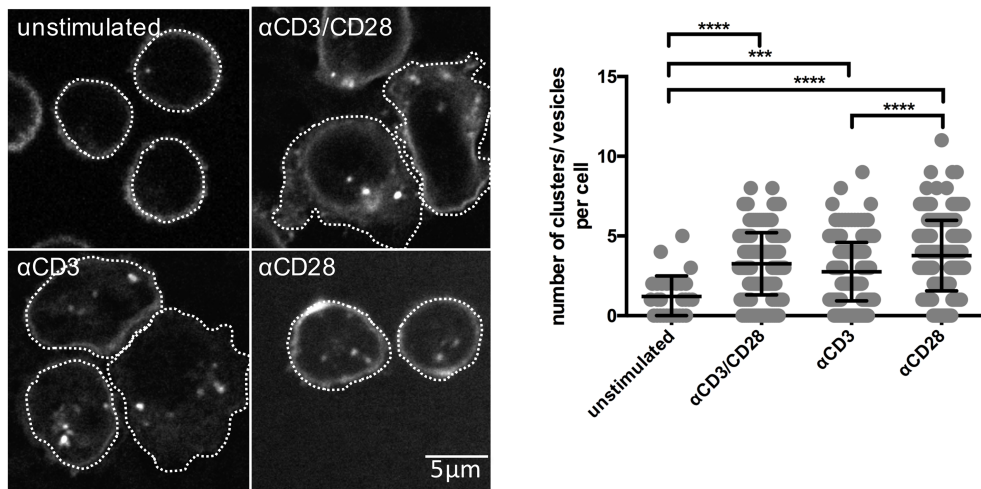


Figure 31: N_3 - C_6 -cer redistribution. Primary T cells were fed with N_3 - C_6 -cer and stimulated on planar antibody-coated surfaces. The diagram on the right depicts the cluster quantification per cell. Lines show means with standard deviation for $n=3$ independent experiments.

A similar spreading response was observed when the cells were activated by α CD3 ligation alone, but expectedly not upon ligation of α CD28 alone (bottom images, Figure 31). This experimental setting allowed to study whether the modified ceramides also redistribute into activation clusters. The primary cells were fed with N_3 - C_6 -cer for 30 min and exposed to α CD3-, α CD28- or α CD3/CD28-antibodies for 15 min on ice. The cells were transferred to the surface coated with the cross-linking antibodies, and the dye was applied for 15 min at 37 °C before immediate imaging of the samples. In the unstimulated cells, no clusters were visible, while for all stimulation conditions ceramide clusters appeared at or near to the plasma membrane, as well as vesicles endocytosed from there (see 3D reconstruction in Figure 32 for α CD28-stimulated cells).

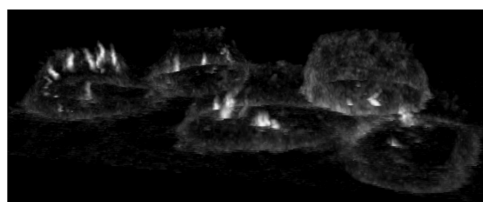


Figure 32: 3D reconstruction for α CD28-stimulated T cells. Primary T cells were fed with N_3 - C_6 -cer and stimulated on a planar antibody-coated surface.

The ceramide-enriched domains were quantified by counting spots exhibiting higher fluorescent intensity than measured for the membrane ring. In unstimulated cells, on average 1,21 clusters were visible per cell, while the amount increased for co- and α CD3-stimulation to 3,26 and 2,76 clusters per cell, respectively. Most clusters were generated in response to α CD28-stimulation (3,77 per cell). This strongly indicates that N_3 - C_6 -cer redistributed along with the natural ceramide into clusters enriched in ceramide (Figure 31). This is because α CD28-ligation (but not CD3 or CD3/CD28 co-

ligation) activates ASM which promotes formation of ceramide-enriched membrane domains within the outer leaflet of the plasma membrane [103]. If redistribution of N_3 - C_6 -cer followed that of endogenously generated by ASM activity, inhibition of the enzyme during CD28 ligation should ablate the N_3 - C_6 -cer clustering.

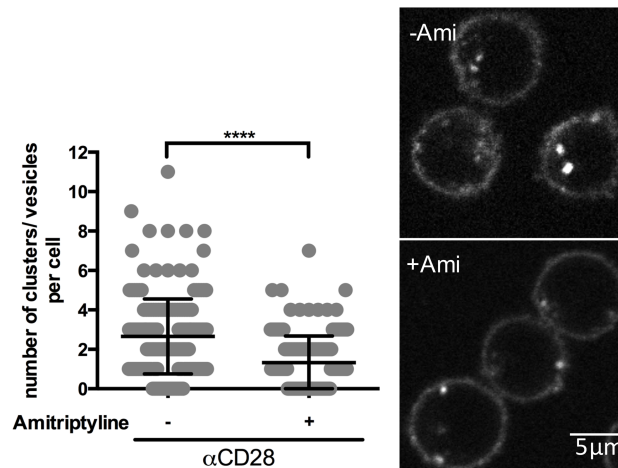


Figure 33: Role of the ASM for N_3 - C_6 -cer redistribution. Primary T cells were treated with amitriptyline prior to feeding with N_3 - C_6 -cer and stimulated on planar α CD28-coated surfaces. The diagram on the left depicts the cluster quantification per cell. Lines show means with standard deviation for $n=3$ independent experiments.

To study this, primary T cells were pre-treated with the ASM inhibitor amitriptyline prior to α CD28 ligation. In the absence of inhibitor treatment, on average 2,65 clusters per cell were formed, while amitriptyline treatment reduced this number to 1,32 which was comparable to levels measured on unstimulated cells. This shows that the modified ceramides co-redistributed into activation clusters within endogenous ceramides (Figure 33).

To further analyse redistribution of N_3 - C_6 -cer into ceramide-enriched domains, primary T cells were treated with extracellular bacterial sphingomyelinase. This induced formation of ceramide-enriched domains on the cell surface as shown by antibody staining (Figure 34, left image). The same clusters appeared after incubation of N_3 - C_6 -cer supplemented and clicked T cells with bacterial sphingomyelinase for 30 min.

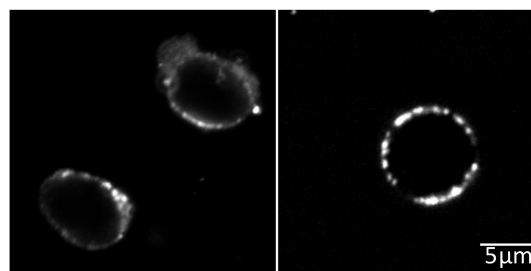


Figure 34: Bacterial sphingomyelinase generated ceramide clusters. Primary T cells were incubated with bSMase for 30 min, fixed, and ceramides were stained with an α -ceramide antibody (left image) or fed with N_3 - C_6 -cer prior to bSMase treatment and clicked to DIBO 488 afterwards (right image).

Altogether, these experiments show that the modified ceramide is recruited into clusters along with endogenous ceramides released by sphingomyelin hydrolysis.

4.1.8 Ceramide Localisation in T Cell/DC Conjugates

Ceramides re-distributed upon activation on planar surfaces and treatment of cells with molecules and enzymes, promoting the formation of ceramides on the cell surface (Figure 31 to Figure 34). In a third approach, the localisation of N_3 - C_6 -cer was analysed in T cells conjugated to antigen-presenting cells (APCs).

Based on antibody stainings, ceramides were found to be excluded from the APC/T cell interface and to accumulate in vesicles beneath the immune synapse [69]. To verify whether this was also the case with the modified ceramides, Jurkat T cells were fed with N_3 - C_6 -cer, the click reaction was performed, and cells were mixed with co-stimulatory beads and imaged after 15 min of incubation. The labelled N_3 - C_6 -cer was excluded from the T cell/bead synapse and accumulated in clearly discernible vesicular compartments proximal to the IS (Figure 35, arrowheads indicate ceramide accumulations).

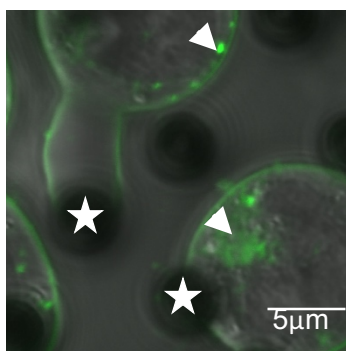


Figure 35: N_3 - C_6 -cer in Jurkat T cell/bead contacts. Cells were fed with N_3 - C_6 -cer and contacted with co-stimulatory dyna beads for 15 min before the click reaction was performed with DIBO 488 and pseudo-immune synapses were imaged. Arrowheads indicate ceramide accumulations; stars indicate the localisation of the beads.

As described for the bead conjugation experiment with Jurkat T cells, primary T cells, compound fed and clicked, were mixed with mature DCs loaded with Staphylococcus enterotoxin A/E, and the distribution of N_3 - C_6 -cer in the IS was recorded. Similar to the bead experiment, about 70 % of all immune synapses analysed were devoid of modified ceramides (Figure 36), and vesicular, synapse proximal ceramide-enriched compartments were visible (images Figure 36, arrowheads point at ceramide compartments).

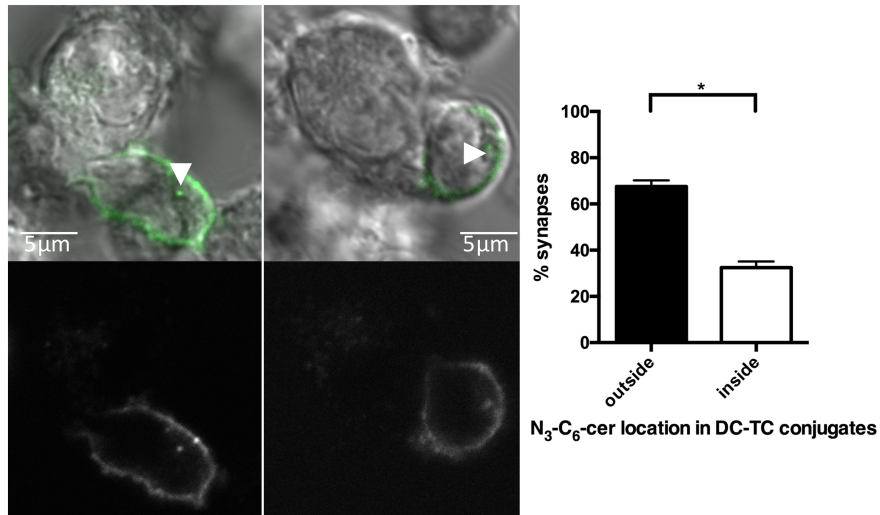


Figure 36: N_3 - C_6 -cer in primary T cell/DC contacts. T cells were fed with N_3 - C_6 -cer and contacted with SEE-loaded DCs for 15 min before the click reaction was performed with DIBO 488 and the IS was imaged. Approximately 20 contacts were analysed per experiment. Bars show means with standard deviation for $n=3$. Arrowheads indicate ceramide accumulations, upper images show DIBO 488 (green), overlaid with DIC, lower images show the DIBO 488 signal only.

4.2 Membrane and Vesicle Dynamics

Vesicle movement relies on rearrangement, deformation and extension of both the membrane and the underlying cytoskeleton. Previous experiments revealed a major impact of the NSM on membrane dynamics [69]. In T cell co-stimulation, the cells spread on a planar stimulatory surface (Figure 31), and this effect was significantly enhanced upon NSM ablation [69]. The appearance of ceramide-containing vesicles was also observed in stimulated T cells (Figure 31 and Figure 36). The vesicles appeared near the contact plane or the immune synapse and then appeared to move away from the reaction interface. To evaluate the importance of the NSM for endocytic processes in general, TCR endocytosis, which occurs in response to interaction with peptide-loaded MHC, was analysed in control and NSM ablated cells. The NSM was ablated in primary T cells by siRNA knockdown, and the knockdown efficiency was controlled by NSM activity assays (average knockdown rate: 60 to 70 %). These and control cells (nucleofected with unspecific siRNA) were contacted with SEE-loaded mature DCs for 15 min prior to fixation and staining for the CD3 ϵ chain, which is part of the TCR complex. The number of cells showing vesicles proximal to the immune synapse was counted (vesicles marked by the arrowhead in Figure 37). Quantification of the signals revealed that CD3 ϵ endocytosis was enhanced upon NSM ablation as compared to controls, indicating that the NSM indeed – possibly negatively – regulates receptor endocytosis (Figure 37).

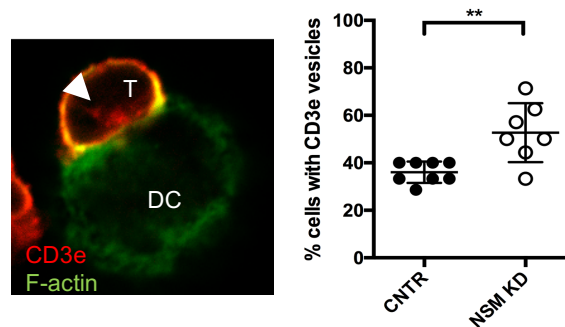


Figure 37: $CD3\epsilon$ endocytosis. Primary T cells (T) were contacted with SEE-loaded DCs and $CD3\epsilon$ was stained and quantified for vesicle formation behind the IS. The arrowhead points at $CD3\epsilon$ vesicles proximal to the IS. Diagram shows percentage of cells with vesicles, each dot indicating the quantification of cells per image (about 5). Lines show means with standard deviation for 7-8 images from $n=3$ independent experiments.

4.2.1 T Cell/Bead Contact Formation

To study whether NSM generally impacts membrane dynamics, primary control and NSM knockdown T cells were generated and contacted with uncoated $6\ \mu\text{m}$ beads which, as not decorated with stimulatory antibodies, do not specifically activate the T cells.

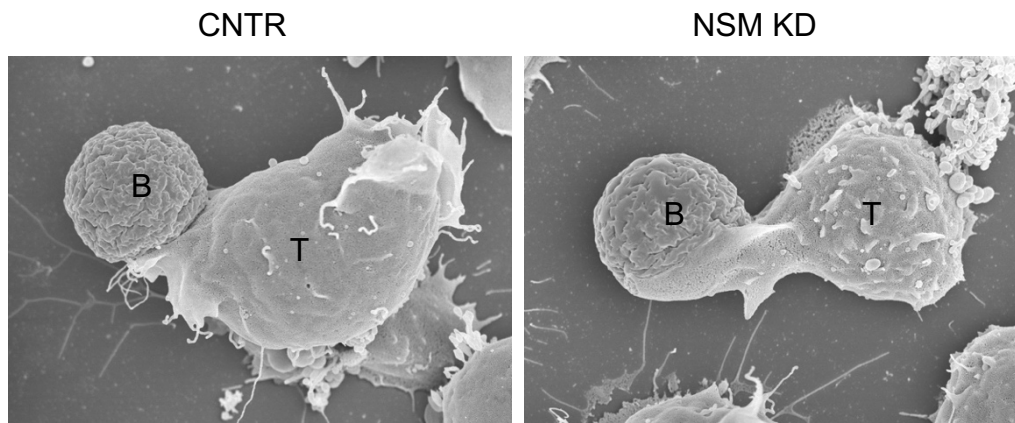


Figure 38: EM image for T cell/bead contacts. Primary T cells (T) were contacted with $6\ \mu\text{m}$ beads (B) for 15 min and processed for electron microscopy. Images show two representative cells.

As revealed by scanning electron microscopy analysis, control siRNA-treated cells contacted, but did not engulf the beads, while NSM siRNA nucleofected cells extended their membranes to create extended interaction surfaces with the beads which were partially engulfed (representative images shown in Figure 38). This shows a role for the NSM in regulation of membrane processes also independent of stimulation.

To comparatively analyse the impact of the NSM in stimulation-dependent and stimulation-independent conjugate formation, T cell/bead interactions with uncoated and co-stimulatory beads were analysed. Beads with diameters of $3\ \mu\text{m}$ and $6\ \mu\text{m}$ were coated with $\alpha CD3/\alpha CD28$ antibodies or were left untreated. They were mixed with control or

NSM KD cells, and T cell/bead contact formation was analysed by FACS after 15 min or 1 h. Irrespective of bead coating, NSM ablation led to enhanced contact formation (Figure 39). For the smaller beads, this difference became more obvious for co-stimulatory beads, while for non-stimulating beads (uncoated) the level of NSM-related increase of conjugate efficiency did not reach statistical relevance.

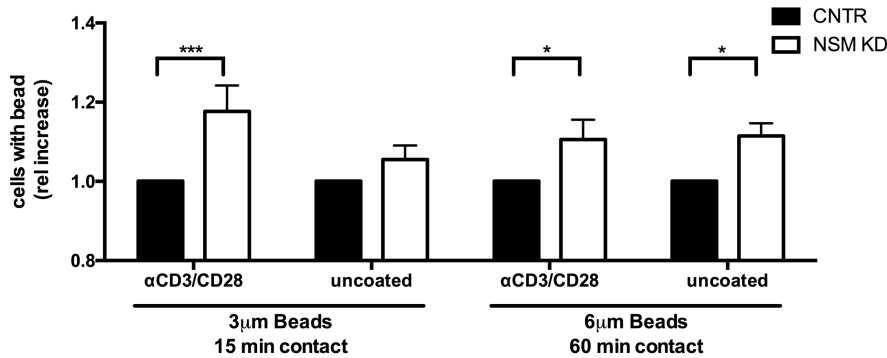


Figure 39: T cell/bead contact formation. Control and NSM KD T cells were mixed with 3 µm or 6 µm beads which carry or do not carry αCD3/αCD28 antibodies. The contacts were quantified by FACS according to the FSC/SSC pattern. Graph shows means with standard deviation of n=6.

NSM KD cells conjugated more efficiently to larger beads than control cells, irrespective of coating, indicating that NSM might impact cytoskeletal or membrane activity required for conjugate formation. Upon NSM ablation, T cells interact with beads and activate both cytoskeleton and membrane dynamics even in the absence of stimulation.

4.2.2 Migration of N₃-C₆-cer Labelled T Cells

The NSM was found to regulate receptor endocytosis and membrane dynamics, and it appeared possible that it regulates subcellular redistribution of ceramides in these processes. A suitable model to study membrane dynamic processes including endo- and exocytosis, is cell migration. Cell motility on a substrate requires recruitment and transport of membranes from the retracting uropod towards the extending leading edge. Additionally, receptors and adhesion molecules need to be re-organised in the cell and translocated to membrane domains where they cluster and interact with their ligands and interaction partners to induce cellular responses.

For the analysis of ceramide dynamics in migrating primary T cells, these were loaded with the modified N₃-C₆-cer and clicked with DIBO 488.

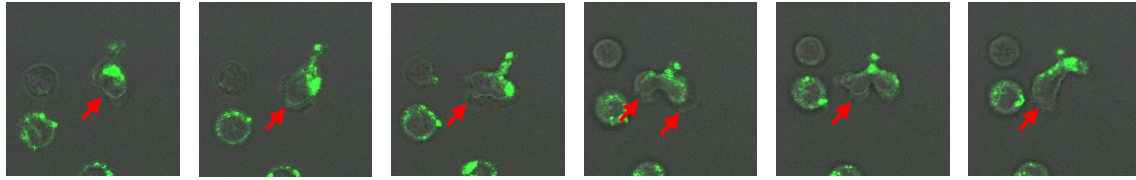


Figure 40: Ceramide vesicle movement in migrating T cells. Cells were exposed to N_3 -C₆-cer and clicked with DIBO 488 before settling onto FN. Images were taken every 10 secs to show cell movement and ceramide distribution. Red arrows point at the leading edge and the fine ceramide layer in the cell.

The cells were seeded onto fibronectin-coated slides and imaged for 10 min. A thin layer of ceramides was detected at the leading edge of the cells (Figure 40, red arrow), but the majority of ceramides was located to the rear of the cell within vesicular structures which changed dynamically in size and position when the cell was moving. These observations support a dynamic re-localisation of ceramide in migrating T cells. Whether ceramide generation by sphingomyelin breakdown by sphingomyelinases contributes to T cell motility along a chemokine gradient is analysed in subsequent experiments.

4.3 NSM in Directed T Cell Migration

4.3.1 Influence of the NSM on 2D Migration

T cells show locomotion towards specific chemokines when seeded onto extracellular matrix components like collagen or fibronectin, or onto endothelial cells. They differentially express various different chemokine receptors and can so respond specifically to chemokines secreted by organs like lymph nodes (LN), tissue resident cells or immune effector cells. In the following experiments CXCL12 (also SDF-1 α) was used as a ligand for CXCR4, which is highly expressed on lymphocytes and induces chemokinesis, but also directed chemotaxis along a chemokine gradient towards higher chemokine concentrations.

For analysis of 2D migration T cells were treated with either of the two NSM inhibitors (GW4869 and ES048) or a solvent control and seeded onto μ -slides coated with collagen type I. After cell attachment, an SDF-1 α gradient was applied, and the cells were imaged for 90 min at 37°C with images recorded every 45 sec. Based on manual tracking of individual cells, directional movement of control cells towards the SDF-1 α source was confirmed (Figure 41, left panel).

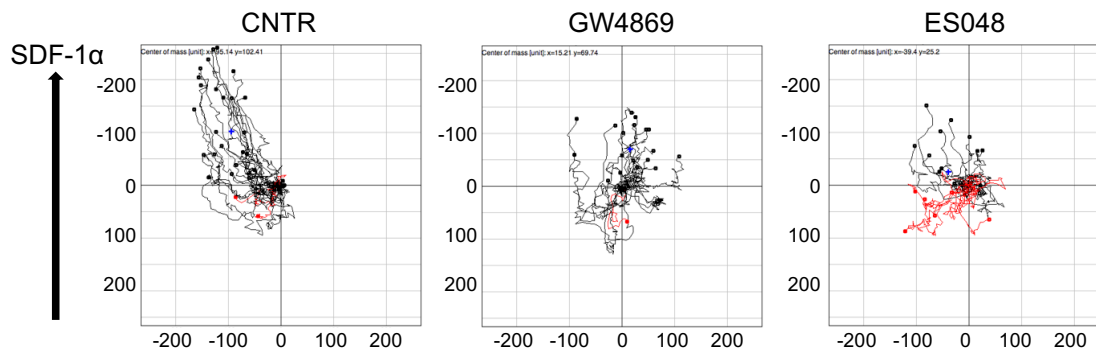


Figure 41: Tracks of T cells in a 2D environment. Primary T cells were inhibitor treated and seeded onto collagen surfaces. SDF-1 α was applied to one site of the channel (top in the images), and cells were imaged for 90 min. The tracks of each individual cell are depicted in the coordinate system, setting the starting points into the middle. Black lines indicate movement to the top, red ones to the bottom. X and Y axes show the distance in μm .

NSM inhibition caused a loss of directionality of cell movement which was visually evident by the tracking profiles (Figure 41, middle and right panels) and also at a quantitative basis (Figure 42). Calculations were based on directionality values, ranging from “1” (indicating straight migration) to lower values (for decreasing movement straightness), and yielded a NSM-inhibitor-related drop in directionality from 0,32 (measured in controls) to 0,25 (in NSM-inhibition).

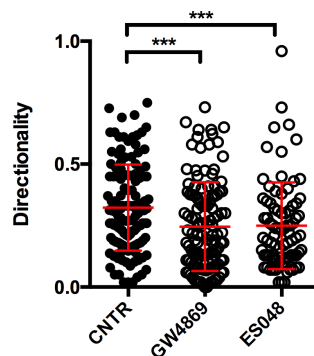


Figure 42: Directionality of primary T cells. Cells were inhibitor treated and seeded onto collagen surfaces. SDF-1 α was applied to one site of the channel, and cells were imaged for 90 min. Values for directionality were calculated with Fiji software; each dot indicates one cell. Lines are means with standard deviation for $n=4$ with approximately 30 cells per experiment.

Additionally, the speed of the cell movement was influenced by NSM inhibition. While control cells moved with a mean velocity of 2,2 $\mu\text{m}/\text{min}$, those exposed to NSM inhibitors appeared to move slightly faster (2,3 and 2,4 $\mu\text{m}/\text{min}$).

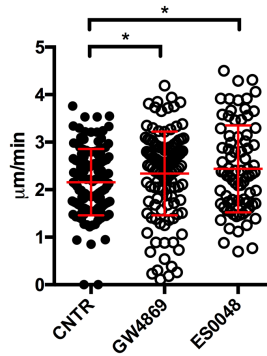


Figure 43: Velocity of primary T cells. Cells were inhibitor treated and seeded onto collagen surfaces. SDF-1 α was applied to one site of the channel and cells were imaged for 90 min. The velocity was calculated with Fiji software; each dot indicates one cell. Lines are means with standard deviation for n=4 with approximately 30 cells per experiment.

Hence, the NSM seems to influence the movement of T cells, and here especially the directionality of the locomotion.

4.3.2 Transendothelial Migration

The 2D migration experiments might be regarded as surrogates for motility of T cells on surfaces provided by the extracellular matrix, but also endothelia. To evaluate the importance of the NSM for the capability of T cells to adhere to endothelia, human brain microvascular endothelial cells (HBMECs) were seeded in 96-well plates and grown to confluency. T cells are labelled with CFSE, applied onto the HBMECs and allowed to adhere for 1 h before washing off non-adherent cells. After cell lysis, the retained fluorescent label can be used to define the efficiency of T cell adhesion. The principle of this assay was first verified by application of various concentrations of CFSE-labelled T cells which rendered a linear curve for the fluorescence signal up to half a million cells per well (see Figure 44).

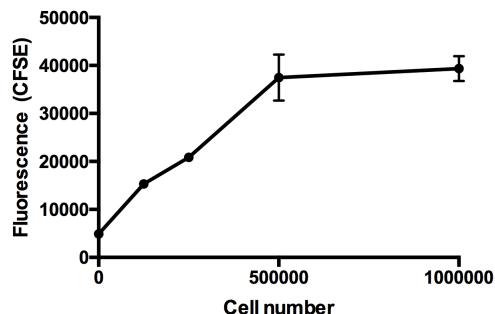


Figure 44: Titration of T cells for the adhesion assay. Primary T cells were labelled with CFSE and $1,25 \cdot 10^5$ to $1 \cdot 10^6$ cells were applied to each well and were lysed. The CFSE signal was measured with a fluorescent plate reader. The graph shows a linear curve for cell numbers lower than $5 \cdot 10^5$ T cells. The graph shows average values for n=2 independent repetitions.

To distinguish between a non-specific adhesion and that fostered by inflammation, HBMEC cultures were used untreated (resting) or after activation by $TNF\alpha/IFN\gamma$ which leads to an upregulation of adhesion receptors (see Figure 11).

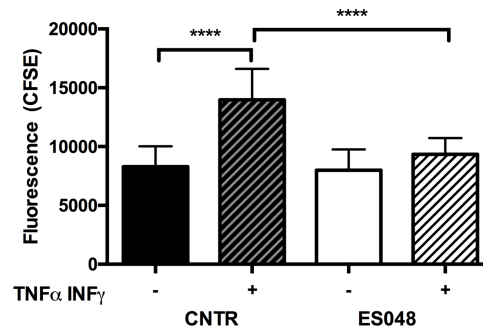


Figure 45: T cell adhesion to HBMECs. HBMECs were seeded in 96-well plates and left in a resting state (-) or stimulated with $TNF\alpha/IFN\gamma$ (+) over night. CFSE-labelled T cells were added to the cells and allowed to adhere. After washing away non-adhered cells, adhesive T cells were measured by their fluorescence label. Graph shows means with standard deviation for n=3 experiments.

Using these conditions, control and inhibitor-treated cells did adhere equally well to resting endothelia (compare black and white bar in Figure 45). Adhesion of control cells to the activated endothelium (+ $TNF\alpha/IFN\gamma$) was clearly enhanced while this could not be observed upon a pre-exposure of T cells to the NSM inhibitor (Figure 45). These findings strongly support the hypothesis that the NSM is required for essential steps of T cell adhesion to an inflamed endothelium.

After adhering, T cells need to move through the endothelium, which can be experimentally addressed by transmigration assays. For these, HBMECs were grown in filter inlets to confluency, and the density of the monolayer was controlled by TEER value measurement, inserts with HBMEC cells were used in transmigration assays when the TEER value lay between 50 and 60 Ω/cm^2 . SDF-1 α was applied to the bottom and T cells to the upper compartment from where they should follow the chemokine gradient. Transmigrated cells were counted and normalised for adhesion by counting T cells adhering to the HBMECs in the filter inserts and stratifying transmigrated cells accordingly. Passage through the resting endothelium was inefficient with NSM KD, control and especially ASM KD T cells (Figure 46, blank bars).

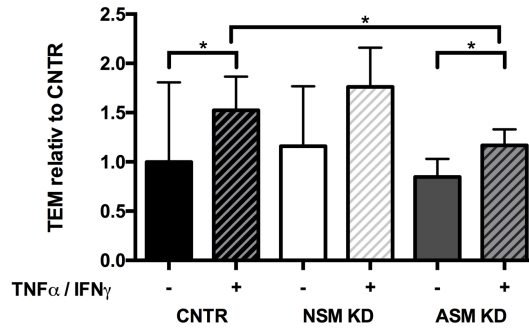


Figure 46: T cell TEM through HBMEC layer. HBMECs were seeded in filter inlets and left in a resting state or stimulated o.n. with $TNF\alpha/IFN\gamma$. T cells were added to the wells and allowed to transmigrate towards $SDF-1\alpha$ in the lower well for 1 h. Transmigrated T cells were counted with counter beads by FACS and stratified for the number of cells adhering to the HBMEC cell layer in the filter insert. Graph show means with standard deviation for $n=5$ experiments.

Adhering control and NSM KD cells passed the activated endothelium with greater efficiency and equally well (Figure 46, striped bars), even though only the increase for control T cells reached statistical significance. ASM KD cells also passed the inflamed endothelium slightly better than the resting ones, but still significantly worse than control cells. Altogether, this indicates that NSM activity is more important for adhesion to than for passage through the endothelium, while ASM activity plays an important role in the transmigration process through the HBMECs.

4.3.3 Influence of the NSM on 3D Migration

As T cells in the organism need to move also through 3D environments, the impact of NSM ablation in 3D environments (as an equivalent for tissue passage) was tested using collagen type I matrices. Primary NSM KD T cells were generated and embedded into a collagen matrix in which an $SDF-1\alpha$ gradient was formed. The T cells now needed to move through a more confined environment where collagen fibres built a meshwork. Per experiment 30 moving cells were tracked for 90 min. As evident by manual tracking, movement of control-siRNA nucleofected cells covered a larger area than that of NSM knockdown cells (Figure 47, tracks in upper panel).

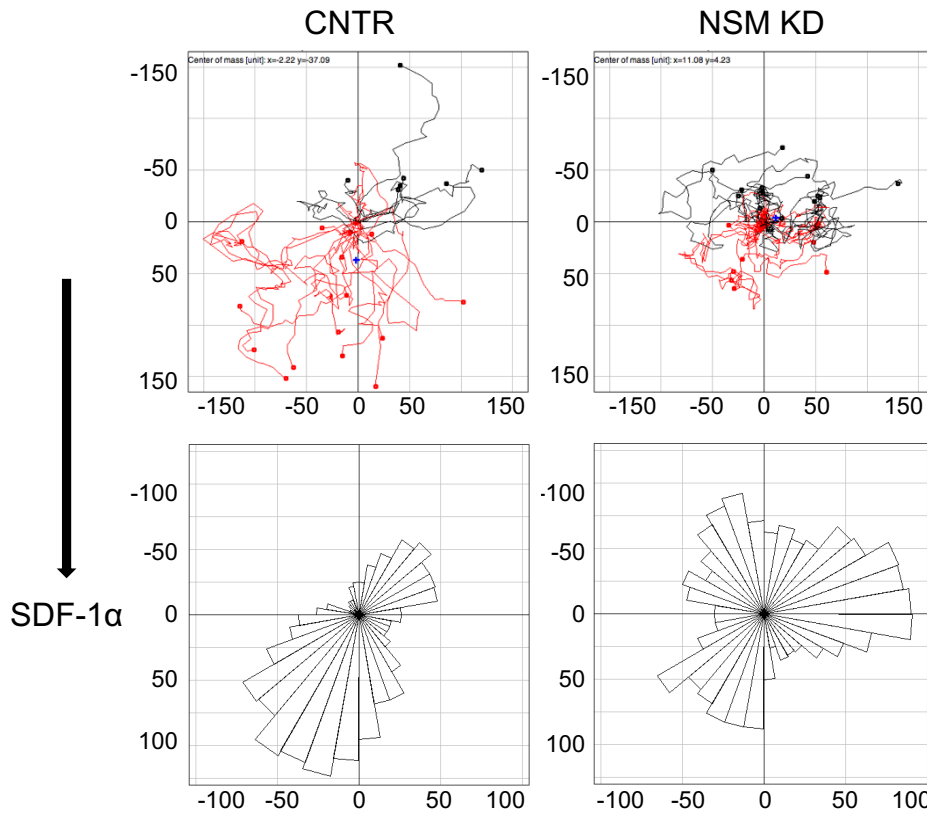


Figure 47: Tracks of T cells in a 3D environment. Control or NSM KD T cells were embedded in collagen matrices. SDF-1 α was applied to one site of the channel (bottom in the images), and cells were imaged for 90 min. The track of each individual cell is depicted in the coordinate system, setting the starting points into the middle. Black lines indicate movement to the top, red ones to the bottom (top diagrams). X and Y axes show the distance in μm . The bottom row shows rose diagrams visualising the number of cells moving into each direction.

The rose diagrams depict the number of cells moving into each direction (Figure 47, bottom row). The importance of the NSM for directional movement in a 3D environment towards SDF-1 α became apparent because control cells efficiently followed the gradient (69,6 %, Figure 47 top left, red tracks), while directional movement of NSM KD cells was significantly impaired (46,1 %, Figure 47 top right, red tracks). On a quantitative basis, directionality values were 0,30 for control and 0,24 for NSM-ablated T cells (Figure 48).

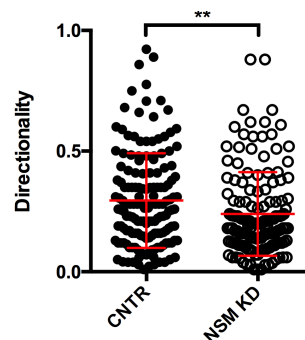


Figure 48: Directionality of primary T cells. Control or NSM KD T cells were introduced into collagen matrices. SDF-1 α was applied to one site of the channel and cells were imaged for 90 min. The directionality was calculated with Fiji software and each dot indicates one cell. Lines are means with standard deviation for $n=4$ with approximately 30 cells per experiment.

In the 2D model, the NSM-inhibited T cells (NSMi) moved slightly faster than the control cells (Figure 43). In the 3D environment, the velocity of NSM sufficient control cells corresponded to that measured in the 2D system (2,3 $\mu\text{m}/\text{min}$, Figure 43 and Figure 49), while that of NSM KD T cells was lower (1,9 $\mu\text{m}/\text{min}$, Figure 49) indicating that NSM might not only control the directionality, but also the speed of T cell migration in confined environments.

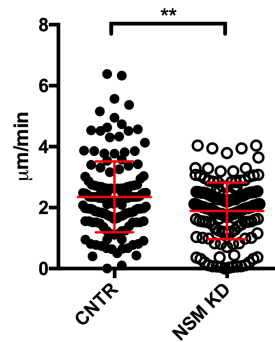


Figure 49: Velocity of primary T cells. Control or NSM KD T cells were embedded into collagen matrices. SDF-1 α was applied to one site of the channel and cells were imaged for 90 min. The velocity was calculated with Fiji software and each dot indicates one cell. Lines are means with standard deviation for n=4 with approximately 30 cells per experiment.

The importance of the NSM for the movement in confined environments can be analysed upon decreasing or increasing the density of the collagen meshwork. The forward migration index in y-direction (y FMI) is a value calculated from the distance between the starting and end point of a migrating cell and the accumulated distance it actually travelled. Hence, it represents the efficiency of the forward migration of cells. In this experiment a positive value for the y FMI indicates that the cell moved towards the chemokine source.

In a loose network, the NSM inhibition does not influence the range of movement of the T cells to a large extent even though it does not show any directionality towards the chemokine gradient (Figure 50). With increasing density of the network, directional movement of the NSMi cells was significantly impaired as compared to solvent-treated controls.

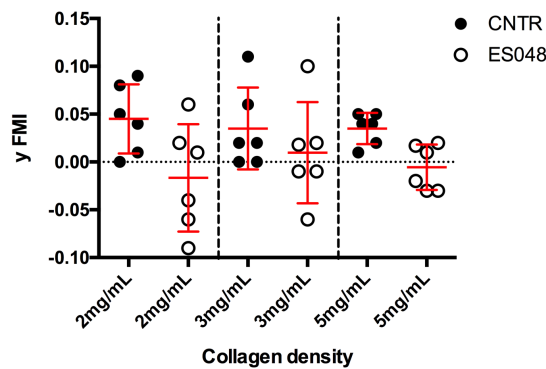


Figure 50: y FMI of primary T cells. Control or ES048 treated T cells were embedded in collagen matrices with densities of 2, 3 or 5 mg/mL. SDF-1 α was applied to one site of the channel and cells were imaged for 90 min. The forward migration index in y-direction is calculated with Fiji software, each dot indicates one experiment with about 30 cells. Lines are means with standard deviation for n=3 experiments.

The analysis of the 2D and 3D migration clearly shows an important impact of a functional NSM on the migration capacity of primary T cells, which is most obvious when the environment is restrictive, and therefore extensive cytoskeletal and membrane deformations are needed.

4.3.4 In Vitro Migration of Murine T Cells

To investigate whether these findings obtained *in vitro* with human T cells are of any importance *in vivo*, homing experiments in mice were conducted, involving transfer of NSM-sufficient and -inhibited T cells. As a prerequisite for the *in vivo* experiments, the 3D migration assay was repeated with murine CD4⁺ T cells. CD4⁺ T cells were isolated from LN of WT donor mice and treated o.n. with the NSM inhibitor ES048 which reduced NSM activity in mouse CD4⁺ T cells by 48 % with the inhibitor continuously present (not shown). Following the cell transfer into animals, the inhibitor would no longer be available, and therefore, durability of the inhibition in the absence of the inhibitor was analysed by washout experiments. Two hours following the inhibitor treatment, the activity of the enzyme was reduced by 54 % (similar as for an over night inhibition, see above), and remained almost constant within the following 9 hours. It was still visible (23 % reduction as compared to control cells) after 16 hours (Figure

51). Therefore, one would expect a considerable reduction of the NSM activity for up to 9 hours, and a mild reduction at 16 hours following T cell transfer into the animals.

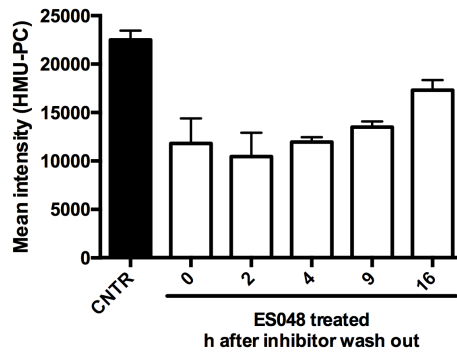


Figure 51: NSM assay with murine T cells. $CD4^+$ T cells were treated with $1,5 \mu M$ ES048 for 2 h, the inhibitor was washed away and cells were prepared for NSM activity assay after 2, 4, 9 and 16 h to measure the residual inhibition. Bars show means with standard deviation of $n=3$.

For the 3D migration assay, $CD4^+$ murine T cells were embedded into the collagen matrix as before, and murine SDF-1 α was applied which diffused into the matrix to form a gradient. Data obtained with regard to the directionality of movement for murine cells perfectly recapitulated those measured for human cells: NSM inhibition led to a loss of directionality in murine $CD4^+$ T cells (Figure 52).

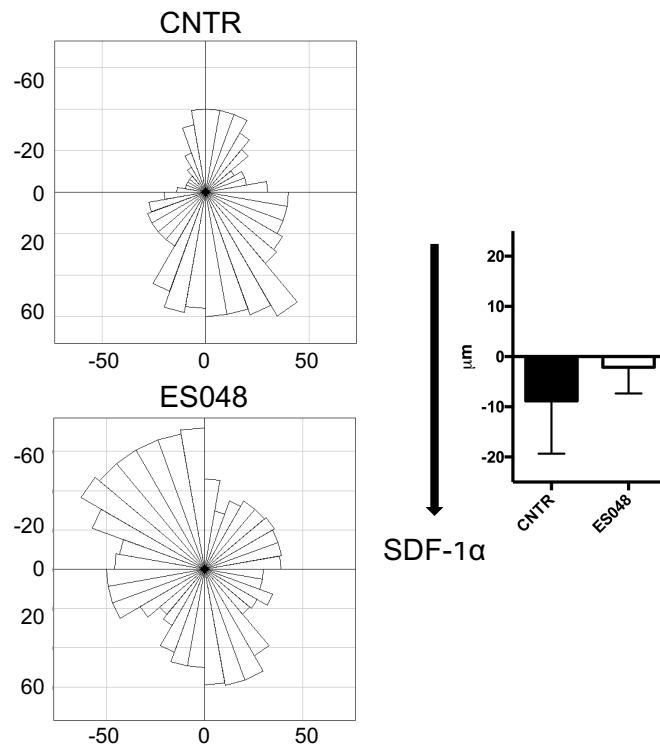


Figure 52: Murine T cell migration. $CD4^+$ T cells were isolated and treated with ES048 before embedding them into a collagen matrix. Mouse SDF-1 α was applied to one side of the channels (bottom of the image) and T cell movement was tracked for 90 min. The rose diagrams on the left depict the direction into which the cells moved, with X and Y axes showing the distance in μm . The distance of the cells' movement is shown in the graph on the right. The displacement of the cells into the y-direction is calculated for 30 cells per experiment with the software Fiji. Bars show means with standard deviation of $n=3$.

4.3.5 In Vivo Migration of Murine T Cells

Having confirmed the importance of the NSM for directed T cell migration *in vitro* also for murine T cells, the behaviour of NSMi T cells should now be comparatively analysed with that of unmodified T cells in *in vivo* homing assays. To study the steady-state homing efficiency of T cells, their recruitment into the LN without an inflammatory stimulus is a suitable system. For the experiment, CD4⁺ T cells were isolated from Thy1.1⁺ donor mice and divided into two populations. One was treated with ES048 over night and labelled with CFSE, whereas the other was treated with the solvent as a control and labelled with eFlour 670. Both populations were mixed at a 1:1 ratio and injected into the tail vein of congenic Thy1.2⁺ WT acceptor mice. T cells were allowed to home for 16 hours or 1 hour, and thereafter, their presence in blood, spleen and LN was analysed by flow cytometry of the respective cell suspensions.

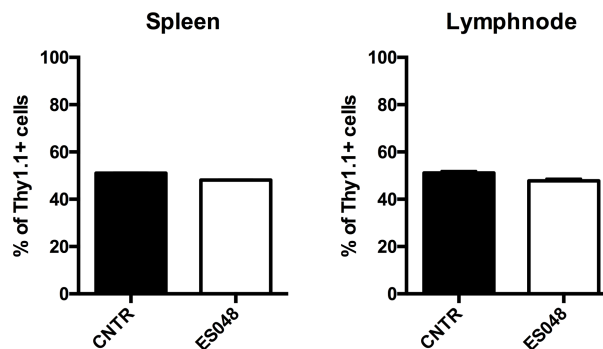


Figure 53: 16 h homing of CD4⁺ T cells into secondary lymphoid tissues. T cells were isolated, inhibitor treated, labelled and re-injected into acceptor mice. After 16 h spleen and LNs were isolated and implanted T cells were quantified. Bars show means with standard deviation for n=3 mice.

At 16 h following transfer, numbers of transferred CD4⁺ T cells were equal for inhibitor-treated and control populations in spleen and LNs (Figure 53). The impact of NSM inhibition was, however, clearly evident, when the frequencies of these populations were analysed 1 h following transfer: while the ratio of control to NSMi T cells is still 1:1 in the blood, slightly more control than NSMi T cells had moved to the spleen (the ratio 1:0,91), and this difference was even more pronounced in LNs (the ratio 1:0,67) where the frequency of control T cells exceeded that of NSMi T cells by more than 30 % (Figure 54).

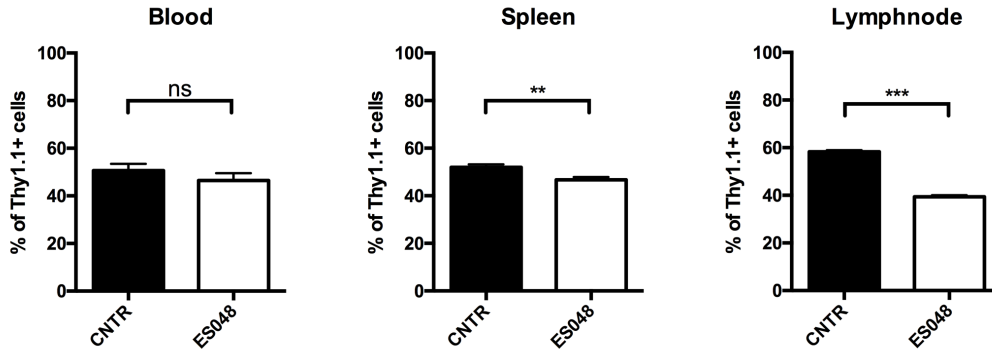


Figure 54: 1 h homing of CD4⁺ T cells into secondary lymphoid tissues. T cells were isolated, inhibitor treated, labelled and re-injected into acceptor mice. After 1 h blood, spleen and LNs were isolated, and implanted T cells were quantified. Bars show means with standard deviation for n=3 mice.

These data underscore the importance of the NSM for migration also *in vivo*, but how the NSM influences the migration is still unknown.

4.3.6 CXCR4 Expression on T Cells

To detect SDF-1 α and to convert the signal into directional movement, T cells need to express and polarise CXCR4, re-organise their cytoskeleton and thereby their morphology. One reason for the diminished response of NSM-ablated T cells could be a defect at the level of receptor expression. To investigate this point, CXCR4 was measured on the surface of control and NSM KD T cells by flow cytometry. As shown in Figure 55, CXCR4 expression levels on both cell populations were equal, so the reduced response is not due to a lack of receptor surface expression.

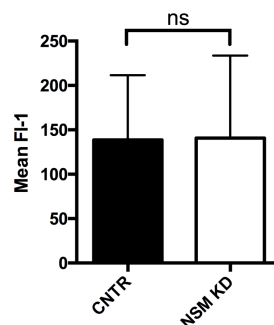


Figure 55: CXCR4 surface staining. FACS measurement of CXCR4 expression on primary control and NSM KD T cells. Bars show means with standard deviation for n=3 experiments.

Next, SDF-1 α -induced re-localisation of surface CXCR4 was analysed by immunofluorescence. In CNTR T cells CXCR4 localises to the leading edge of the polarised T cells, whereas in NSM KD cells the receptor is detected in spot-like localisations at various areas on the cell membrane (Figure 56, arrowheads mark CXCR4 localisation in the CNTR T cells).

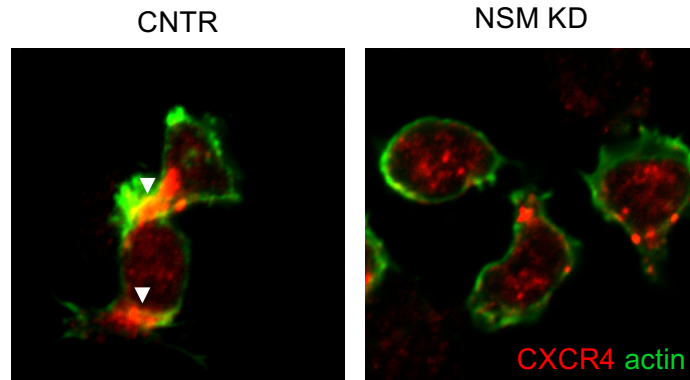


Figure 56: CXCR4 on polarised T cells. Primary control and NSM KD T cells were settled onto FN and stained for CXCR4 (red) and F-actin (green). Arrowheads point at CXCR4 accumulation at the leading edge of CNTR T cells. Images show representative cells for $n=3$ experiments.

On quantification, in 65 % of the control cells the receptor was found to localise at the leading edge, while this occurred in only 40 % of NSM KD cells (Figure 57). It is therefore possible that although CXCR4 is expressed and may sense the signal, this does not lead to a polarised response because the signal is not received in a spatially meaningful manner.

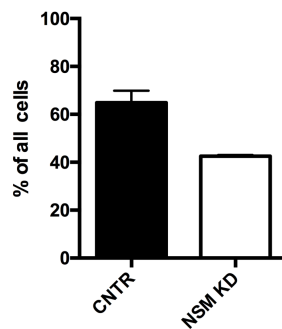


Figure 57: CXCR4 re-localisation in polarised T cells. Quantification of CXCR4 localisation at the leading edge of primary control and NSM KD T cells polarised on FN. Bars show means with standard deviation for $n=3$ experiments.

4.3.7 Sphingomyelinase Activity upon SDF-1 α Contact

The NSM ablation could influence T cell migration by interfering with CXCR4 signal perception because it is needed for CXCR4 signalling directly. To investigate this, the activity levels of the ASM and NSM were determined after exposure of primary human T cells to SDF-1 α over time. These did not provide any evidence for a role of either SMase in CXCR4 signalling (Figure 58).

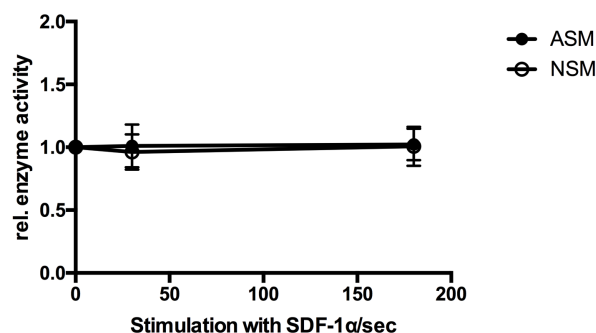


Figure 58: ASM and NSM activity after SDF-1 α stimulation. T cells were stimulated with 500 ng/mL SDF-1 α for 30 secs and 3 min, and ASM and NSM activity was measured with the respective assay. Graph shows means with standard deviation of n=3.

It is concluded that basal rather than stimulated NSM most likely influences T cell motility and migration.

To analyse if NSM activity is important for signalling downstream of CXCR4 engagement primary T cells were stimulated with 500 ng/mL SDF-1 α , and the phosphorylation of Src-kinases and Erk 1/2 was measured after 5, 15 and 30 secs (Figure 59).

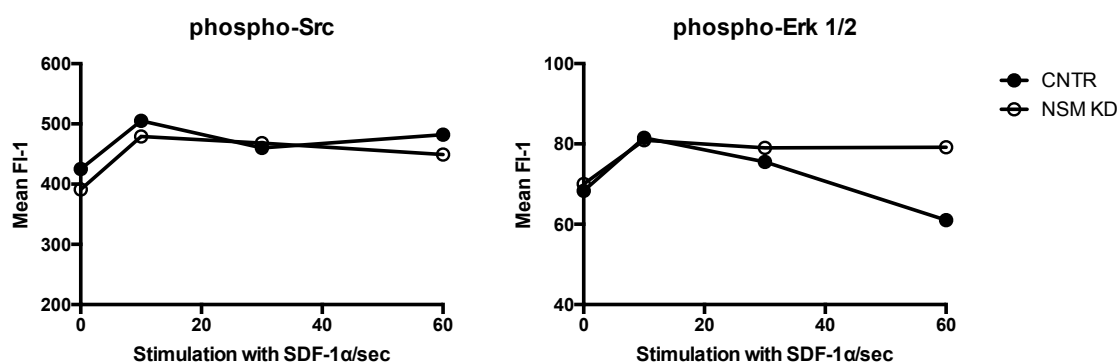


Figure 59: Src and Erk 1/2 phosphorylation after SDF-1 α stimulation. Primary control and NSM KD T cells were stimulated with 500 ng/mL SDF-1 α for 10, 30 and 60 secs. Phosphorylation was measured with phospho-specific antibodies by flow cytometry. Graph shows means of n=2.

Already after 5 secs, both enzymes were phosphorylated, reaching a maximum after several further seconds. Surprisingly, the NSM ablation does not alter this response to the stimulus.

4.3.8 LFA-1 Affinity Maturation

Chemokine receptor engagement leads to affinity maturation of adhesion molecules such as LFA-1, which induces phosphorylation of downstream effector molecules upon binding its ligand ICAM-1. As the NSM might influence the receptor organisation, it could also have an impact on LFA-1 affinity maturation, and thereby on signalling. Integrins switch into their open conformation which displays a higher affinity towards their ligand upon crosslinking, and this step could be sensitive to basal NSM activity. To

measure this effect, upregulation of the open/high affinity isoform on T cells exposed to the NSM inhibitor or not prior LFA-1 activation with the antibody NKI-L16 [108] was determined by flow cytometry using conformation-specific LFA-1 antibodies. The stimulation with NKI-L16 induced a switch to the open form of LFA-1 in control cells, as shown by the threefold increase in the mean fluorescence signal (Figure 60, black bars). In NSM ablation, the signal did not even double, clearly indicating that NSM activity is needed for the conformational change into the open form of LFA-1 in response to stimulation.

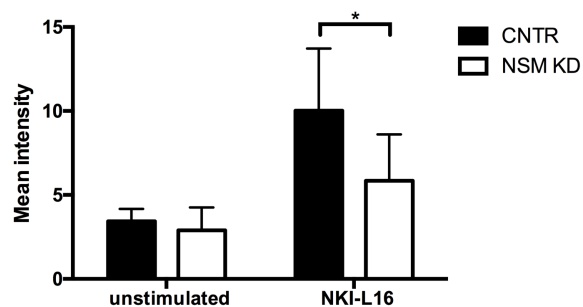


Figure 60: LFA-1 open conformation after NKI-L16 stimulation. T cells were treated with the NSM inhibitor or left untreated prior to stimulation with 100 ng/mL NKI-L16 for 30 min. The open LFA-1 isoform was stained for FACS. Bars represent means with standard deviation for n=4.

In addition to its conformational changes, polarised redistribution of LFA-1 is important for its function [30], which could well be targeted by NSM activity at the membrane level.

Immunofluorescence staining using again conformation-specific LFA-1 antibodies revealed that the closed conformation of the integrin (Figure 61, red signal, both panels) is present on the membrane of FN-seeded control and NSM KD T cells with no detectable compartmentalisation. In contrast, the active form concentrated in a polarised fashion in control cells which was much less prominent in NSM KD cells where LFA-1 in open conformation appeared to cluster at multiple places in the outer membrane (Figure 61, green signal, both panels).

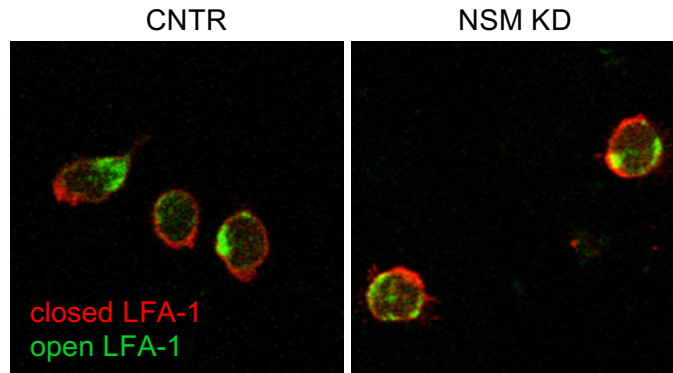


Figure 61: LFA-1 localisation. Primary NSM KD or control cells were applied to FN-coated slides and allowed to polarise. With specific antibodies the open and closed form of LFA-1 was stained. Pictures show representative images for $n=3$ independent experiments.

Defects in high affinity LFA-1 clustering showed even clearer in immunofluorescence staining of open LFA-1 on Jurkat T cells adhering to HBMEC cells. The HBMECs have been seeded in slides suitable for immunofluorescence and were stimulated with $TNF\alpha/INF\gamma$ over night.

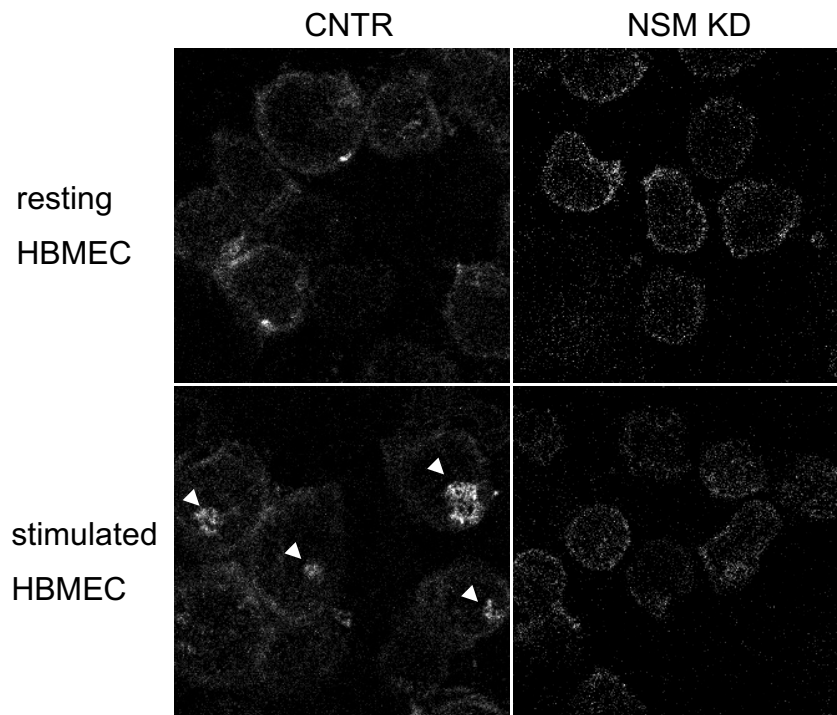


Figure 62: Open LFA-1 clusters on Jurkat T cells on a HBMEC layer. HBMECs were seeded in slides suitable for immunofluorescence and left in a resting state (top row) or stimulated with $TNF\alpha/INF\gamma$ o.n. (bottom row). Control or NSM KD Jurkat T cells were added to the wells on the slide and allowed to adhere for 1 h. Cells were fixed and stained with an antibody specific for the open conformation of LFA-1. Arrowheads point at clusters of LFA-1, only present in the lower left image. Images show representative cells of $n=3$ experiments.

Under resting conditions, open LFA-1 clusters (arrowheads in Figure 62) were present in 14,5 % of control Jurkat T cells and this increased to 37 % of all cells under inflammatory conditions (Figure 63, black and dark grey striped bars). These clusters only showed on about 7 % of NSM KD Jurkat T cells, independent of the stimulation status of the HBMECs (Figure 63, white and white striped bars).

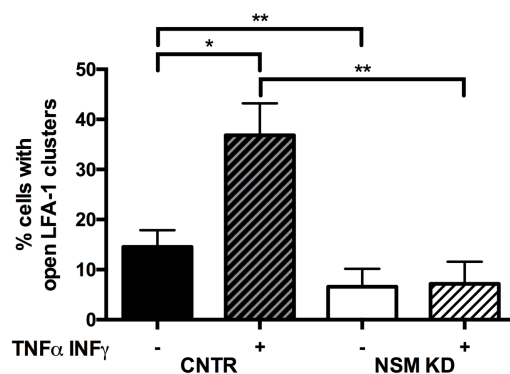


Figure 63: Open LFA-1 clusters on Jurkat T cells on a HBMEC layer. HBMECs were seeded in slides suitable for immunofluorescence and left in a resting state or stimulated with TNF α /IFN γ over night. Jurkat T cells were added to the wells on the slide and allowed to adhere for 1 h. Cells were fixed and stained with an antibody specific for the open conformation of LFA-1. Z-stack images were taken, and clusters were analysed manually by counting cells showing LFA-1 accumulations. Graph shows means with standard deviation for n=3 experiments.

These observations are in perfect agreement with those made for total CXCR4 (Figure 60), indicating that the polarisation is defective in NSM ablation, but for LFA-1 also affinity maturation is sensitive to basal NSM activity.

This might indicate that the basal activity of the NSM is needed for membrane domain formation, enabling or favouring the recruitment of active integrins.

4.3.9 Phosphorylation of Src, ZAP70 and Erk 1/2

Though conversion to the active LFA-1 conformation was only slightly affected upon NSM ablation, its aberrant polarisation might relate to impaired signalling and function. This was addressed by cross-linking of LFA-1 using α LFA-1 antibody-coated beads, followed by analysis of the accumulation of phosphorylated Src-kinases, ZAP70 and Erk 1/2 over time by flow cytometry. Expectedly, each of these enzymes was found activated already after 5 min following cross-linking in control cells, and activation levels were maintained over the observation period. Except for ZAP70, which appeared slightly less activated at all time points, activation of the membrane proximal LFA-1 signalling components analysed in NSMi cells paralleled that seen in control cells (Figure 64).

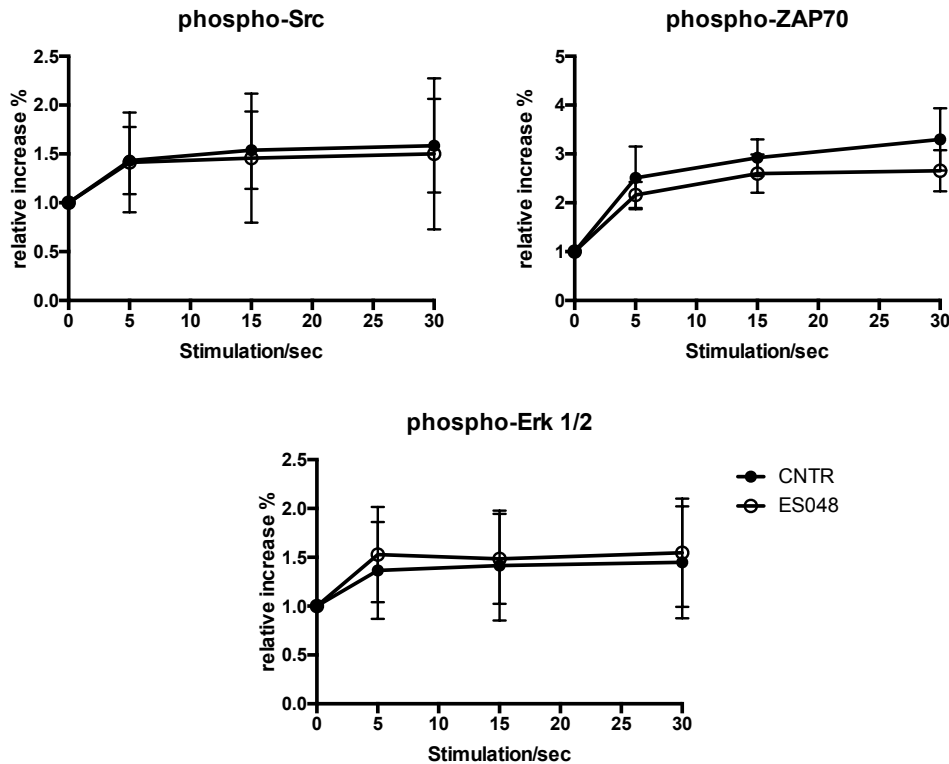


Figure 64: Src, ZAP70 and Erk 1/2 phosphorylation after LFA-1 cross-linking. T cells were treated with the NSM inhibitor ES048 and α LFA-1 coated beads were added. The reaction was stopped after 5, 15 or 30 min, and enzyme phosphorylation was measured with specific antibodies by FACS. Graph shows means with standard deviation of $n=4$.

4.3.10 T Cell Polarisation

From the analysis of CXCR4 and LFA-1 expression described so far it became apparent that the NSM predominantly affected the polarised redistribution of receptors rather than their signalling function (Figure 55 to Figure 64). Therefore, it appeared likely that the dramatic impact of NSM ablation on T cell motility and migration *in vitro* and *in vivo* might reflect a general lack of cell polarity, representatively shown for aberrant receptor sorting. This should also target actin cytoskeletal dynamics and its regulators.

When T cells attach to an extracellular matrix or endothelial cells and initiate migration, their shape changes from round to stretched and elongated. This morphological change can be quantified by measuring the “roundness” of a cell. A roundness value of “1” depicts a perfect circle; the more the value drops, the more the cell becomes irregular and elongated. Potential NSM relating alterations of morphological restructuring were first analysed by investigating circularity of primary T cells exposed to the NSM inhibitor or not prior to CFSE labelling and seeding onto a dense HBMEC monolayer.

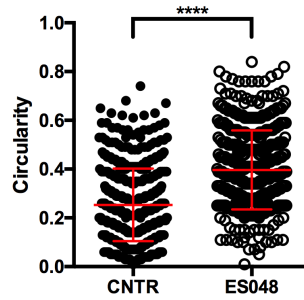


Figure 65: T cell polarisation on endothelia. HBMECs were grown to a confluent monolayer before application of CFSE-labelled T cells which were untreated or treated with ES048 for 2 h. Images were taken, and the T cells' shape was analysed with Fiji software. Each dot represents one cell, lines represent means with standard deviation of $n=3$, approximately 150 cells were analysed per experiment.

The cells were fixed and analysed microscopically by taking images and analysing the shape of approximately 500 T cells with the Fiji software. In the absence of inhibitor, T cells revealed a circularity value of on average 0,25, while NSMi cells significantly retained their round, circular shape (value on average 0,40, Figure 65).

Morphological changes require actin cytoskeleton remodelling. This can be measured by increases of phalloidin binding, a surrogate marker for filamentous actin (F-actin), by flow cytometry. Primary T cells were treated with NSM siRNA to knock down the NSM activity, stimulated with SDF-1 α for 30, 60 and 180 secs, fixed and stained. In control cells (transfected with control siRNA), the F-actin content readily increased with SDF-1 α addition and was retained within the following 30 seconds before it declined to basal levels. In stark contrast, F-actin content only slightly increased in NSM KD cells to levels never approaching those seen in controls (Figure 66).

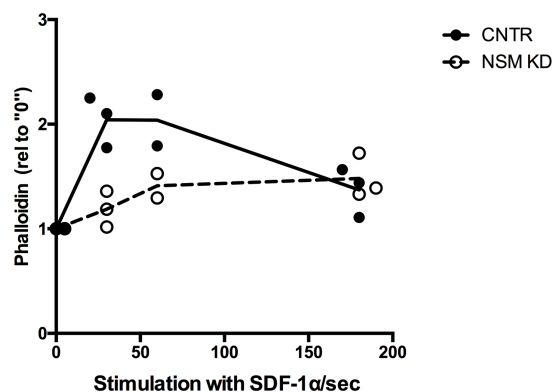


Figure 66: Actin polymerisation. Primary control and NSM KD T cells were stimulated with SDF-1 α for 30 secs, 1 and 3 min, labelled with phalloidin as a marker for F-actin and analysed by FACS. Dots represent data from one experiment, lines the mean of $n=3$.

This indicates that NSM activity is required for remodelling the actin cytoskeleton upon polarising signals. This involves the activity of actin remodelling protein complexes (including small GTPases such as Cdc42), but also that of proteins dynamically linking

the actin cytoskeleton to the plasma membrane (such as the ezrin-radixin-moesin (ERM) proteins).

To evaluate the impact of the NSM on this intracellular organisation the localisation of phospho-ezrin, phospho-moesin and Cdc42 was analysed. Phospho-ezrin and phospho-moesin represent the activated ERM species in T cells which link the actin cytoskeleton to the membrane and usually locate to the uropod in migrating T cells. Cdc42 is found at the leading edge where it organises filopodial extensions; it is crucial for gradient sensing and cell polarisation. To achieve optimal polarisation, control and NSM KD T cells were seeded onto fibronectin for 15 min before fixation and staining. To define the leading edge, cells were co-stained for actin. In control cells, actin-based lamellipodial structures at the leading edge can be clearly discerned from pERM-enriched protrusions at the uropod (Figure 67, left panel).

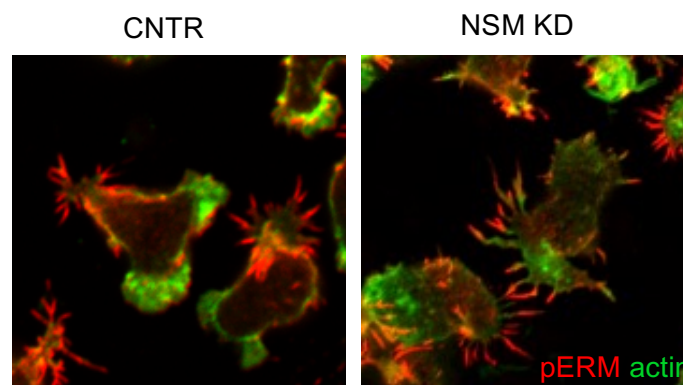


Figure 67: pERM on polarised T cells. Primary control and NSM KD T cells were settled onto FN and stained for pERM (red) and F-actin (green). Images show representative cells for $n=3$ experiments.

In NSM KD, polarisation of both actin and pERM proteins was much less compartmentalised and confined, and in some cells even revealed an overlapping accumulation pattern not restricted to the uropod (see Figure 67, right panel, and Figure 68 for a quantitative assessment).

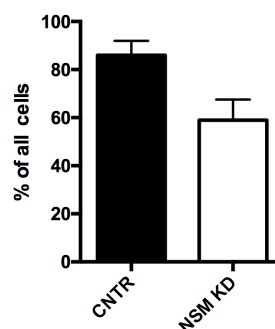


Figure 68: pERM re-localisation in polarised T cells. Primary control and NSM KD T cells were settled onto FN and stained for pERM, pERM re-localisation to the uropod was analysed manually. Graph shows means with standard deviation for $n=3$ independent experiments with approximately 30 cells each.

A similar and even clearer defect was seen for Cdc42 re-localisation which was recruited to the leading edge in only 40% of analysed NSM KD cells (Figure 69).

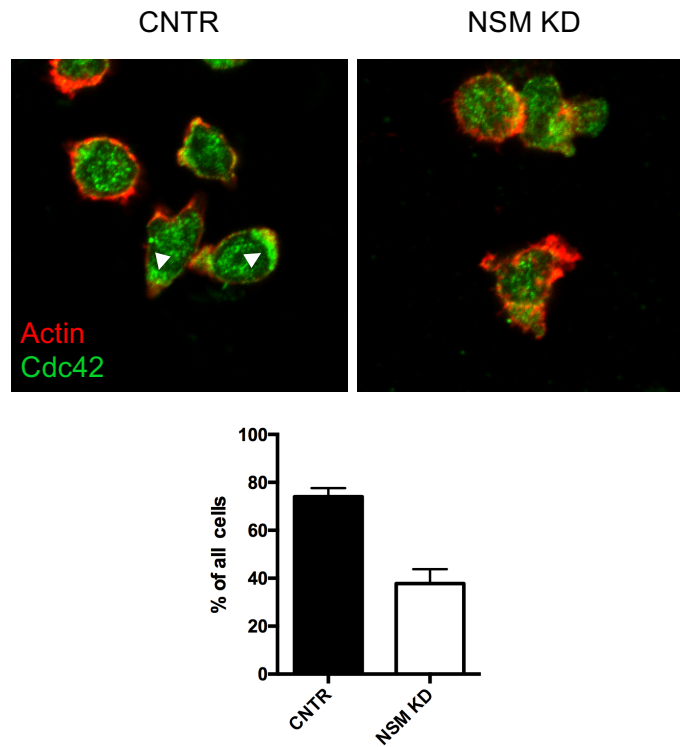


Figure 69: Cdc42 re-localisation in polarised T cells. Primary control and NSM KD T cells were settled onto FN and stained for Cdc42, re-localisation was analysed manually. Arrowheads in the upper image mark Cdc42 accumulation at the rear of the T cell. Images show representative cells, and the graph shows quantification of re-localisation with means and standard deviation for $n=3$ independent experiments with approximately 30 cells each.

5 Discussion

5.1 N₃-ceramides Allow for Analysis of Ceramide Redistribution in Living T cells

In the first part of this thesis the establishment of a working protocol for the labelling of N₃-ceramides in living primary human T cells and Jurkat T cells was shown. N₃-ceramides with terminal alkynes in combination with the cyclooctyne dyes (DIBO 488 and DBCO-Sulfo-Cy5) allowed for the rapid detection and tracing of N₃-ceramides in cells.

Ideally, tools suitable for ceramide labelling should not influence the physicochemical properties of those and not interfere with the T cell functionality. In T cells, the N₃-ceramides did not negatively affect cell viability (Figure 14) or interfere with cell activation (Figure 29 and Figure 30). Parallel to the N₃-ceramides, N-oleyl-serinol has also been tested as ceramide mimicking molecules to image the cell membrane in a variety of cell types, including Jurkat T cells and HBMECs. These also did not exhibit any cell toxicity for either of the cell types at concentrations of 25 µM, while allowing for cell membrane imaging already after 5 min of incorporation time [107].

Lipid-protein interactions often require the entry of lipids into deep binding pockets, a process that is very sensitive to changes within the lipid molecules [109]. Additionally, proteins located in the plasma membrane depend on fluidity, hydrophobicity and curvature of the membrane environment for proper compartmentalisation [110].

Incorporation of N₃-C₆-cer into the outer leaflet of the plasma membrane did not influence SMase activity because they appeared to be co-recruited along with ceramides endogenously generated upon CD28 ligation into ceramide-enriched platforms in T cells (Figure 31). Confirming the specificity of this finding, the clustering of N₃-C₆-cer was not observed on ASM inhibition (Figure 33).

It has been shown that a ceramide surface display is only enhanced after CD28 ligation (induction of ASM activity), but not after CD3 or CD3/CD28 ligation. Co-stimulation even abrogates ASM activity, only retaining NSM activity which is also measurable when CD3 is ligated alone [69]. It is therefore surprising that there is condensation of ceramides in the outer leaflet in co-stimulated or CD3-stimulated cells (see Figure 31) because upon this stimulation ceramide is generated dependent on NSM in the inner

leaflet where the fed ceramides are not likely to localise. This indicates that N_3 - C_6 -cer is actively flipped, and therefore, the enriched domains would be in the inner leaflet. This would require that the modified ceramides, even after the addition of dye are still recognised by the specific proteins which actively flip lipids, as the spontaneous flipping is very slow [111]. Alternatively, N_3 - C_6 -cer condensation occurs in the outer leaflet due to transbilayer communication with ceramides condensing into clusters on the inner leaflet upon NSM activation [112]. To analyse the exact localisation of the ceramides at the inner or the outer leaflet of the membrane the resolution of confocal microscopy is insufficient.

Ceramide compartmentalisation in T cells following APC contact (Figure 35 for T cell/bead conjugates and Figure 36 for T cell/DC conjugates) was in agreement with that shown previously by detection with specific antibodies in T cell/bead conjugates and on planar co-stimulatory surfaces [69]. Ceramide exclusion from the IS centre could result from lateral redistribution towards the IS periphery or via endocytosis. A role of the NSM in the latter process was evidenced in the experiments shown in Figure 37 to Figure 39. There, ablation of the enzyme was associated with increased contact formation between NSM KD T cells and beads (independent of co-stimulation), indicating that the activity of the enzyme is required for regulation of cytoskeletal and membrane dynamics, as well as endocytosis by regulation of the SM/ceramide ratio. This could explain the disappearance of ceramides (along with molecules enriched within these domains), as due to induced SM breakdown at the inner leaflet, ceramides are generated which could favour endocytosis. In fact, ceramide-enriched vesicles were detected proximal to the IS both by antibody detection and by feeding with labelled ceramides (Figure 35, Figure 36 and [69]).

In migrating T cells, studies involving N_3 - C_6 -cer revealed that ceramide-enriched vesicles appeared at the rear of a moving cell (Figure 40); however their origin has not been resolved. Possibly, these represent ceramide-enriched vesicles that were endocytosed at the uropod to deliver membrane molecules to the extending front. The origin and destination of proximal IS and uropod vesicles could be further investigated by detection of Rab family members in more detail. Rabs located at the plasma membrane could be first targets to look at for vesicle characterisation [113]. Especially, Rab5 regulates endocytic internalisation and early endosome fusion, and it might be a candidate for analysis. Altogether 12 Rabs have been localised to the endocytic pathway and could shed light on the question where the ceramide enriched vesicles originate [114].

For the time being, this cannot be addressed using N₃-C₆-cer, as no co-detection with antibody staining is possible due to fixation problems.

The Golgi is the site of high sphingolipid turnover, and it is likely that also the N₃-C₆-cer, which accumulates there, is metabolised at this site (Figure 25) [115]. A similar effect has been shown for other modified ceramides [116, 117].

The N₃-modification of the N₃-C₆-cer would allow for mass-spectrometric analysis of ceramide conversion products, which has, however, not been performed in this study, where rather incorporation rates of N₃-C₆-cer and N₃-C₁₆-cer were determined by lipidomic analysis (Figure 21 and Figure 23). This was possible because the molecules analysed were included into the measurement as standards. For the detection of conversion products, the possible molecules needed to be generated with the N₃ group to be included into the analysis as standards.

Short chain ceramides (C₂, C₄, C₆, C₈) are cell permeable, and are not natural components of the plasma membranes of mammalian cells [118]. Their known toxicity and ability to induce apoptosis are exploited in anti-cancer applications [119]. C₆-cer was indeed found to be toxic in Jurkat T cells at concentrations of 50 μM and higher, but only after incubation times of 6 h to 16 h, even though high C₆-cer concentrations (50 – 100 μM) already slightly increased ROS production 30 min after application [120]. At the concentration (25 μM) used here and for the relatively short timespans (up to 2 h) the N₃-C₆-cer was not toxic (Figure 14). The impact of N₃-C₆-cer on cell viability after long term feeding or long term experiments after N₃-C₆-cer incorporation was not analysed here.

In contrast, NBD-C₆-ceramide proved to be toxic for T cells already after 1 hour (Figure 14 and Figure 24). Because the attached dye is the major difference between the NBD-C₆-ceramide and the N₃-C₆-cer molecules, the role of dye coupling for cell toxicity was addressed. DIBO 488-coupled N₃-C₆-cer did, however, not differ from N₃-C₆-cer with regard to toxicity (Figure 15), indicating that increased toxicity of NBD-C₆-ceramide must result from other molecule-specific attributes.

N₃-C₁₆-cer would be a more physiologic ceramide-analogue to study toxicity and redistribution, but due to its low incorporation rates no extensive analysis was possible (Figure 22 and Figure 23). Prolonged feeding of this compound over night to Jurkat T cells was not toxic, and it was found to accumulate in the cell membrane rather than in the Golgi (Figure 26). As efficient incorporation required long feeding periods, it is possible

that trafficking kinetics of this molecule are also slower, and thus, a Golgi localisation would only show after even longer times.

Additionally, the solubility of N₃-C₆-cer and especially N₃-C₁₆-cer proved to be limited in the aqueous feeding solution (lipidomic analysis, data not shown), which negatively influenced the incorporation efficiency. Increasing the solubility of N₃-C₆-cer by addition of pluronic F-127 to the feeding media improved the uptake rate into primary T cells (Figure 27), showing that solubility is an important issue determining the ceramide uptake. Further on, stimulation-dependent membrane changes impacted on the incorporation of N₃-C₆-cer. High density culture, co-stimulation, and especially contact with co-stimulatory beads enhanced N₃-C₆-cer and also N₃-C₁₆-cer uptake rates into primary T cells (Figure 28). N₃-C₆-cer was taken up by Jurkat T cells more readily than by primary T cells (Figure 21), which could be due to differences in cell size or stimulation-dependent membrane properties. Jurkat T cells are in a constantly pre-stimulated state, as they are an immortalised cell line, and N₃-C₆-cer uptake is increased in the stimulated primary T cells, indicating a role of stimulation-dependent membrane changes in N₃-C₆-cer uptake.

In this part of the study, a novel tool for the analysis of ceramide redistribution in live cell applications was established that is suitable for a detailed analysis of the role ceramides play in the cell function.

5.2 NSM Ablation

In this study NSM function was reduced in primary T cells either by siRNA mediated knockdown or treatment with the NSM inhibitors GW4869 or ES048.

The knockdown efficiency of the NSM varied between T cells from different donors from about 50 to 70 % (representative assay shown in Figure 8). Therefore, a residual NSM activity of 50 to 30 % was always retained in the assays, and it reduced the measurable effect of NSM ablation.

When treating cells with chemical compounds to inhibit enzyme function, off-target effects always have to be taken into account, as the specificity for the target enzyme may be strongly dose-dependent. Also, the control cells were only treated with a solvent control, but not with a molecule mimicking possible unspecific effects, as done when transfecting control T cells with scrambled siRNA. For the *in vivo* transfer experiment, the inhibitor was washed away before transfer into the mice, and over time the

effect vanishes (Figure 51), which may have masked an effect of NSM inhibition also in the long term (16 h) experiment.

5.3 NSM in T Cell Polarisation

2D and 3D migration experiments revealed a role for the NSM in directional T cell movement (Figure 42 and Figure 48). For directional migration, T cells need to sense a chemokine gradient and polarise the respective receptors towards the source of the attractant (its highest concentration) to receive spatially organised signals [121]. Overall cell surface expression of CXCR4 was unaffected upon NSM KD (Figure 55), but organisation towards the leading edge of the cell was inefficient (Figure 56 and Figure 57). Still, the signalling after SDF-1 α binding (Src-kinase- and Erk 1/2-phosphorylation, Figure 59) was not influenced by NSM ablation. Therefore, it is likely, that T cells are able to sense the chemokine gradient and relay receptor signalling; they can, however, not transform this information in a spatially meaningful way because the signal is not received in a polarised manner. Additionally, this lack of spatial signalling information might also translate into non-polarised actin dynamics in the absence of NSM activity. This is evident by the formation of extensive protrusions from the entire cell body rather than by visible cell polarisation and organisation of a lamellipodium at the leading edge, as revealed by F-actin detection (Figure 67).

NSM activity impacts TCR signalling, and NSM inhibition leads to T cell hyperactivity, revealing that the NSM can directly influence signalling pathways [69]. While the NSM is activated upon TCR engagement, this is not the case for CXCR4 signalling (Figure 58). Apparently, membrane receptor organisation relies on basal rather than stimulated NSM activity in polarising and migrating T cells. The lipid composition of the plasma membrane plays a role for receptor compartmentalisation. As it was recently shown that cholesterol directly modulates the chemokine receptor function [122], it is possible that organisation of steady state membrane domains enriched in ceramide might influence receptor organisation. It is also possible that not only large-scale receptor organisation might influence the T cell response, but also microdomain organisation of CXCR4. CXCR4 forms dimers upon SDF-1 α binding, and this allows for optimal downstream signalling [123]. To enable homodimer formation, the receptor needs to be spatially organised in such a way that single molecules are in close lateral proximity. No evidence for disturbed association of CXCR4 with membrane-microdomains was ob-

tained by floatation analysis (not shown). The resolution of lipid raft analysis is, however, limited, and therefore, the application of methodology allowing for nanodomain analysis would be required in order to reveal or discard a role of the NSM in the organisation of CXCR4 nanodomains.

Not only CXCR4 redistribution was reduced by NSM ablation, but also the front/rear polarisation of pERM (Figure 67 and Figure 68) and Cdc42 (Figure 69). Ezrin, radixin and moesin link membrane domains to the actin cytoskeleton, and Cdc42 is directly involved in actin polymerisation. The organisation of pERM to the rear [124] and Cdc42 to the leading edge [125] of T cells is crucial for polarisation and actin polymerisation to enable T cell locomotion. In line with this reduced compartmentalisation of members of the actin polymerisation machinery, F-actin formation itself was lower in NSM KD T cells following SDF-1 α stimulation (Figure 66).

Actin dynamic is needed for cell movement especially in confined environments, as shown in an “under agarose assay” with latrunculin A treated T cells. The inhibitor prevents actin assembly, and the so treated T cells were still able to move through nanogrooves without confinement, but the cells were nearly non-motile in a confined agarose environment [126]. Indicating a direct impact of the NSM on actin dynamics, the radius of T cell movement after NSM inhibition in dense collagen matrices was considerably reduced compared to control cells (Figure 50). Overall, T cell polarisation and cytoskeletal organisation seem to depend on basal NSM function, which is also reflected by the lack of gross morphological changes of NSM KD T cells settled onto HBMEC cells (Figure 65).

5.4 Adhesion and Transendothelial Migration

The formation of a polarised phenotype of T cells settled onto endothelial cells was reduced upon NSM ablation (Figure 65), possibly as a result of diminished actin reorganisation and front/rear polarisation. How this affects the T cell movement through an organism, which requires not only directional movement but also adhesion to and migration through endothelia, was analysed *in vitro* and *in vivo*.

In vivo transfer of control and NSM inhibitor treated (NSMi) T cells revealed a role for the NSM in steady-state homing into secondary lymphoid organs. 16 h after T cell transfer, equal amounts of control and NSMi T cells had reached the spleen and the LNs of WT acceptor mice (Figure 53). This shows that the treatment of the T cells

(inhibitor/solvent and CFSE/eFluor 670 labelling) did not affect cell viability and movement capacity of the cells, but also did not reveal an impact of NSM inhibition in this process. The effect of NSM inhibition on T cell migration became evident in the short-term analysis performed 1 h after transfer. In the blood, equal amounts of control and NSMi T cells were present, but NSMi T cells reached the spleen and especially the LNs less efficiently (Figure 54). The difference in the spleen was less pronounced than in LNs, possibly because the entry into the spleen is not restricted, while for entry into LNs T cells have to cross the endothelium of the high endothelial venule (HEV) [45, 46, 49]. The lack of a difference after 16 h might be due to a vanishing effect of NSM inhibition, which, at least *in vitro*, was still measurable at this time point (Figure 51). More likely, in spite of their reduced motility, NSMi T cells might finally reach their destination when given sufficient time to catch up with their unmodified controls.

For homing into the LN, the T cells move through the lymphatic vessels to the LN; there they need to adhere to the endothelium and transmigrate. For the analysis of T cells in the LNs, the whole organs were isolated and processed for flow cytometric analysis. Hence, no data about T cell localisation within the organ is available, addressing the question if NSMi T cells after crossing the HEV entered the cortex or moved into wrong LN compartments, and whether different subpopulations reached their correct destination within the organ. In future experiments, parts of the LNs should be processed for histochemical analysis to allow a detailed topological analysis of the entry of T cell subsets into the LN.

Adhesion and TEM were analysed independently in *in vitro* assays using HBMECs in resting and inflamed state to define a potential role of the NSM. Control and NSMi T cells adhered equally well to the resting endothelium. It was only in the inflamed situation that the control cells showed an increased adhesion. This was not seen with NSMi cells (Figure 45).

As evident from a more detailed analysis, the NSM appeared to impact adhesion, possibly through its crucial function for LFA-1 clustering, which is nearly completely absent in NSM KD T cells (Figure 62 and Figure 63). LFA-1 function has been shown to be sensitive to the plasma membrane lipid-nano-environment, and the ceramide content proved to be especially important for integrin mobility and ligand encounter [101].

On the inflamed endothelium, adhesion receptors like ICAM-1 are upregulated on the surface (Figure 11) to increase efficient T cell adhesion and thereby recruitment to the site of inflammation [127]. To respond to this increased ICAM-1 expression, the LFA-

1 on the T cells needs to be clustered and to be stabilised in its high affinity conformation [128]. Overall levels of high affinity (but not total) LFA-1 were substantially reduced on the surface of NSM KD T cells (Figure 60), as was their clustering upon adherence to inflamed HBMECs (Figure 62 and Figure 63). This finding indicates that NSM is required for outside-in signalling of LFA-1 which, being the major integrin for T cell adhesion, explains the reduced adhesion to the stimulated HBMECs. How this is exerted mechanistically, can only be speculated. The regulation of the LFA-1 conformation is directly linked to actin dynamics via talin. Interactions between the α - and the β -chains of LFA-1 stabilise the molecule in its bent conformation; upon talin binding to the β -chain this interaction is relieved, and LFA-1 unfolds to expose the ligand binding domain. Talin is the prime regulator for this process, as it has been shown that talin overexpression results in a majority of LFA-1 molecules to switch into their open conformation [129]. Talin also is an actin cross-linking protein, and so it relays changes in the cytoskeletal dynamics, as occurring in NSM ablation, to integrin function [130]. Whether talin itself is subject to changes in the lipid membrane domain composition is yet unknown.

As several experiments showed a role for the NSM in receptor organisation, polarisation and actin dynamics, it was a surprising finding that TEM through the resting endothelium did not change upon NSM inhibition in neither the resting nor the inflamed environment. It appeared, however, that ASM function in T cells is needed for TEM in the resting and the inflamed state, as in both situations the efficiency of T cell crossing of the HBMEC cell layer was significantly reduced upon ASM inhibition (Figure 46). Interestingly, ASM activity in endothelial cells was also required for efficient transmigration [131], and it would be interesting to see whether NSM would also be dispensable in endothelial cells for T cell transmigration.

For diapedesis, protrusion formation, pushing of the leading edge under the epithelium and nucleus lobulation is needed [35, 36], and apparently at least one of these processes is sensitive for the sphingolipid composition of the outer leaflet of the plasma membrane. The different impact of the NSM and the ASM on the two processes of adhesion and transmigration may be due to the different cytoskeletal mechanisms involved. Migratory T cells show a lamellipodia/uropod-based phenotype which is converted into a blebbing/transmigratory phenotype by microtubule depolymerisation and increased RhoA/ROCK activity [132]. The NSM proved to be important for the organisation of both the lamellipodium and the uropod (as shown for LFA-1, pERM and

Cdc42 organisation: Figure 60 - Figure 63 and Figure 67 - Figure 69), and therefore impacts both migration and adhesion. While for directional migration especially the lamellipodia formation and receptor organisation in the front is important, for transmigration, cells need to generate a pushing force to scan the endothelium and find spots suitable for TEM (e.g., not through the endothelial cell's nucleus) [133], form invasive podosomes [36] and contract their uropod to fulfil the process. The final step is initiated by microtubule depolymerisation, which causes the release of Rho-GEF-H1, activating RhoA and ROCK, and therefore enhances cell contractility [134, 135].

Ceramide-enriched regions in the outer leaflet have been associated with the induction of membrane curvature, promoting formation of membrane invaginations [89]. It is possible that ceramide-enriched domains generated by the ASM are needed to enable the cell to extensively deform the membrane and to also allow for rapid retraction of the uropod by regulating endocytosis of surplus membrane parts. ASM-generated ceramides have been shown to abrogate the formation of actin-based extensions, as shown for murine WT and Asm KO T cells seeded onto FN. WT T cells form surface protrusions which are increased in Asm KO cells, but SMase activation upon MV contact induced a loss of these membrane ruffles in WT cells. The same loss of membrane extensions was observed after bSMase treatment or feeding of C₁₆-ceramides [103]. In TEM for uropod retraction actin extensions also need to collapse in a locally defined space; this might be regulated by local ASM activity.

As the impact of the ASM did not depend on the status of the endothelium (resting or inflamed), it most likely does not relate to receptor organisation, as this would have an increased effect on the migration under inflamed conditions. The *in vivo* assays were performed under resting conditions, and the *in vitro* assays showed no impact of NSM inhibition without an inflamed endothelium. The effects seen in the *in vivo* assay therefore only reflect consequences of defective directional migration. In animal experiments including an inflammatory stimulus and the resulting recruitment of effector T cells into the tissue, NSM inhibition will probably have a higher impact, as enhanced T cell adhesion to the inflamed endothelium depends on the NSM function, and so control cells will increasingly be recruited into the tissue, but NSMi cells cannot respond to this stimulus.

6 Summary

Sphingolipids are important components of the plasma membrane, and among them ceramides both serve as building hubs for complex sphingolipids and also organise membrane domains crucial for receptor organisation. Especially in T cells, ceramide-enriched membrane microdomains are known to modulate TCR signalling.

This study describes the application of a novel azido-functionalised ceramide, allowing for bio-orthogonal click-reactions to fluorescent labels and thereby live tracking of incorporated ceramides. T cell activation was not influenced after uptake of the compound. It was shown that N₃-C₆-cer was incorporated into the plasma membrane and localised into microdomains formed in response to ASM activation after CD28 ligation. In agreement with previous antibody-based findings in fixed cells, N₃-C₆-cer was excluded from the centre of the immune synapse formed between T cells and beads or DCs. N₃-C₆-cer concentrated at the rear of migrating T cells, but did not inhibit their movement, underscoring the potency of this novel tool to study the subcellular redistribution of ceramides in live cell applications.

SMases not only directly influence the plasma membrane sphingolipid composition, but also impact cytoskeletal dynamics, cell polarisation and receptor organisation. The NSM has already proven to be important for T cell activation and now showed to regulate directed T cell migration and adhesion. *In vivo* NSM inhibition reduced early lymph node homing of T cells. Detailed *in vitro* analysis revealed that basal NSM activity is needed for directional T cell motility in response to SDF-1 α , especially in confined environments. It was important for T cell polarisation, including redistribution of CXCR4 and pERM proteins on HBMECs or FN, and for F-actin polymerisation upon SDF-1 α stimulation. Additionally, adhesion to the endothelium and integrin affinity maturation, as well as LFA-1 compartmentalisation on TNF α /IFN γ stimulated HBMECs depended on NSM function. Finally, proper ASM function showed to be needed for transendothelial migration, whereas NSM function was dispensable.

Altogether, this study reveals the central role of SMases in T cell migration under resting and inflamed conditions. NSM function regulates polarised redistribution of receptors and cytoskeletal components, allowing for directed migration and adhesion.

7 Zusammenfassung

Sphingolipide sind wichtige Komponenten der Plasmamembran, und besonders Ceramid stellt das Grundgerüst für komplexere Sphingolipide dar. Darüber hinaus bildet Ceramid Mikrodomänen aus, die für die Organisation von Rezeptoren, z. B. dem T-Zell-Rezeptorkomplex entscheidend sind und somit die Funktion von T-Zellen beeinflussen.

In dieser Arbeit wurden neue azid-funktionalisierte Ceramide angewendet, die durch eine bio-orthogonale Click-Reaktion mit fluoreszenten Farbstoffmolekülen kovalent verbunden werden können. Dies ermöglicht die live-Verfolgung der Ceramide durch lebende und auch stimulierte Zellen, da die Aktivierbarkeit von T-Zellen durch die Zufütterung nicht beeinflusst wurde. Es konnte gezeigt werden, dass N_3 - C_6 -cer in die Plasmamembran interkaliert und sich in Mikrodomänen, die durch eine Aktivierung der ASM nach CD28 Bindung entstehen, bewegt. Darüber hinaus wurde N_3 - C_6 -cer aus dem Zentrum der immunologischen Synapse zwischen T-Zellen und dendritischen Zellen oder Mikrokügelchen ausgeschlossen, wie zuvor in fixierten und mit Antikörper gefärbten T-Zellen gezeigt wurde. In migrierenden T-Zellen sammelte sich das N_3 - C_6 -cer am hinteren Ende der Zelle und beeinflusste die Bewegung der Zellen nicht. Dies unterstreicht die Anwendbarkeit dieser neuen Methode, um die subzelluläre Verteilung von Ceramiden in Lebendzell-Experimenten zu untersuchen.

Sphingomyelinasen beeinflussen durch ihre Funktion die Verhältnisse von Sphingolipiden in der Plasmamembran und haben so Einfluss auf die Zytoskelettdynamik, die Zellpolarisation und die Rezeptororganisation. Es wurde bereits zuvor gezeigt, dass die neutrale Sphingomyelinase wichtig ist für die T-Zellaktivierung. Nun wurde darüber hinaus ihre Rolle in der gerichteten Migration und Adhäsion dargestellt. *In vivo* Hemmung der NSM reduzierte die frühe Wanderung von T-Zellen in die Lymphknoten, und detaillierte *in vitro* Analysen zeigten, dass die basale Aktivität der neutralen Sphingomyelinase für die gerichtete Migration entlang eines SDF-1 α -Gradienten notwendig ist. Darüber hinaus ist ihre Funktion wichtig für die T-Zell Polarisierung und hier besonders die Organisation von CXCR4 und pERM. Außerdem spielt die neutralen Sphingomyelinase eine Rolle in der Polymerisierung von F-Aktin nach einer Stimulation der T-Zellen mit SDF-1 α . Auch die Adhäsion an das TNF α /IFN γ -stimulierte Endothel sowie

die Ausbildung und Organisation der offenen Form von LFA-1 hängen von der neutralen Sphingomyelinase ab. Für den Prozess der Transmigration war im Gegensatz hierzu nur die Funktion der sauren Sphingomyelinase von Bedeutung.

Zusammenfassend konnte in dieser Arbeit die zentrale Rolle der Sphingomyelinasen für die T-Zell-Migration im ruhenden und stimulierten Zustand gezeigt werden. Die neutrale Sphingomyelinase reguliert die polarisierte Organisation von Rezeptoren und Zytoskelett-Komponenten, welche für eine gerichtete Migration und Adhäsion unabhängig sind.

8 Bibliography

1. Gaublomme, J.T., et al., *Single-Cell Genomics Unveils Critical Regulators of Th17 Cell Pathogenicity*. Cell, 2015. **163**(6): p. 1400-12.
2. Starr, T.K., S.C. Jameson, and K.A. Hogquist, *Positive and negative selection of T cells*. Annu Rev Immunol, 2003. **21**: p. 139-76.
3. Kurd, N. and E.A. Robey, *T-cell selection in the thymus: a spatial and temporal perspective*. Immunological Reviews, 2016. **271**(1): p. 114-126.
4. Sprent, J., et al., *T cell homeostasis*. Immunol Cell Biol, 2008. **86**(4): p. 312-319.
5. Erard, F. and G. Le Gros, *Th2-like CD8 T cells: Their role in protection against infectious diseases*. Parasitology Today, 1994. **10**(8): p. 313-315.
6. Conti, L., et al., *Role of the cytokine environment and cytokine receptor expression on the generation of functionally distinct dendritic cells from human monocytes*. European Journal of Immunology, 2008. **38**(3): p. 750-762.
7. Zlotnik, A., O. Yoshie, and H. Nomiya, *The chemokine and chemokine receptor superfamilies and their molecular evolution*. Genome Biol, 2006. **7**(12): p. 243.
8. Moser, B., et al., *Chemokines: multiple levels of leukocyte migration control*. Trends Immunol, 2004. **25**(2): p. 75-84.
9. Griffith, J.W., C.L. Sokol, and A.D. Luster, *Chemokines and chemokine receptors: positioning cells for host defense and immunity*. Annu Rev Immunol, 2014. **32**: p. 659-702.
10. Förster, R., A. Braun, and T. Worbs, *Lymph node homing of T cells and dendritic cells via afferent lymphatics*. Trends in Immunology, 2012. **33**(6): p. 271-280.
11. Lorenz, N., et al., *Plasmin and regulators of plasmin activity control the migratory capacity and adhesion of human T cells and dendritic cells by regulating cleavage of the chemokine CCL21*. Immunol Cell Biol, 2016. **94**(10): p. 955-963.
12. Arimont, M., et al., *Structural Analysis of Chemokine Receptor-Ligand Interactions*. Journal of Medicinal Chemistry, 2017.
13. Nombela-Arrieta, C., et al., *A central role for DOCK2 during interstitial lymphocyte motility and sphingosine-1-phosphate-mediated egress*. The Journal of Experimental Medicine, 2007. **204**(3): p. 497-510.
14. Sai, J., et al., *Parallel phosphatidylinositol 3-kinase (PI3K)-dependent and Src-dependent pathways lead to CXCL8-mediated Rac2 activation and chemotaxis*. J Biol Chem, 2008. **283**(39): p. 26538-47.
15. Hesselgesser, J., et al., *Identification and Characterization of the CXCR4 Chemokine Receptor in Human T Cell Lines: Ligand Binding, Biological Activity, and HIV-1 Infectivity*. The Journal of Immunology, 1998. **160**(2): p. 877-883.
16. Tachibana, K., et al., *The chemokine receptor CXCR4 is essential for vascularization of the gastrointestinal tract*. Nature, 1998. **393**(6685): p. 591-594.
17. Busillo, J.M. and J.L. Benovic, *Regulation of CXCR4 signaling*. Biochim Biophys Acta, 2007. **1768**(4): p. 952-63.
18. Ward, S.G., *T lymphocytes on the move: chemokines, PI 3-kinase and beyond*. Trends in Immunology, 2006. **27**(2): p. 80-87.
19. Geiselhart, L.A., et al., *IL-7 Administration Alters the CD4:CD8 Ratio, Increases T Cell Numbers, and Increases T Cell Function in the Absence of Activation*. The Journal of Immunology, 2001. **166**(5): p. 3019-3027.
20. Prabhu, N., et al., *Gamma interferon regulates contraction of the influenza virus-specific CD8 T cell response and limits the size of the memory population*. J Virol, 2013. **87**(23): p. 12510-22.
21. Zhang, X., et al., *Tissue trafficking patterns of effector memory CD4+ T cells in rheumatoid arthritis*. Arthritis & Rheumatism, 2005. **52**(12): p. 3839-3849.

22. Huang, M.-T., et al., *ICAM-2 mediates neutrophil transmigration in vivo: evidence for stimulus specificity and a role in PECAM-1-independent transmigration*. *Blood*, 2006. **107**(12): p. 4721-4727.
23. *T Lymphocyte-Endothelial Cell Interactions*. Annual Review of Immunology, 2004. **22**(1): p. 683-709.
24. Abbassi, O., et al., *Neutrophil adhesion to endothelial cells*. *Blood Cells*, 1993. **19**(2): p. 245-59; discussion 259-60.
25. Abbassi, O., et al., *E-selectin supports neutrophil rolling in vitro under conditions of flow*. *J Clin Invest*, 1993. **92**(6): p. 2719-30.
26. Jones, D.A., et al., *P-selectin mediates neutrophil rolling on histamine-stimulated endothelial cells*. *Biophys J*, 1993. **65**(4): p. 1560-9.
27. Strazza, M., et al., *PLCepsilon1 regulates SDF-1alpha-induced lymphocyte adhesion and migration to sites of inflammation*. *Proc Natl Acad Sci U S A*, 2017.
28. Cannon, J.L., et al., *PKCtheta regulates T cell motility via ezrin-radixin-moesin localization to the uropod*. *PLoS One*, 2013. **8**(11): p. e78940.
29. Luster, A.D., R. Alon, and U.H. von Andrian, *Immune cell migration in inflammation: present and future therapeutic targets*. *Nat Immunol*, 2005. **6**(12): p. 1182-90.
30. Shulman, Z., et al., *Lymphocyte crawling and transendothelial migration require chemokine triggering of high-affinity LFA-1 integrin*. *Immunity*, 2009. **30**(3): p. 384-96.
31. Cernuda-Morollon, E., S. Gharbi, and J. Millan, *Discriminating between the paracellular and transcellular routes of diapedesis*. *Methods Mol Biol*, 2010. **616**: p. 69-82.
32. Ostermann, G., et al., *JAM-1 is a ligand of the beta(2) integrin LFA-1 involved in transendothelial migration of leukocytes*. *Nat Immunol*, 2002. **3**(2): p. 151-8.
33. Millan, J., et al., *Lymphocyte transcellular migration occurs through recruitment of endothelial ICAM-1 to caveola- and F-actin-rich domains*. *Nat Cell Biol*, 2006. **8**(2): p. 113-123.
34. Barzilai, S., et al., *Leukocytes Breach Endothelial Barriers by Insertion of Nuclear Lobes and Disassembly of Endothelial Actin Filaments*. *Cell Rep*, 2017. **18**(3): p. 685-699.
35. Rottenstreich, A., et al., *Active malignancy in patients with renal vein thrombosis: influence upon clinical course and survival*. *Clin Exp Nephrol*, 2017. **21**(1): p. 49-54.
36. Carman, C.V., et al., *Transcellular diapedesis is initiated by invasive podosomes*. *Immunity*, 2007. **26**(6): p. 784-97.
37. Skau, C.T. and C.M. Waterman, *Specification of Architecture and Function of Actin Structures by Actin Nucleation Factors*. *Annu Rev Biophys*, 2015. **44**: p. 285-310.
38. Blanchoin, L., et al., *Actin dynamics, architecture, and mechanics in cell motility*. *Physiol Rev*, 2014. **94**(1): p. 235-63.
39. Machesky, L.M. and R.H. Insall, *Scar1 and the related Wiskott-Aldrich syndrome protein, WASP, regulate the actin cytoskeleton through the Arp2/3 complex*. *Curr Biol*, 1998. **8**(25): p. 1347-56.
40. Pollard, T.D. and J.A. Cooper, *Actin, a Central Player in Cell Shape and Movement*. *Science*, 2009. **326**(5957): p. 1208-1212.
41. Gomez-Mouton, C., et al., *Segregation of leading-edge and uropod components into specific lipid rafts during T cell polarization*. *Proc Natl Acad Sci U S A*, 2001. **98**(17): p. 9642-7.
42. Nordenfelt, P., H.L. Elliott, and T.A. Springer, *Coordinated integrin activation by actin-dependent force during T-cell migration*. *Nat Commun*, 2016. **7**: p. 13119.
43. Cueni, L.N. and M. Detmar, *The lymphatic system in health and disease*. *Lymphat Res Biol*, 2008. **6**(3-4): p. 109-22.
44. Baluk, P., et al., *Functionally specialized junctions between endothelial cells of lymphatic vessels*. *The Journal of Experimental Medicine*, 2007. **204**(10): p. 2349-2362.
45. Girard, J.-P., C. Moussion, and R. Forster, *HEVs, lymphatics and homeostatic immune cell trafficking in lymph nodes*. *Nat Rev Immunol*, 2012. **12**(11): p. 762-773.

46. Teijeira, A., et al., *T Cell Migration from Inflamed Skin to Draining Lymph Nodes Requires Intralymphatic Crawling Supported by ICAM-1/LFA-1 Interactions*. Cell Rep, 2017. **18**(4): p. 857-865.
47. Forster, R., A.C. Davalos-Miszlitz, and A. Rot, *CCR7 and its ligands: balancing immunity and tolerance*. Nat Rev Immunol, 2008. **8**(5): p. 362-371.
48. Schwab, S.R. and J.G. Cyster, *Finding a way out: lymphocyte egress from lymphoid organs*. Nat Immunol, 2007. **8**(12): p. 1295-1301.
49. Manevich-Mendelson, E., et al., *Talin1 is required for integrin-dependent B lymphocyte homing to lymph nodes and the bone marrow but not for follicular B-cell maturation in the spleen*. Blood, 2010. **116**(26): p. 5907-5918.
50. Ruddle, N.H. and E.M. Akirav, *Secondary lymphoid organs: responding to genetic and environmental cues in ontogeny and the immune response*. J Immunol, 2009. **183**(4): p. 2205-12.
51. Airola, M.V. and Y.A. Hannun, *Sphingolipid metabolism and neutral sphingomyelinases*. Handb Exp Pharmacol, 2013(215): p. 57-76.
52. El Alwani, M., et al., *Bioactive sphingolipids in the modulation of the inflammatory response*. Pharmacol Ther, 2006. **112**(1): p. 171-83.
53. Ogretmen, B. and Y.A. Hannun, *Biologically active sphingolipids in cancer pathogenesis and treatment*. Nat Rev Cancer, 2004. **4**(8): p. 604-616.
54. Mesmin, B., et al., *A Four-Step Cycle Driven by PI(4)P Hydrolysis Directs Sterol/PI(4)P Exchange by the ER-Golgi Tether OSBP*. Cell, 2013. **155**(4): p. 830-843.
55. Hanada, K., et al., *Molecular machinery for non-vesicular trafficking of ceramide*. Nature, 2003. **426**(6968): p. 803-809.
56. Sugiki, T., et al., *Structural basis for the Golgi association by the pleckstrin homology domain of the ceramide trafficking protein (CERT)*. J Biol Chem, 2012. **287**(40): p. 33706-18.
57. Kitatani, K., J. Idkowiak-Baldys, and Y.A. Hannun, *The sphingolipid salvage pathway in ceramide metabolism and signaling*. Cell Signal, 2008. **20**(6): p. 1010-8.
58. Kim, M.Y., et al., *Identification of sphingomyelin turnover as an effector mechanism for the action of tumor necrosis factor alpha and gamma-interferon. Specific role in cell differentiation*. J Biol Chem, 1991. **266**(1): p. 484-9.
59. Tepper, A.D., et al., *Effect of Overexpression of a Neutral Sphingomyelinase on CD95-Induced Ceramide Production and Apoptosis*. Biochemical and Biophysical Research Communications, 2001. **280**(3): p. 634-639.
60. Piccinini, M., et al., *Deregulated sphingolipid metabolism and membrane organization in neurodegenerative disorders*. Mol Neurobiol, 2010. **41**(2-3): p. 314-40.
61. Boini, K.M., et al., *Sphingolipids in obesity and related complications*. Front Biosci (Landmark Ed), 2017. **22**: p. 96-116.
62. Pasternack, D.A., et al., *Sphingosine Kinase Regulates Microtubule Dynamics and Organelle Positioning Necessary for Proper G1/S Cell Cycle Transition in Trypanosoma brucei*. MBio, 2015. **6**(5): p. e01291-15.
63. Jacobi, J., et al., *Targeting acid sphingomyelinase with anti-angiogenic chemotherapy*. Cell Signal, 2017. **29**: p. 52-61.
64. Bollinger, C.R., V. Teichgraber, and E. Gulbins, *Ceramide-enriched membrane domains*. Biochim Biophys Acta, 2005. **1746**(3): p. 284-94.
65. Rajagopalan, V., et al., *Critical determinants of mitochondria-associated neutral sphingomyelinase (MA-nSMase) for mitochondrial localization*. Biochimica et Biophysica Acta (BBA) - General Subjects, 2015. **1850**(4): p. 628-639.
66. Milhas, D., et al., *Anterograde and retrograde transport of neutral sphingomyelinase-2 between the Golgi and the plasma membrane*. Biochimica et Biophysica Acta (BBA) - Molecular and Cell Biology of Lipids, 2010. **1801**(12): p. 1361-1374.
67. Tonnetti, L., et al., *A Role for Neutral Sphingomyelinase-mediated Ceramide Production in T Cell Receptor-induced Apoptosis and Mitogen-activated Protein Kinase-mediated Signal Transduction*. The Journal of Experimental Medicine, 1999. **189**(10): p. 1581-1589.

68. Avota, E., E. Gulbins, and S. Schneider-Schaulies, *DC-SIGN mediated sphingomyelinase-activation and ceramide generation is essential for enhancement of viral uptake in dendritic cells*. PLoS Pathog, 2011. **7**(2): p. e1001290.
69. Mueller, N., et al., *Neutral sphingomyelinase in physiological and measles virus induced T cell suppression*. PLoS Pathog, 2014. **10**(12): p. e1004574.
70. Singer, S.J. and G.L. Nicolson, *The Fluid Mosaic Model of the Structure of Cell Membranes*. Science, 1972. **175**(4023): p. 720-731.
71. Simons, K. and E. Ikonen, *Functional rafts in cell membranes*. Nature, 1997. **387**(6633): p. 569-572.
72. Salaün, C., D.J. James, and L.H. Chamberlain, *Lipid Rafts and the Regulation of Exocytosis*. Traffic (Copenhagen, Denmark), 2004. **5**(4): p. 255-264.
73. Fujiwara, T., et al., *Phospholipids undergo hop diffusion in compartmentalized cell membrane*. The Journal of Cell Biology, 2002. **157**(6): p. 1071-1082.
74. Karnovsky, M.J., et al., *The concept of lipid domains in membranes*. J Cell Biol, 1982. **94**(1): p. 1-6.
75. Bian, F., et al., *Lipid rafts, ceramide and molecular transcytosis*. Front Biosci (Landmark Ed), 2016. **21**: p. 806-38.
76. Brown, D.A. and J.K. Rose, *Sorting of GPI-anchored proteins to glycolipid-enriched membrane subdomains during transport to the apical cell surface*. Cell, 1992. **68**(3): p. 533-44.
77. Munro, S., *Lipid Rafts: Elusive or Illusive?* Cell, 2003. **115**(4): p. 377-388.
78. Miyaji, M., et al., *Role of membrane sphingomyelin and ceramide in platform formation for Fas-mediated apoptosis*. The Journal of Experimental Medicine, 2005. **202**(2): p. 249-259.
79. Cremesti, A., et al., *Ceramide enables fas to cap and kill*. J Biol Chem, 2001. **276**(26): p. 23954-61.
80. Grassme, H., et al., *CD95 signaling via ceramide-rich membrane rafts*. J Biol Chem, 2001. **276**(23): p. 20589-96.
81. Mateos-Gil, P., et al., *Super-Resolution Imaging of Plasma Membrane Proteins with Click Chemistry*. Front Cell Dev Biol, 2016. **4**: p. 98.
82. Erdmann, R.S., et al., *Super-resolution imaging of the Golgi in live cells with a bioorthogonal ceramide probe*. Angew Chem Int Ed Engl, 2014. **53**(38): p. 10242-6.
83. Bhabak, K.P., et al., *Development of a novel FRET probe for the real-time determination of ceramidase activity*. Chembiochem, 2013. **14**(9): p. 1049-52.
84. Peyrot, S.M., et al., *Tracking the subcellular fate of 20(s)-hydroxycholesterol with click chemistry reveals a transport pathway to the Golgi*. J Biol Chem, 2014. **289**(16): p. 11095-110.
85. Hoglinger, D., et al., *Trifunctional lipid probes for comprehensive studies of single lipid species in living cells*. Proc Natl Acad Sci U S A, 2017. **114**(7): p. 1566-1571.
86. Glebov, O.O. and B.J. Nichols, *Lipid raft proteins have a random distribution during localized activation of the T-cell receptor*. Nat Cell Biol, 2004. **6**(3): p. 238-243.
87. Viola, A., et al., *T lymphocyte costimulation mediated by reorganization of membrane microdomains*. Science, 1999. **283**(5402): p. 680-2.
88. Andrews, N.W., P.E. Almeida, and M. Corrotte, *Damage control: cellular mechanisms of plasma membrane repair*. Trends Cell Biol, 2014. **24**(12): p. 734-42.
89. Draeger, A., et al., *Dealing with damage: plasma membrane repair mechanisms*. Biochimie, 2014. **107 Pt A**: p. 66-72.
90. Antonucci, F., et al., *Microvesicles released from microglia stimulate synaptic activity via enhanced sphingolipid metabolism*. EMBO J, 2012. **31**(5): p. 1231-40.
91. Herz, J., et al., *Acid sphingomyelinase is a key regulator of cytotoxic granule secretion by primary T lymphocytes*. Nat Immunol, 2009. **10**(7): p. 761-8.
92. Li, X., E. Gulbins, and Y. Zhang, *Oxidative stress triggers Ca-dependent lysosome trafficking and activation of acid sphingomyelinase*. Cell Physiol Biochem, 2012. **30**(4): p. 815-26.
93. Trajkovic, K., et al., *Ceramide triggers budding of exosome vesicles into multivesicular endosomes*. Science, 2008. **319**(5867): p. 1244-7.

94. Kosaka, N., et al., *Secretory mechanisms and intercellular transfer of microRNAs in living cells*. J Biol Chem, 2010. **285**(23): p. 17442-52.
95. Schneider, B., et al., *Lipid microdomain-dependent macropinocytosis determines compartmentation of Afipia felis*. Traffic, 2007. **8**(3): p. 226-40.
96. Anes, E., et al., *Selected lipids activate phagosome actin assembly and maturation resulting in killing of pathogenic mycobacteria*. Nat Cell Biol, 2003. **5**(9): p. 793-802.
97. Utermohlen, O., et al., *Fusogenicity of membranes: the impact of acid sphingomyelinase on innate immune responses*. Immunobiology, 2008. **213**(3-4): p. 307-14.
98. Goswami, D., et al., *Nanoclusters of GPI-Anchored Proteins Are Formed by Cortical Actin-Driven Activity*. Cell, 2008. **135**(6): p. 1085-1097.
99. Head, B.P., H.H. Patel, and P.A. Insel, *Interaction of membrane/lipid rafts with the cytoskeleton: impact on signaling and function: membrane/lipid rafts, mediators of cytoskeletal arrangement and cell signaling*. Biochim Biophys Acta, 2014. **1838**(2): p. 532-45.
100. van Gijssel-Bonnello, M., et al., *Pantethine Alters Lipid Composition and Cholesterol Content of Membrane Rafts, With Down-Regulation of CXCL12-Induced T Cell Migration*. Journal of Cellular Physiology, 2015. **230**(10): p. 2415-2425.
101. Eich, C., et al., *Changes in membrane sphingolipid composition modulate dynamics and adhesion of integrin nanoclusters*. Scientific Reports, 2016. **6**: p. 20693.
102. Lingwood, D. and K. Simons, *Lipid Rafts As a Membrane-Organizing Principle*. Science, 2010. **327**(5961): p. 46-50.
103. Gassert, E., et al., *Induction of membrane ceramides: a novel strategy to interfere with T lymphocyte cytoskeletal reorganisation in viral immunosuppression*. PLoS Pathog, 2009. **5**(10): p. e1000623.
104. Muller, N., et al., *Measles virus contact with T cells impedes cytoskeletal remodeling associated with spreading, polarization, and CD3 clustering*. Traffic, 2006. **7**(7): p. 849-58.
105. Collenburg, L., et al., *A Functionalized Sphingolipid Analogue for Studying Redistribution during Activation in Living T Cells*. J Immunol, 2016. **196**(9): p. 3951-62.
106. Römer, P.S., et al., *Preculture of PBMCs at high cell density increases sensitivity of T-cell responses, revealing cytokine release by CD28 superagonist TGN1412*. Blood, 2011. **118**(26): p. 6772-6782.
107. Walter, T., et al., *Incorporation and visualization of azido-functionalized N-oleoyl serinol in Jurkat cells, mouse brain astrocytes, 3T3 fibroblasts and human brain microvascular endothelial cells*. Chem Commun (Camb), 2016. **52**(55): p. 8612-4.
108. Keizer, G.D., et al., *A monoclonal antibody (NK1-L16) directed against a unique epitope on the alpha-chain of human leukocyte function-associated antigen 1 induces homotypic cell-cell interactions*. The Journal of Immunology, 1988. **140**(5): p. 1393-1400.
109. Haberkant, P. and J.C.M. Holthuis, *Fat & fabulous: Bifunctional lipids in the spotlight*. Biochimica et Biophysica Acta (BBA) - Molecular and Cell Biology of Lipids, 2014. **1841**(8): p. 1022-1030.
110. Balla, T., *Phosphoinositides: Tiny Lipids With Giant Impact on Cell Regulation*. Physiological Reviews, 2013. **93**(3): p. 1019-1137.
111. Pomorski, T.G. and A.K. Menon, *Lipid somersaults: Uncovering the mechanisms of protein-mediated lipid flipping*. Prog Lipid Res, 2016. **64**: p. 69-84.
112. Contreras, F.X., et al., *Sphingomyelinase activity causes transbilayer lipid translocation in model and cell membranes*. J Biol Chem, 2003. **278**(39): p. 37169-74.
113. Hutagalung, A.H. and P.J. Novick, *Role of Rab GTPases in Membrane Traffic and Cell Physiology*. Physiological Reviews, 2011. **91**(1): p. 119-149.
114. Somsel Rodman, J. and A. Wandinger-Ness, *Rab GTPases coordinate endocytosis*. Journal of Cell Science, 2000. **113**(2): p. 183-192.
115. Deng, Y., et al., *Sphingomyelin is sorted at the trans Golgi network into a distinct class of secretory vesicle*. Proc Natl Acad Sci U S A, 2016. **113**(24): p. 6677-82.

116. Milne, S.B., et al., *Capture and release of alkyne-derivatized glycerophospholipids using cobalt chemistry*. *Nat Chem Biol*, 2010. **6**(3): p. 205-207.
117. Thiele, C., et al., *Tracing Fatty Acid Metabolism by Click Chemistry*. *ACS Chemical Biology*, 2012. **7**(12): p. 2004-2011.
118. Jiang, F., et al., *Liposomal C6 Ceramide Activates Protein Phosphatase 1 to Inhibit Melanoma Cells*. *PLOS ONE*, 2016. **11**(9): p. e0159849.
119. Furlong, S.J., N.D. Ridgway, and D.W. Hoskin, *Modulation of ceramide metabolism in T-leukemia cell lines potentiates apoptosis induced by the cationic antimicrobial peptide bovine lactoferricin*. *Int J Oncol*, 2008. **32**(3): p. 537-44.
120. Villena, J., et al., *Ceramide-induced formation of ROS and ATP depletion trigger necrosis in lymphoid cells*. *Free Radical Biology and Medicine*, 2008. **44**(6): p. 1146-1160.
121. Hauser, M.A. and D.F. Legler, *Common and biased signaling pathways of the chemokine receptor CCR7 elicited by its ligands CCL19 and CCL21 in leukocytes*. *J Leukoc Biol*, 2016. **99**(6): p. 869-82.
122. Legler, D.F., et al., *Modulation of Chemokine Receptor Function by Cholesterol: New Prospects for Pharmacological Intervention*. *Molecular Pharmacology*, 2017. **91**(4): p. 331-338.
123. Contento, R.L., et al., *CXCR4-CCR5: a couple modulating T cell functions*. *Proc Natl Acad Sci U S A*, 2008. **105**(29): p. 10101-6.
124. Martinelli, S., et al., *Ezrin/Radixin/Moesin Proteins and Flotillins Cooperate to Promote Uropod Formation in T Cells*. *Frontiers in Immunology*, 2013. **4**(84).
125. Gérard, A., et al., *The Par polarity complex regulates Rap1- and chemokine-induced T cell polarization*. *The Journal of Cell Biology*, 2007. **176**(6): p. 863-875.
126. Kwon, K.W., et al., *Nanotopography-Guided Migration of T Cells*. *The Journal of Immunology*, 2012. **189**(5): p. 2266-2273.
127. Kim, M., et al., *The primacy of affinity over clustering in regulation of adhesiveness of the integrin α _L β ₂*. *The Journal of Cell Biology*, 2004. **167**(6): p. 1241-1253.
128. Comrie, W.A., A. Babich, and J.K. Burkhardt, *F-actin flow drives affinity maturation and spatial organization of LFA-1 at the immunological synapse*. *The Journal of Cell Biology*, 2015. **208**(4): p. 475-491.
129. Comrie, W.A. and J.K. Burkhardt, *Action and Traction: Cytoskeletal Control of Receptor Triggering at the Immunological Synapse*. *Front Immunol*, 2016. **7**: p. 68.
130. Critchley, D.R., *Cytoskeletal proteins talin and vinculin in integrin-mediated adhesion*. *Biochem Soc Trans*, 2004. **32**(Pt 5): p. 831-6.
131. Lopes Pinheiro, M.A., et al., *Acid Sphingomyelinase-Derived Ceramide Regulates ICAM-1 Function during T Cell Transmigration across Brain Endothelial Cells*. *The Journal of Immunology*, 2016. **196**(1): p. 72-79.
132. Takesono, A., et al., *Microtubules regulate migratory polarity through Rho/ROCK signaling in T cells*. *PLoS One*, 2010. **5**(1): p. e8774.
133. Stroka, K.M., H.N. Hayenga, and H. Aranda-Espinoza, *Human neutrophil cytoskeletal dynamics and contractility actively contribute to trans-endothelial migration*. *PLoS One*, 2013. **8**(4): p. e61377.
134. Chang, Y.-C., et al., *GEF-H1 Couples Nocodazole-induced Microtubule Disassembly to Cell Contractility via RhoA*. *Molecular Biology of the Cell*, 2008. **19**(5): p. 2147-2153.
135. Krendel, M., F.T. Zenke, and G.M. Bokoch, *Nucleotide exchange factor GEF-H1 mediates cross-talk between microtubules and the actin cytoskeleton*. *Nat Cell Biol*, 2002. **4**(4): p. 294-301.

9 Abbreviations

°C	-	degree Celsius
2D	-	two dimensional
3D	-	three dimensional
ACKR	-	atypical chemokine receptor
APC	-	antigen presenting cell
APS	-	ammonium persulfate
Arp 2/3	-	actin-related proteins 2 and 3
ASM	-	acid sphingomyelinase
ATP	-	adenosine triphosphate
BSA	-	bovine serum albumin
bSMase	-	bacterial sphingomyelinase
C	-	cysteine
CD	-	cluster of differentiation
Cdc42	-	cell division control protein 42 homolog
CERT	-	ceramide transfer protein
CFSE	-	carboxyfluorescein succinimidyl ester
CRISPR	-	clustered regularly interspaced short palindromic repeats
cyclic AMP	-	cyclic adenosine monophosphate
DC	-	dendritic cell
ddH ₂ O	-	bi-distilled water
DIBO	-	di-benzocyclooctyne
DMSO	-	dimethyl sulfoxide
DNA	-	deoxyribonucleic acid
DOCK2	-	dedicator of cytokinesis 2
EDTA	-	ethylenediaminetetraacetic acid
ELMO	-	engulfment and cell motility
ER	-	endoplasmatic reticulum
ERM	-	ezrin/radixin/moesin
F-actin	-	filamentous actin
FA	-	formaldehyde
FACS	-	fluorescence-activated cell sorting
FCS	-	fetal calf serum

FITC	-	fluorescein isothiocyanate
FN	-	fibronectin
FSC	-	forward scatter
g	-	gram
GM-CSF	-	granulocyte-macrophage colony stimulating factor
GPCR	-	G-protein coupled receptor
GTP	-	guanosine triphosphate
h	-	hour/hours
HBMEC	-	human brain microvascular endothelial cells
HBSS	-	Hank's balanced salt solution
HEV	-	high endothelial venules
HIV	-	human immunodeficiency virus
HRP	-	horseradish peroxidase
ICAM	-	intracellular adhesion molecules
IF	-	immunofluorescence
IFN γ	-	interferon γ
Ig	-	immunoglobulin
IL	-	interleukin
IS	-	immunological synapse
JAM-1	-	junctional adhesion molecule-1
KD	-	knockdown
kDa	-	kilo Dalton
l	-	litre
LFA	-	lymphocyte function-associated antigen
LN	-	lymph node
LPS	-	lipopolysaccharide
M	-	molar
MEM	-	minimal essential media
MFI	-	mean fluorescence intensity
MHC	-	major histocompatibility complex
min	-	minute/minutes
moDC	-	monocyte derived dendritic cell
mRNA	-	messenger ribonucleic acid
NaCl	-	sodium chloride

NBD	-	nitro-2-1,3-benzoxadiazol-4-yl
NSM	-	neutral sphingomyelinase
NSMi	-	neutral sphingomyelinase inhibited
o.n.	-	over night
PAGE	-	polyacrylamid gel electrophoresis
PBL	-	peripheral blood lymphocytes
PBMC	-	peripheral blood mononuclear cells
PBS	-	phosphate buffered saline
PCR	-	polymerase chain reaction
PECAM-1	-	platelet endothelial cell adhesion molecule
PH	-	pleckstrin homology domain
PI	-	propidium iodide
PI3	-	phosphoinositid-3
PKC	-	protein kinase C
PLC γ	-	phospholipase
PLL	-	poly-L-lysin
PMA	-	paramethoxy amphetamine protein
Rac	-	ras-related C3 botulinum toxin substrate
rmp	-	revolutions per minute
ROS	-	reactive oxygen species
RPMI	-	Roswell Park Memorial Institute
RT	-	room temperature
S1P	-	sphingosine-1-phosphate
SDF-1 α	-	stromal cell-derived factor 1 α
SDS	-	sodium-dodecylsulfat
SEA	-	Staphylococcus Enterotoxin A
SEB	-	Staphylococcus Enterotoxin B
sec/sec	-	second/seconds
SH3	-	Src-homology 3
siRNA	-	small interfering RNA
SM	-	sphingomyelin
SMase	-	sphingomyelinase
SNARE	-	soluble N-ethylmaleimide-sensitive factor attachment

Src	-	c-Src: <u>c</u> ellular, <u>sar</u> coma
SSC	-	sideward scatter
START	-	StAR-related lipid-transfer
TCR	-	T cell receptor
TEM	-	transendothelial migration
Th	-	T-helper
TNF α	-	tumor necrosis factor α
U	-	unit
UV	-	ultraviolet
VCAM	-	vascular cell adhesion protein
WASP	-	Wiskott-Aldrich-Syndrom-Protein
WT	-	wild type
yCoM	-	centre of mass displacement in y-direction
yFMI	-	forward migration index in y-direction
ZAP70	-	zeta-associated protein of 70 kDa
x g	-	gravitational constant

10 Acknowledgements

I would like to express my deep gratitude to Prof. Dr. Sibylle Schneider-Schaulies for her patient guidance, enthusiastic encouragement and useful critiques of this research work. Her guidance helped me in all the time of research and in the writing of this thesis.

Besides my advisor, I would like to thank my other thesis committee members PD Dr. Niklas Beyersdorf and Prof. Dr. Markus Sauer for their insightful comments on my dissertation and for their continuous encouragement.

For the fluorescence microscopy the advice and assistance provided by Dr. Nora Müller has been a great help.

My special thanks go to all members of the DFG-Forschergruppe SpingoFOR 2123 for excellent collaboration, discussions and advice. I would like to especially thank Prof. Dr. Jürgen Seibel, Tim Walter and Dr. Lukasz Japtok for their work on the click chemistry project.

I thank my colleagues Elita, Charlene, Claudia, Philipp and Sherry, for the assistance, discussions and for all the fun we have had in the last three years.

Last not least, I thank my friend Sebastian Peschko and my family for patiently learning a lot about biology over the years, and for always tirelessly supporting me.

11 Publication List

Incorporation and visualization of azido-functionalized N-oleoyl serinol in Jurkat cells, mouse brain astrocytes, 3T3 fibroblasts and human brain microvascular endothelial cells.

Walter T, Collenburg L, Japtok L, Kleuser B, Schneider-Schaulies S, Müller N, Becam J, Schubert-Unkmeir A, Kong JN, Bieberich E, Seibel J.

Chem Commun (Camb). 2016 Jun 30

(Lena Collenburg and Tim Walter contributed equally to the work.)

A Functionalized Sphingolipid Analogue for Studying Redistribution during Activation in Living T Cells.

Collenburg L, Walter T, Burgert A, Müller N, Seibel J, Japtok L, Kleuser B, Sauer M, Schneider-Schaulies S.

J Immunol. 2016 May 1

(Lena Collenburg and Tim Walter contributed equally to the work.)

Multiepitope tissue analysis reveals SPPL3-mediated ADAM10 activation as a key step in the transformation of melanocytes.

Ostalecki C, Lee JH, Dindorf J, Collenburg L, Schierer S, Simon B, Schliep S, Kremmer E, Schuler G, Baur AS.

Sci. Signal. 2017 March 14

Neutral sphingomyelinase in physiological and measles virus induced T cell suppression.

Mueller N, Avota E, Collenburg L, Grassmé H, Schneider-Schaulies S.

PLoS Pathog. 2014 Dec 18

12 Curriculum Vitae

Name: Lena Collenburg
Date of Birth: 15.07.1988
Place of Birth: Kiel
Nationality: German

Education

Since July 2014 **PhD student at the Universität Würzburg, Würzburg, Germany**

Topic: The role of ceramides and sphingomyelinases for dynamic membrane processes in T cells

April 2013 until June 2014 **PhD student at the Uniklinikum Erlangen, Erlangen, Germany**

2011 to 2012 **Hochschule Mannheim University of Applied Sciences**

Degree: Master of Science in Biotechnology

Master thesis: Merck, Darmstadt

Topic: Influence of BAFF and APRIL targeting therapies on the expression of BCMA, BAFFR and TACI on plasma cells and other B cell populations

2007 to 2011 **Hochschule Mannheim University of Applied Sciences**

Degree: Bachelor of Science in Biotechnology

Bachelor thesis: Evotec, Hamburg

Topic: Development of a cell based cytotoxicity model using high content screening and analysis

1998 to 2007 **Gymnasium Schwarzenbek**

Degree: Abitur